SUBSTRUCTURAL STUDIES AT LARGE STRAINS IN ALUMINUM

by

HONGANAHALLI CHANDRA, B.Sc., B.E., M.E.

A Thesis

Submitted to the School of Graduate Studies

in Partial Fulfilment of the Requirements

for the Degree

Doctor of Philisophy

McMaster University.

December 1979

SUBSTRUCTURAL STUDIES AT LARGE STRAINS IN ALUMINUM

DOCTOR OF PHILOSOPHY (1979)
(Metallurgy and Materials Science)

McMASTER UNIVERSITY
Hamilton, Ontario

TITLE: SUBSTRUCTURAL STUDIES AT LARGE STRAINS IN ALUMINUM

AUTHOR: Honganahalli Chandra, B.Sc. (Bangalore University, India)
B.E. (Indian Institute of Science, India)
M.E. (Indian Institute of Science, India)

SUPERVISOR: Dr. J.D. Embury

NUMBER OF PAGES: xv, 243

ABSTRACT

The nature of the dislocation substructure developed at large strains in single crystals of aluminum has been studied. The detailed characteristics of the substructure have been studied as functions of (a) strain, up to compressive strains of 1.0 and (b) crystal orientation. The crystal orientations have been selected to study the influence of the stability of orientation on the nature of the dislocation substructure developed during deformation.

The Bishop-Hill and yield subsurface analyses have been adopted to predict the operative slip systems. Applicability of these methods to large strain deformation studies has been discussed.

Results of the present study emphasize the influence exerted by crystal orientation via the nature of operative slip systems and the extent of homogeneity of slip on the extent of dynamic recovery and the resulting dislocation substructure. Development of high angle boundaries in the as-deformed condition in crystals deformed to large strains, is associated with inhomogeneity of slip. Origin of these high angle boundaries during deformation and their role in subsequent recrystallization process have been discussed.

ii a

ACKNOWLEDGMENTS

TABLE OF CONTENTS

LIST OF FIGURES

LIST OF TABLES

CHAPTER 1

INTRODUCTION

Statement of Objectives and Summary of the Scope of the Present Work

When metallic materials are deformed at low temperatures (< 0.5 T_m), in general, their flow stress increases due to the imposed strain and the dislocation content of the crystal increases rapidly. Much effort has been devoted to the understanding of the detailed structural changes and dislocation interactions which give rise to the work hardening.

In the majority of cases, the investigations have been performed at low strains. It has been usual to study the effect of deformation by X-ray methods, electron microscopy observations of the dislocation sub-structure and observations of slip plane traces on the surface of the specimen (Nabarro et al., 1964; Basinski and Basinski, 1966; Hirsch, 1975). The emphasis has been on correlating the flow stress with the stored dislocation density and the local configuration of the disloca-tions (Bailey and Hirsch, 1960; Warrington, 1960). Various models have been developed to account for the development of the observed microstruc-tural features and the rates of work hardening (Seeger, 1957; Hirsch, 1959, Basinski, 1959, Kuhlmann-Wilsdorf, 1962, Mott, 1952).

It is important to extend these studies to large strains and to a variety of proportional loading paths. At large strains both work hardening and recovery (i.e., dynamic recovery) occur simultaneously. Thus, the understanding of the substructural features developed at large

1

strains may be of value in assessing the mechanical and thermal stability of the dislocation substructure. It is also of significance to consider the nature of the dislocation substructure developed at large strains in relation to the subsequent recovery and recrystallization behaviour.

The objective of the present work is to gain some understanding of the nature and evolution of the dislocation substructure characteristic of large strains. Particular emphasis was given to:

(a) the understanding of the role of deformation geometry at large strains;

(b) the effect of orientation of the crystal on the evolution of the substructure at large strains, and,

(b) the relation of the substructure to subsequent recovery and recrystallization behaviour.

To simplify the study, the substructure development was studied in single phase, single crystals of high purity aluminum deformed under essentially plane strain conditions in a channel die. The effect of the orientation was investigated by selecting $(1\bar{1}0)$ $[\bar{1}12]$ crystals of stable orientation and $(1\bar{1}1)$ $[\bar{1}23]$ crystals which undergo lattice reorientation during deformation. It is hoped that the data obtained from the present series of experiments may aid in interpreting results possessing a more varied microstructure and subjected to more complex loading paths.

The experimental work described in this thesis includes a determination of the shape changes undergone by the specimens at different stages of the compression process, up to a compressive strain of

about 1.0. Slip plane traces observed on the surfaces of the specimen
at different levels of compressive strain enabled unambiguous determin-
ation of the active slip planes, though not of active slip directions.
The experimental observations were compared with theoretical predictions
of active slip systems based on the Bishop-Hill analysis (1951) and the
yield subsurface method following the approach proposed by Kocks (1970).

A major part of the experimental study was directed towards the
understanding of the evolution of the dislocation substructure during
the compression process for crystals of the two initial orientations.
Transmission electron microscope was used to study the nature and local
configuration of the dislocation substructure. In addition, optical
metallography aided in the study of the spatial distribution of the sub-
structure which in turn could be related to the scale and nature of
the slip plane traces observed on the surface of the compressed crystals.
Particular attention was paid to the homogeneity of deformation.

An important observation was made using the transmission elec-
tron microscope about development of high angle boundaries during de-
formation. These high angle boundaries act as nuclei for recrystalliza-
tion as was observed from hot stage experiments performed on thin foils
in the transmission electron microscope. It is of importance to under-
stand the development of such subdomains of high misorientation during
deformation. Possible mechanisms leading to their formation are con-
sidered.

Although the phenomenon of work hardening is accompanied by an
increase in the level of energy stored in the material, no attempt was
made in the present work to correlate the two. Instead, the formalisms

that are available for describing the stored energy data are considered
and some general comments are offered concerning the correlation of the
stored energy data with the associated work hardening behaviour.

CHAPTER 2

LITERATURE REVIEW

In this chapter, a brief review of the literature relevant to the present work will be provided. In the interest of clarity, it will be presented in sections which parallel the presentation of results later in the thesis. Thus, the first part of the review is devoted to the description of methods of predicting the geometry of slip for general deformation conditions and the correlation of these predictions, with experimental observations. In order to determine the active slip systems, observation of the arrangement of slip plane traces on the surface must be made and thus the second section of the review is devoted to a brief summary of the findings concerning the slip plane traces on the surfaces of deformed crystals.

One of the important problems in plastic deformation is understanding the evolution of the dislocation substructure during deformation and thus it is appropriate to review the known data concerning the dislocation substructure developed particularly at large strains (> 0.2). Clearly the description of the dislocation substructure is a complex problem and traditionally the approach has been to attempt to relate parameters such as the flow stress of the material to average parameters such as the scale of the substructure or the average lattice misorientation measured across the cell walls. However, for many problems such as the determination of the nucleation event in recrystallization

5

or the establishment of criterion for flow stability, the paramters
which describe the average quantities may not suffice. Thus, in the
third section of this chapter dealing with dislocation substructure,
attention is given to the structural features associated with hetero-
geneity of deformation.

Although as opined above the description of the evolution of
the substructure is of great importance in understanding the cold worked
state it is also of importance to understand the stability of the dislo-
cation substructure and the changes which occur upon subsequent recovery
and recrystallization. Thus the fourth section of this chapter is de-
voted to this topic.

Clearly all the topics outlined above cannot be reviewed in a
comprehensive and critical manner. Thus, at various points in the
review, references are made to recent detailed review articles. In
addition, for the sake of brevity and relevance, the review given here
emphasizes results obtained for aluminum and other fcc metals.

2.1 Prediction of Slip Systems

In this section, the yield criterion defined by Schmid (1924)
for deformation of single crystals under uniaxial conditions and its
modification for multiaxial loading will be considered. The models
available to predict active slip systems as proposed by Taylor (1938),
Bishop-Hill (1951), Kocks (1970), Chin et al. (1966) are considered.
The application of the above criteria to available experimental data
obtained under approximate plane strain deformation mode will be
discussed.

2.1.1 Yield Criterion in Terms of Schmid Law

The Schmid Law relates the stress σ applied in uniaxial mode to the shear stress τ resolved on a given slip system as:

$$\tau = \cos \phi \cos \theta \, \sigma \tag{2.1}$$

As shown in Fig. 2.1, θ and ϕ are the angles between the loading axis and the slip direction and slip plane normal, respectively. Yield occurs when τ reaches a critical value τ_c which is assumed to be the same on all equivalent slip systems. The product of the direction cosines $\cos \theta \cos \phi$ is referred to as "m", the Schmid factor.

Under multiaxial loading conditions, Eq. (2.1) can be modified to

$$\tau^s = m_{ij}^s \, \sigma_{ij} \tag{2.2*}$$

where σ_{ij} is a general applied stress tensor. The superscript s refers to a given slip system s. Characterizing the slip system s by $\underline{p}^s$, the vector along the slip plane normal and $\underline{q}^s$ along the slip direction, and defining the coordinate system in which the applied stress tensor is given by the unit vectors $(\underline{a}_1, \underline{a}_2, \underline{a}_3)$. the components of m_{ij}^s can be calculated as

$$m_{ij}^s = (\underline{p}^s \cdot \underline{a}_i)(\underline{q}^s \cdot \underline{a}_j) \tag{2.3}$$

Based on Eq. (2.2), yield criterion can be defined for a single crystal deforming under multiaxial loading conditions, as

$$m_{ij}^s \, \sigma_{ij} \leq \tau_c^s \tag{2.4a}$$

for each inactive slip system, and

$$m_{ij}^s \, \sigma_{ij} = \tau_c^s \tag{2.4b}$$

for each active slip system.

The yield criterion defined in Eqs. (2.4) is based on the following

---

* Einstein summation convention is assumed.

↑LOAD

p

q

φ θ

SLIP
PLANE

SLIP PLANE

p = SLIP PLANE
NORMAL

q = SLIP DIRECTION
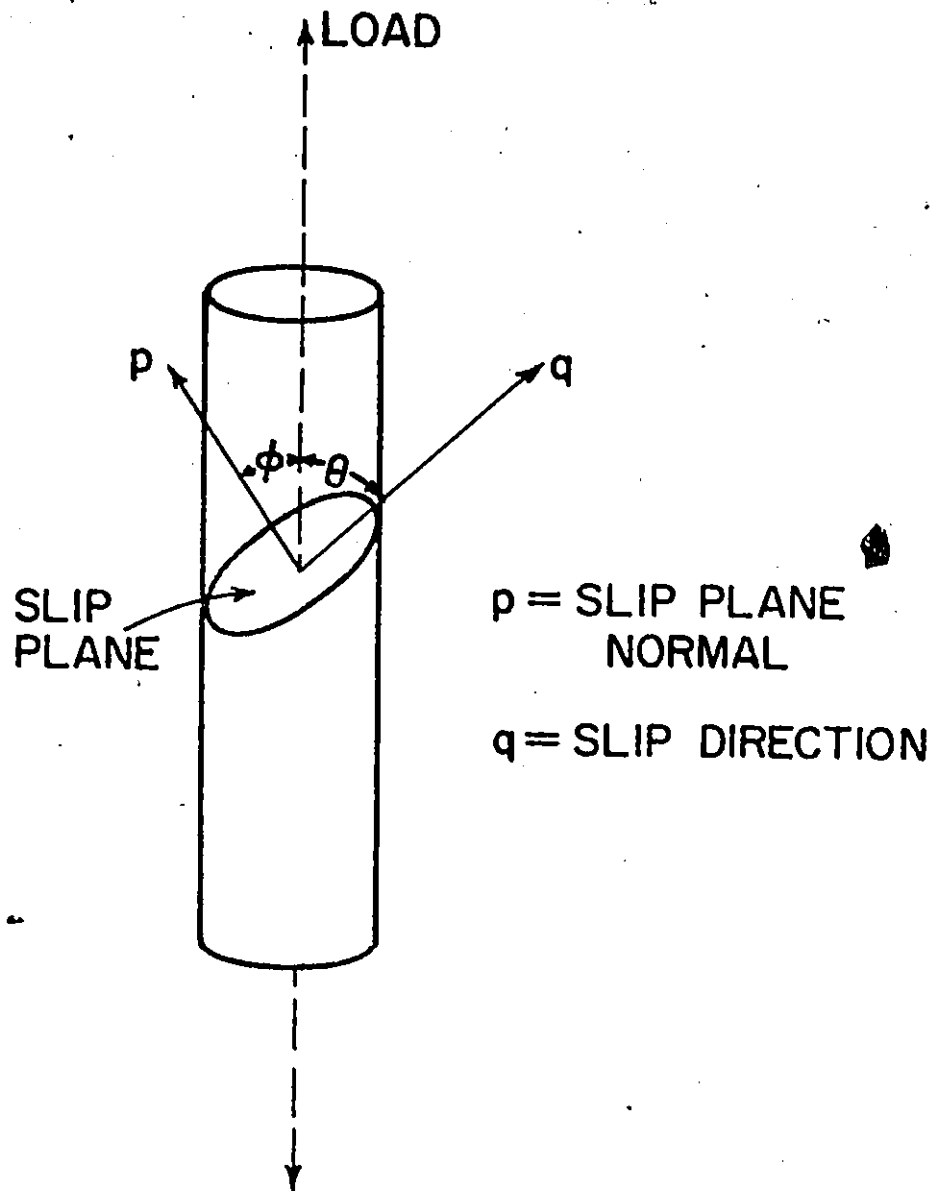
Fig. 2.1   Schematic illustration of a slip system with respect
to the loading axis.

assumptions:

(1) A slip system cannot be activated unless the value of resolved

shear stress reaches τ_c.

(2) The activity on the active slip systems is caused only by the

applied stress σ_{ij}, i.e., there is no secondary slip.

(3) The active and inactive slip systems harden at the same rate, i.e.,

the latent hardening ratio is approximately unity.

The displacement gradient tensor de_{ij} is similarly related to

increments of shear $d\gamma^s$ on each active slip system, defined by the yield

criterion

$$de_{ij} = \Sigma\, m^s_{ij}\, d\gamma^s \tag{2.5}$$

Contribution from each active slip system must be summed up to get the

components on the left-hand side of Eq. (2.5).

By definition the displacement gradient tensor can be divided

into a pure strain tensor $d\epsilon_{ij}$ and a rotation tensor $d\omega_{ij}$ as

$$d\epsilon_{ij} = \Sigma\, \frac{1}{2}\, (m^s_{ij} + m^s_{ji})\, d\gamma^s \tag{2.6}$$

$$d\omega_{ij} = \Sigma\, \frac{1}{2}\, (m^s_{ij} - m^s_{ji})\, d\gamma^s \tag{2.7}$$

The Equations (2.6) and (2.4b) are the basis of predicting slip systems

in the Taylor, Bishop-Hill and yield surface analyses.

2.1.2 Taylor Method

Taylor (1938) proposed, based on Eq. (2.6) that among all the

combinations of available slip systems, the active combination will be

the one for which the sum of the shears is the least. When a general

strain is imposed, five independent slip systems need to be activated

(von Mises condition). In fcc crystals assuming that slip occurs on the

{111} <110> family of slip systems, the Taylor analysis becomes an

exercise in finding the set of slip systems which yield least $\Sigma d\gamma^S$, out

of the available 384 independent combinations. Taylor originally pro-

posed the above hypothesis for a polycrystalline aggregate deforming

under uniaxial tension. The taylor factor, M, scales the applied stress

to the shear stress, and the sum of shears on the active slip systems to

the applied uniaxial strain

$$M = \frac{\Sigma d\gamma^S}{d\varepsilon_{xx}} = \frac{\sigma_{xx}}{\tau} . \qquad (2.8)$$

The Taylor factor, M, depends on the mode of deformation and orientation

(Chin, 1966). Based on the principle of virtual work,

$$M = \frac{d\omega_{ext}}{\tau d\varepsilon_{xx}} \qquad (2.9)$$

where $d\omega_{ext}$ is the amount of work done externally in uniaxial tension on

unit volume of the material. The evaluation of the value of $d\omega_{ext}$ for a

given deformation mode, based on the Bishop-Hill analysis, will be des-

cribed later.

As shown by both Taylor and Bishop and Hill the value of M for a

random polycrystalline material deformed in unaxial tension is 3.06.

This figure can be arrived at by calculating M for specific orientations

of the tensile axis within the standard stereographic triangle and

averaging the results.

Though the criterion of satisfying the yield condition was not

dealt with by Taylor, Kocks (1970), and Chin and Mammel (1969) have

shown that obeying of the yield criterion given in Eq. (2.4) is implicit

in the Taylor hypothesis.

2.1.3 Bishop-Hill Method

The yield criterion of Eq. (2.4) forms the basis of the Bishop-

Hill method. The selection of active slip systems is based on the prin-

ciple of maximum work which follows from the assumed convexity of the

yield surface and normality of the plastic strain increment at the

yield strain. The description of a representative yield surface is

given in Appendix 1. Based on Eq. (2.4), Bishop and Hill developed

polyhedral yield surfaces in stress space for {111} <110> slip in fcc

single crystals deforming under a general applied stress. It has been

shown by Bishop-Hill (1951) that it is sufficient to consider

only 56 sets of slip systems each consisting of either six or eight

independent slip systems, which are activated by stress states corres-

ponding to the vertices of the polyhedral yield surface. Bishop and

Hill referred to the 56 combinations as 56 "stress states" characterized

by distinct values of stress components, given in terms of coefficients

A, B, C, F, G and H. Since the hydrostatic stress component of the

applied stress does not influence yielding, all the six components of

the applied stress need not be considered to specify the shear stresses

set up in a crystal. The relevant stress components are defined in

terms of the coefficients A to H as:

$$A = \sigma_{22} - \sigma_{33} \qquad F = \sigma_{23}$$
$$B = \sigma_{33} - \sigma_{11} \qquad G = \sigma_{31} \qquad (2.10)$$
$$C = \sigma_{11} - \sigma_{22} \qquad H = \sigma_{12}$$

Bishop and Hill (1951) and Kocks (1970) have divided these 56 combinations among five distinct sets of polyslip. The five distinct types of polyslip will be referred to as A*, B*, C*, D* and E* groups. Each polyslip group is characterized by a given "external" loading condition. Following Kocks (1970), the description of the five types of polyslip is given in Table 2.1.

In Table 2.2, the 12 {111} <110> slip systems and their nomenclature according to Bishop and Hill (1951) and Kocks (1970) are given. In Table 2.3, the 56 "stress states" of Bishop and Hill, referred to henceforth as 56 polyslip corners are given along with the values of the coefficients A, B, C, F, G and H and the combination of slip systems intersecting at each corner.

2.1.3.1 Application of Bishop-Hill Method·

Under a general applied stress the external work can be evaluated according to:

$$dw = \sigma_{ij} \, d\varepsilon_{ij} \qquad (2.12)$$

In terms of the coefficient of Eq. (2.11):

$$dw = - Bd\varepsilon_{11} + Ad\varepsilon_{22} + 2Fd\varepsilon_{23} + 2Gd\varepsilon_{13} + 2Hd\varepsilon_{12} \qquad (2.13)$$

The $d\varepsilon$ terms are referred to the cubic coordinate system.

The Bishop-Hill technique of predicting slip systems applies to a case of prescribed stain. The prescribed strain $d\varepsilon_{ij}$ measured in a given reference frame is transformed into components $d\varepsilon_{11}$, etc., given in cubic coordinate system using the direction cosines m_{ij} of Eq. (2.3). Then, based on Eq. (2.13) and the values of coefficients from Table 2.3, the work done at each of the 56 polyslip corners is calculated. That

Table 2.1

Description of the five types of polyslip[†].

Type	A*	B*	C*	D*	E*
Mode of Deformation	[100] Tension	[111] Tension	(100)[010] Shear	[100] Compression + (100)[011] Shear	(100)[010] Shear + (110)[110] Shear
Number of polyslip corners of each type [*]	3	4	3	12	6
Number of slip systems interacting at a given corner of each type	8	6	8	6	8

[†]   Reference: Kocks (1970)

[*]   Remaining 28 corners are negatives of those given here.

Table 2.2

Nomenclature of the $\{111\}<110>$ type slip systems
according to Bishop-Hill (1951) and Kocks (1970).

Slip Systems Plane Direction		Nomenclature according to:	
		Bishop-Hill	Kocks*
(111)	[011]	b_1	a
	[101]	$\bar{b}_2$	b
	[1$\bar{1}$0]	b_3	c
(1$\bar{1}\bar{1}$)	[01$\bar{1}$]	$\bar{c}_1$	d
	[101]	$\bar{c}_2$	e
	[110]	c_3	f
(1$\bar{1}$1)	[011]	$\bar{d}_1$	g
	[10$\bar{1}$]	$\bar{d}_2$	h
	[110]	d_3	i
(111)	[01$\bar{1}$]	a_1	j
	[10$\bar{1}$]	$\bar{a}_2$	k
	[1$\bar{1}$0]	a_3	l

* Nomenclature according to Kocks (1970) is
followed in the present study.

Table 2.3

The fifty-six polyslip corners* contained in the fcc yield surface of Bishop-Hill; values of the coefficients A, B, C, F, G, H and the type of slip systems intersecting at each corner.

Polyslip Type	Polyslip Corner	A $=\sigma_{22}-\sigma_{23}$	B $=\sigma_{33}-\sigma_{11}$	C $=\sigma_{11}-\sigma_{22}$	F $=\sigma_{23}$	G $=\sigma_{31}$	H $=\sigma_{12}$	Slip systems intersecting at the polyslip corner
A*	1	0	1	-1	0	0	0	a b̄ c e f h ī l̄
	2	-1	0	1	0	0	0	a c d̄ f g h j̄ l̄
	3	1	-1	0	0	0	0	a b d e g i j k
B*	1	0	0	0	1/2	1/2	1/2	a b̄ c e f̄ g i l̄
	2	0	0	0	-1/2	1/2	1/2	a c d f̄ h k l̄
	3	0	0	0	1/2	-1/2	1/2	b̄ c̄ d̄ e h̄ j̄ l̄ l̄
	4	0	0	0	1/2	1/2	-1/2	a d̄ e f̄ g j̄ k̄
C*	1	0	0	0	1	0	0	b c e f̄ h i k̄ l̄
	2	0	0	0	0	1	0	a c̄ d e g j̄ l̄ l̄
	3	0	0	0	0	0	1	a b d̄ e g h j̄ k
D*	1	0	-1/2	1/2	0	1/2	1/2	a b̄ d̄ g k̄ l̄
	2	0	-1/2	1/2	0	-1/2	-1/2	a̅ c̄ e f̄ g h i
	3	0	-1/2	1/2	0	1/2	-1/2	d e̅ h̄ i j̄ k̄
	4	0	-1/2	1/2	0	-1/2	1/2	b c f̄ g̅ i̅ k̄
	5	1/2	0	-1/2	1/2	0	1/2	a d̄ e f̄ g j̄
	6	1/2	0	-1/2	-1/2	0	-1/2	b̄ c̄ i̅ h̄ k̄ l̄
	7	1/2	0	-1/2	-1/2	0	1/2	c d̄ h̄ i̅ j̄ k̄
	8	1/2	0	-1/2	1/2	0	-1/2	a̅ d̅ g h̄ k̄ l̄
	9	-1/2	1/2	0	1/2	1/2	0	e̅ f̄ h̄ j̄ k̄ l̄
	10	-1/2	1/2	0	-1/2	-1/2	0	a d̄ e f̄ g h̄ i̅
	11	-1/2	1/2	0	1/2	-1/2	0	c̄ e f̄ h̄ j̄
	12	-1/2	1/2	0	-1/2	1/2	0	b̄ d g i j̄ l̄
E*	1	-1	1/2	1/2	1/2	0	0	a̅ b c d e g i̅ k̄
	2	-1	1/2	1/2	-1/2	0	0	a b c f g h i̅ l̄
	3	1/2	-1	1/2	0	1/2	0	a b d f h i j̄ k̄
	4	1/2	-1	1/2	0	-1/2	0	b c e f g h l̄ l̄
	5	1/2	1/2	1	0	0	1/2	a c e h̄ i̅ j̄ l̄ l̄
	6	1/2	1/2	-1	0	0	-1/2	b c̄ d f g j̄ l̄ l̄

Ref: Bishop-Hill (1951), Kocks (1970)

* Only 28 of the 56 polyslip corners are given here. The rest are the negatives of the ones given.

polyslip corner which maximizes the external work needed to achieve the prescribed strain defines the combination of slip systems that is possibly active during the given deformation. When the external work is maximized at two different polyslip corners, the set of slip systems common to the two corners are considered to be active.

Chin and Mammel (1969) have shown that both the Taylor and Bishop-Hill methods are equivalent. The Bishop-Hill method is a search among only 56 polyslip corners unlike the Taylor method which for fcc crystals slipping on {111} <110> systems is a search among 384 possible combinations. It can be shown following the work of Chin and Mammel (1969), that the set of active slip systems selected based on the Taylor theory is always contained in the polyslip corner selected based on the Bishop-Hill model. Henceforth in the present work only the treatment proposed by Bishop and Hill will be followed because it is simpler to apply and the results will be treated as being equivalent to the predictions of Taylor's theory.

2.1.4 The Yield Subsurface Analysis Developed by Kocks

The basis of the yield subsurface analysis (1970) is the generalized Schmid Law of Eq. (2.2). Instead of considering a general yield surface as proposed by Bishop and Hill, Kocks considered "yield subsurfaces" appropriate to given deformation mode. Thus the yield subsurface analysis can also be treated as a particular form of the Bishop-Hill method.

2.1.4.1 Method of Construction of the Yield Subsurface for Deformation in the Channel Die

The yield subsurface is constructed based on Eq. (2.2). The stresses acting on a crystal during deformation in a channel die are σ_{xx},

the primary compression stress, σ_{yy} and σ_{xy}, the reaction stresses.
(The axes x, y and z are defined in Figure 3.5. The concept of these
stresses will be dealt with in greater detail in Chapter 4.) Eq. (2.2)
can be rewritten in terms of these stress components, as:

$$\tau^s = m^s_{xx}\,\sigma_{xx} + m^s_{yy}\,\sigma_{yy} + (m^s_{xy} + m^s_{yx})\,\sigma_{xy} \qquad (2.13)$$

m^s_{xx} etc. are calculated according to Eq. (2.3). Eq. (2.13) defines the
location of the slip system "s" in a yield subsurface constructed in the
stress coordinate system of σ_{xx}, σ_{yy} and σ_{xy}. The paramters m^s_{xx}, m^s_{yy}
and m^s_{xy} define the inverse of the intercepts, the particular slip system
"s" makes along the σ_{xx}, σ_{yy} and σ_{xy} axes, respectively. A value of zero
for a particular m component defines that particular intercept of the
slip plane at infinity. For example, if $m^s_{xx} = 0$ the slip plane "s" is
parallel to the stress axis σ_{xx}. The stress σ_{xx} cannot active the slip
system "s".

Utilizing the "m" matrix and Eq. (2.6), the shape change possible
by slip on the set of slip systems given by Eq. (2.13) can be evaluated.

2.1.5 Lattice Reorientation During Deformation

The yield criterion of Eq. (2.4) defines the slip systems which
could be activated under given deformation conditions, when the orien-
tation of the crystal is known. Whether the same set of slip systems
are active throughout the entire range of deformation and whether the
same ratio of activity is maintained on each slip system depends on
the stability of the crystal orientation during deformation.

In general, slip on a given slip system will lead to both shape
change and lattice reorientation, according to Eqs. (2.6) and (2.7).

The net rotation is given by:

$$|d\omega| = \sqrt{(d\omega_{12}^2 + d\omega_{23}^2 + d\omega_{31}^2)} \qquad (2.14)$$

The rotation occurs about an axis whose direction cosines are:

$$\frac{d\omega_{23}}{|d\omega|}, \quad \frac{d\omega_{31}}{|d\omega|}, \quad \frac{d\omega_{12}}{|d\omega|} \qquad (2.15)$$

Based on the variation of parameter $\dfrac{|d\omega|}{d\epsilon}$, the instantaneous rate of rotation per unit strain, Dillamore et al. (1968) have determined the stability of crystals deforming under plane strain conditions. It was shown that among fcc single crystals with either <110> or <111> axis along the transverse direction, the orientations {1$\bar{1}$0} <001> and {110} <$\bar{1}$12> were stable during deformation. The importance of the stability of orientation will be considered next.

Both in the Taylor and Bishop-Hill models, the strain components, i.e., the shape change of the crystal, is the parameter that is experimentally determined. These methods are applicable to crystals deformed to small strains and crystals whose orientation does not change during deformation. Application of the Bishop-Hill method to crystals subjected to large deformations, is equivalent to assuming that the shape and size of the yield surface remain similar and the direction of prescribed strain vector remains fixed throughout the deformation. The validity of such an assumption is debatable. The problem is more complicated when the orientation of the crystal changes during deformation.

As the orientations of the crystal axes changes during deformation, the components of m_{ij}^s defined in Eq. (2.3) also change. Accordingly, the values of $d\epsilon_{11}$, etc., required to calculate the work done at the 56 polyslip corners based on Eq. (2.12) also change. This changes the

direction of the prescribed strain vector. The implication of these concepts will be discussed in detail in Chapter 4.

The concept of the deformation gradient matrix developed by Chin et al.(1966) is suitable to analyze the behaviour of crystals of unstable orientations and at large strains.

2.1.6 The Deformation Gradient Matrix

The matrix treatment enables one to consider any large strain deformation to be made up of several small measurements of strain. Each strain increment is represented by a deformation gradient matrix. The matrix product of these leads to the large strain deformation.

Chin et al. (1966) assumed the set of slip systems that is active during the deformation of a crystal of known orientation and calculated the shape change that the crystal would therefore undergo. Instead, Johnson (1969) measured the deformation gradient matrix of a given crystal at increments of 0.5% reduction in height. The strain components were determined to an accuracy of ± 0.04% and the orientations of the faces were determined to within ± 1/4° accuracy. The ratio of activity on each of the operative slip systems, which led to the measured shape change of the crystal, was evaluated.

The components of the deformation gradient matrix can be determined experimentally during a given strain increment by measuring the initial and final dimensions and orientations of three noncoplanar lines. Details are given in the papers of Chin et al. (1966) and Johnson (1969).

2.1.7 Application of the Techniques Available for Predicting Slip Systems

In this section, the results available in the literature obtained

by the application of the Bishop-Hill method will be presented.

Emphasis is placed on results obtained for single crystals deformed

under conditions of and approximating to that in a channel die.

The application of the yield subsurface analysis will be treated

in Chapter 4. Except for the present work, no other similar treatment

of the yield subsurface analysis applied to deformation in a channel

die, is available.

2.1.7.1 Results Based on the Bishop-Hill Method

Chin and coworkers have extensively applied the Bishop-Hill

method to predict the slip systems that are active during deformation

in a channel die, similar to the one described in Chapter 3. Results

are available for crystals of copper, Cu - 6Al, Ag - 4Sn (1970),

Mo (1975), Al and Permalloy crystals (1966). Hosford has applied the

Bishop-Hill technique for single crystals of Al and Al - 4Cu deformed in

plane strain compression between two indentors (1966, 1971). Serpoul

and Driver (1979) have applied the Bishop-Hill method to single and

bicrystals of aluminum deformed in the channel die. Results from the

above studies are given in Table 2.4 for Al single crystals.

Most of these experimental studies were aimed at understanding the

effect of orientation on the stress-strain behaviour based on the calcu-

lation of the Taylor effect, M, and the development of deformation tex-

ture. Identification of slip plane traces is reported only for certain

orientations of Permalloy and Al crystals. It was concluded that the

slip systems predicted based on the Bishop-Hill method adequately

explained the experimental results.

Table 2.4

Results of Bishop-Hill analysis.

Orientation	Possible set of slip systems	Taylor Factor M ($\sqrt{6}$)
(110)[1$\bar{1}$0]	$\bar{a}\ \bar{b}\ \bar{c}\ \bar{d}\ e\ \bar{g}\ h\ \bar{j}\ \bar{k}$ [1][2][3]	2 ↓
(110)[001]	$\bar{a}\ \bar{b}\ \bar{j}\ \bar{k}$ [1][3]	1 ↑
(110)[$\bar{1}$12]	$\bar{a}\ \bar{b}\ \bar{d}\ e\ \bar{g}\ h\ \bar{j}\ \bar{k}$ [1]	1 ↑
	$\bar{a}\ k$*	
(110)[111]	$a\ b\ d\ e\ g\ h\ j\ k$ [2]	1.6
	$\bar{a}\ e\ \bar{g}$*	
(001)[$\bar{1}\bar{1}$0]	$a\ b\ j\ k$ [1]	1 ↑ ↓
(100)[010]	$\bar{c}\ \bar{f}\ \bar{i}\ \bar{l}$ [3]	1
(111)[$\bar{1}$10]	$\bar{a}\ \bar{b}\ \bar{d}\ e\ \bar{g}\ \bar{i}\ \bar{j}\ \bar{k}$ [1]	1 ↑
	$\bar{a}\ \bar{b}\ \bar{d}\ e\ \bar{g}\ \bar{i}$*	
(1$\bar{1}$1)[$\bar{1}$12]	$\bar{a}\ \bar{b}\ f\ \bar{i}$ [1][2]	1.5
($\bar{1}$12)[$\bar{1}$11]	$\bar{a}\ \bar{b}\ f\ \bar{i}$ [2]	
($\bar{1}$23)[4 $\bar{2}$5 18]	$\bar{b}\ \bar{c}\ e\ f\ \bar{h}\ i\ k\ l$	1.75

(1̀)   Ref: Wonsiewicz and Chin (1970)

(2)   Ref: Hosford (1966)

(3)   Ref: Serpont and Driver (1979)

*   with finite shear

↓   decreasing M,   ↑ increasing M

↑   constant M (during deformation)

2.2 Slip Plane Trace Observations

In this section, the salient features of the results available in the literature concerning the slip plane traces formed on the surface during deformation of single crystals will be reviewed. The observations obtained, derived from a variety of strain levels will be discussed with reference to single phase fcc single crystals. In order to comment on the accuracy of the determination of the slip systems and the spatial distribution of slip, a brief review is given concerning the nature of the information that is required and the various metallographic techniques available for the study of the nature and scale of slip plane traces. In this review section, emphasis will be laid on the following aspects:

(1) How do the scale and distribution of slip vary with the level of imposed strain?

(2) Does the scale of slip observed on the surface relate to the evolution of the dislocation substructure in the interior of the crystal?

(3) How is the homogeneity of deformation reflected in the observed slip traces?

In treating the information derived from slip plane traces as representative of the entire deformation process, it is implicitly assumed that all the slip that occurs can be observed via the slip plane traces. Fine slip may be beyond the resolution of the technique presently available. The resolutions and limitations of the various techniques available to study the slip plane traces are given in Table 2.5. These aspects have been discussed in detail by Brown (1952), Nabarro et al. (1964), Basinski and Basinski (1966) and Hirsch (1975).

Table 2.5

Techniques available to study slip plane traces,
the resolution possible and limitations of the technique.

Technique	Resolution	Limitations
Ordinary optical metallography (white light with green filter)	2400 Å	Fine slip cannot be studied; step height cannot be measured.
Nomarski interference method	150 Å in height	Surface has to be extremely flat; cannot study electrolytically prepared surfaces.
Replica technique	50 – 80 Å in length and spacing 15 – 20 Å in height	Extreme care necessary in handling the film; spurious structure may be produced due to replication.

2.2.1 Identification of Active Slip Systems
Based on the Analysis of Slip Plane Traces.

Slip plane traces are formed on the surface of a deformed crystal

as the steps due to groups of dislocations which emerge from the crystal.

The traces are the intersections which the active slip planes make with

the surface. Steps are formed on the surfaces where a component of the

Burgers vector of the emerging dislocation is normal to the surface.

Identification of the directions of the trace and the surface on which

the correponding steps are formed for two non-parallel surfaces, leads

to the identification of the active slip system. Barrett (1952) has

dealt with the procedure of identifying the active slip systems based

on slip plane trace information.

2.2.2 Techniques of Studying the Slip Plane Traces

The various methods available to study the slip plane traces are

based on either optical or electron microscopy. The optical microscopy

technique utilizes either direct or oblique illumination. In oblique

illumination better contrast and therefore improved resolution can be

attained. The theoretical resolution, δ, of a microscope is defined as

$$\delta = \frac{0.61\lambda}{NA} \tag{2.16}$$

where NA is the numerical aperature.

To study fine details of the slip plane traces, particularly the

step heights, the Nomarski interference technique is used (Mitchell et

al., 1966). Fringe displacement across a slip step is analyzed to deter-

mine the step height. A resolution of approximately 150 $\overset{\circ}{A}$ in height is

possible. To be able to study such small differences in height, it is

imperative to have extremely flat surfaces for examination. Electroly-

tically polished surfaces do not meet this requirement.

In the electron microscope technique, the slip plane traces are examined by preparing a replica of the surface. Both oxide and carbon replicas have been used. In the case of aluminum, the Al_2O_3 film from the surface itself can be used (Wilsdorf, 1952). A resolution of 50 – 80 Å in spacing and length and of 15 – 20 Å in step height, can be obtained using the electron microscope. The self-structure of the oxide film, and its fragility necessitate extreme care in handling the replica and in interpreting the information that is obtained.

2.2.3 Nature of Slip Plane Traces in Crystals Deformed at Low Strains

2.2.3.1 Crystal Oriented for Single Slip

A typical stress-strain behaviour exhibiting the three stages of hardening for a fcc single crystal of copper deformed at ordinary temperature ($T < 0.2\ T_m$) in tension is shown in Figure 2.2. In Stage I, known as the easy glide region, homogeneously distributed long, straight and fine traces of primary slip system are observed. Typical length of the traces is $\sim$ 1000 μm and often approximates to the dimensions of the specimen. Only the height of the traces seems to vary (Mader, 1963), both the length and spacing remaining unaltered as strain increases in the easy glide region.

In the linear hardening stage, the traces of the primary slip system are still the traces which predominate on the surface, though electron microscope observation shows a large number of secondary dislocations within the crystal (details to be discussed later in Section 2.3). This could be due to the fact that the secondary dislocations move over

very short distances within the crystal and so do not cause any observable traces on the surface. It is also possible that the resolution attainable in the present-day techniques is not sufficient to observe extremely fine slip (Basinski and Basinski, 1966). Some coarse slip traces belonging to cross slip systems are observed. The slip traces are usually inhomogeneously distributed. In Stage II, the length of the slip plane traces varies with inverse of the strain (Mader, 1963). The height of the slip plane traces is not uniform over the entire surface. New slip line traces appear with increasing strain.

Slip bands of primary slip systems associated with cross slip are commonly observed in Stage III. Slip bands are groups of fine slip plane traces. Blewitt et al. (1955) reported the appearance of "fragmented" slip lines in copper deformed at room temperature. No evidence of cross slip was present. The mean length of the "fragmented" slip lines was found to vary linearly with strain, up to a shear strain of 1.2.

In crystals oriented for single slip, local changes in slip plane trace pattern is observed from one area to another in the crystal indicating occurrence of abrupt lattice curvature associated with kink bands (Honeycombe, 1951-52). When bands of secondary slip are observed, indicating inhomogeneous deformation, changes are observed in the associated slip plane trace patterns (Honeycombe, 1951-52; Rosi, 1954). Traces of secondary slip planes were observed even in Stage I near deformation bands (Kelly, 1956; Basinski and Basinski, 1966).

2.2.3.2 Crystals Oriented for Multiple Slip

In fcc single crystals of multiple orientation deformed at temperatures $(T < 0.3\ T_m)$ the slip plane trace distribution depends,

among other factors, on the initial orientation of the crystal and the stability of orientation during deformation.

In crystals oriented for duplex slip in tension, for example, crystal of the [112] type orientation, traces of both primary and conjugate slip planes are observed on the surface. The traces in general are long and straight.

[111] oriented aluminum single crystals showed short and wavy traces belonging to a number of slip systems (Kocks, 1960) from the start of deformation. Because of the wavy nature, it is difficult to accurately identify the nature of the slip systems. No attempt was made to measure the variation of the scale with strain.

During room temperature deformation, [100] oriented single crystals of aluminum exhibited a strikingly different work hardening behaviour compared to [111] oriented crystals (Kocks, 1960; Hosford et al., 1960; Sakei and Miura, 1977). After an initial stage of work hardening in which multiple slip plane traces were observed, the rate of hardening decreased to extremely low levels, associated with a slip plane trace distribution which varied both spatially and sequentially. Only a few of the available eight slip systems were operative in a given region at a given strain. Both uniform and clustered cross slip traces were observed.

Ambrosi et al. (1974, 1978) observed that length of slip bands in [100] and [111] oriented copper single crystals deformed at room temperature, varied with the inverse of strain.

2.2.4 Nature of Slip Plane Traces in Crystals Deformed to Large Strains

The nature of the slip plane trace distribution observed on the surfaces of the crystal deformed to large strains appears to depend on the stability of the orientation of the crystal during deformation. The observation was done based on an incremental straining technique following Crussard (1945). In crystal of orientation (110) [1$\bar{1}$2], which is a stable orientation under plane strain deformation mode, slip plane traces belonging to the primary and conjugate slip systems were observed during deformation. The average length of the traces was about 200 – 400 μm after about 90% rolling (Hu et al., 1966).

Traces corresponding to duplex slip on primary and conjugate slip systems were also observed on (110) [$\bar{1}$12] crystals deformed under approximately plane strain conditions in the channel die (Chin et al., 1966). After an incremental straining at a thickness reduction of about 50%, the length of the slip plane traces varied between 100 – 400 μm. The distribution of the slip plane traces was found to be quite homogeneous on the surface of crystals of stable orientations.

In crystals of unstable orientation, inhomogeneities in slip plane trace distribution particularly associated with formation of deformation bands have been reported (Wonsiewicz and Chin, 1970; Ahlborn, 1966).

For crystals deformed to large strains, not much quantitative data is available with regard to the variation of the scale of slip plane traces with strain. Most of the data is concerned with the occurrence of variations in slip plane trace pattern corresponding to inhomogeneity in deformation.

2.2.5 Importance of Slip Plane Trace Observation

If it is assumed that the length of the slip plane traces remains proportional to the mean free path of dislocations, a determination of the scale of the slip plane traces is important to establish a correlation with the scale of the dislocation substructure. Such an observation may provide an answer to the question "Does the slip plane trace pattern observed on the surface reflect the scale on which slip occurs, and the nature of the dislocation substructure which develops during deformation?"

From the previous review it is clear that there are few quantitative observations of slip plane traces at large strain. The information that is available indicates mainly the homogeneity or inhomogeneity of flow. Observation of slip plane traces by incremental straining at various stages of large strain deformation is of importance as it enables one to:

(1)   determine whether the same slip systems are active throughout the deformation; and,

(2)   compare the variation of the scale of slip plane traces with the scale and evolution of the dislocation substructure.

2.3 Nature of Dislocation Substructure
Characteristic of The Deformed Condition

In this section, the nature of the dislocation substructure characteristic of deformed metals will be considered. In discussing the available data emphasis will be laid on:

(1) the geometric arrangement of dislocation tangles and cell walls with respect to the orientation of the active slip planes;

(2) the effects of the degree of deformation, mode of deformation and initial crystal orientation on the scale of the dislocation substructure and the misorientation which characterizes the cell walls; and,

(3) the structural features characteristic of the inhomogeneity of deformation at large strains.

In addition, the stability of cell walls and the correlation of the mechanical behaviour of the material and the dislocation substructure will be discussed.

2.3.1 Dislocation Substructure at Low Strains

The configuration of dislocations in the as-deformed condition, its correlation with slip plane traces and variation of its nature and scale with strain and orientation of the crystal have been discussed in great detail for crystals deformed in the low and moderate strain regimes in the review articles of Nabarro et al. (1964), Basinski and Basinski (1966), Mitchell (1964), and Hirsch (1975). Detailed investigations have been carried out for single crystals of copper by Steeds (1966), polycrystals of iron by Keh and Weissman (1963), polycrystals of aluminum and its alloys by Swann (1963). As the emphasis in this thesis concerns

the nature of dislocation substructure at large strains, the data con-
cerned with low strain regime will be treated only very briefly.

A typical stress-strain curve of an fcc single crystal exhibiting
three stages of hardening in tension is given in Figure 2.2 of Section
2.2. The evolution of the dislocation substructure during such a deform-
ation path has been surmised by T.E.M. observations of thin foils of
samples predeformed to a given strain. While considering the information
available from T.E.M. observations it must be borne in mind that it is
restricted to a two-dimensional view of the overall configuration and
that possible rearrangement and loss of dislocations may occur during
the preparation of the thin foil. The latter aspect has been treated
in detail by Hirsch et al. (1965).

Based on the observations in T.E.M., the evolution of the disloca-
tion substructure during the deformation of an fcc single crystal can
be summarized as follows. In the early stages of deformation, only
dipoles and bundles of primary edge dislocations lying in the primary
slip plane along the primary edge direction or along the traces of con-
jugate or critical slip planes are observed. No contrast is observed
across the bundles indicating that they are made up of approximately
equal number of positive and negative dislocations. The slip in this
stage is concentrated on the primary slip plane; most of the crystal is
free of dislocation debris and the rate of hardening is low, of the
order of 10^{-4} μ. There is no equivalence between the scale of the slip
plane traces and accumulated dislocations.

In Stage II, bundles of primary dislocations appear connected by
groups of secondary dislocations. Such arrangements start accumulating
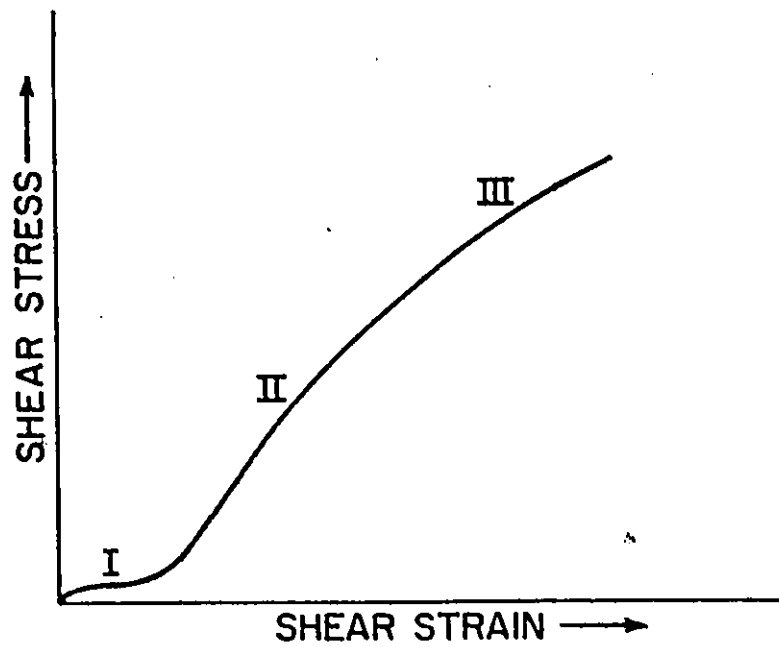
Fig. 2.2 Schematic illustration of the shear stress-strain
curve for an fcc single crystal exhibiting three
stages of hardening.

in planes parallel to and perpendicular to primary slip planes. In
crystals deformed well into Stage II, well-connected dislocation net-
works appear, made up of primary and secondary dislocations. The rate
of hardening in Stage II is high, about $\mu/300$. The densities
of primary and secondary dislocations are approximately equal, though
most of the slip plane traces belong to the primary systems, as described
in Section 2.2. The length of the slip plane traces is found to be pro-
portional to the spacing between dislocation groups. When these disloc-
ation networks extend into the three dimensions of the crystal, the
arrangement of dislocations is referred to as cellular in nature. Cells
are regions relatively free of dislocations and enclosed by cell walls
made up of dense dislocation networks. A number of models have been pro-
posed to explain the formation of cells in terms of the available driving
force (Weertman, 1963; Kuhlmann - Wilsdorf, 1977 and Holt, 1970).

Cells are characterized by their scale, shape and misorientation
and thickness of the cell walls. In two dimensions, the scale is defined
by the length and width of the cells. The misorientation associated with
the cells is the local lattice reorientation across the cell walls caused
by the dislocations constituting the cell walls.

Cells are observed even at the end of Stage II. As deformation
progresses into Stage III and large strain regime, due to work hardening
effects the cell size gets refined and the lattice misorientation in-
creases. Depending on the extent of dynamic recovery, dislocations in
the cell walls could get rearranged into simpler configurations. An
irregular arrangement of dislocations is usually referred to as tangles
while cells in which dislocations are arranged in lower energy configur-

ations are termed subgrains.

Single crystals oriented for multiple slip do not exhibit any Stage I hardening regime. Cellular substructure appears in the early stages of deformation. Good correlation between cell wall directions and traces of slip planes is observed in single crystals of copper oriented for duplex slip and deformed at 4.2°K (Basinski and Dove, 1963). However, no correlation has been observed between slip plane traces and cell walls in crystals oriented for multiple slip, particularly in aluminum single crystals oriented along the <111> axis as was observed by Warrington (1960), Price and Washburn (1963) and more recently by Hasegawa and Kocks (1979) and Kawasaki (1979).

2.3.2 Dislocation Substructure at Large Strains

The general dislocation substructural features, observed in fcc materials of moderate to high SFE deformed at ordinary temperatures to large strains is the cellular arrangement of dislocations. At large strains the arrangement of dislocations in cell walls is simplified by the influence of dynamic recovery.

No correlation was found between the cell walls and active slip planes. Instead, the arrangement of the dislocation substructure appears to follow the pattern of externally imposed flow. This has been observed in drawn pearlitic steels by Embury et al. (1966), in wire drawn iron by Langford and Cohen (1969), in copper deformed under plane strain conditions by Slakhorst and Tien Bouwhuijs (1977).

Not much quantitative data is available relating the scale of the dislocation substructure with the scale of slip plane traces. In Section 2.2 of this chapter, the length of slip plane traces at large strains was

given to be of the order of 100 μm.   In contrast from recent T.E.M.

observations of dislocation substructure, it is known that cell sizes

are of the order of 1 - 2 μm.   In one of the early observations based

on microbeam x-ray measurements, the cell size in rolled Al, Cu, Fe,

etc. was found to approximate to the spacing between slip plane traces.

The aspects of dislocation substructure which have been examined

in detail at large strains are the influence of:

(1)   the level of strain,

(2)   the mode of deformation, and,

(3)   initial orientation of the crystal on the spread in the scale and

misorientation of the substructure.

Attention has also been paid to the details of structural features which

are characteristic of inhomogeneity in deformation.

2.3.3   Variables Affecting the Scale of Dislocation Substructure

2.3.3.1   Variation of Cell Size With Strain

The effects of strain on the scale of the substructure developed

in aluminum during various modes of deformation - tension, rolling and

wire drawing are shown in Fig. 2.3.   The cell size decreases rapidly in

the beginning of deformation and at a much lower rate at larger strains.

Thus, cell wall creation predominates in the initial stage of deforma-

tion, whereas annihilation and creation of dislocation walls must occur

simultaneously at larger strains (Sevillano et al., 1979).   Langford and

Cohen (1969) demonstrate this aspect by plotting the effect of deforma-

tion on the remaining fraction of cells which had formed originally.

The variation of cell sizes shown in Fig. 2.3 apparently seems to

have reached a saturation value when produced by rolling and not in wire
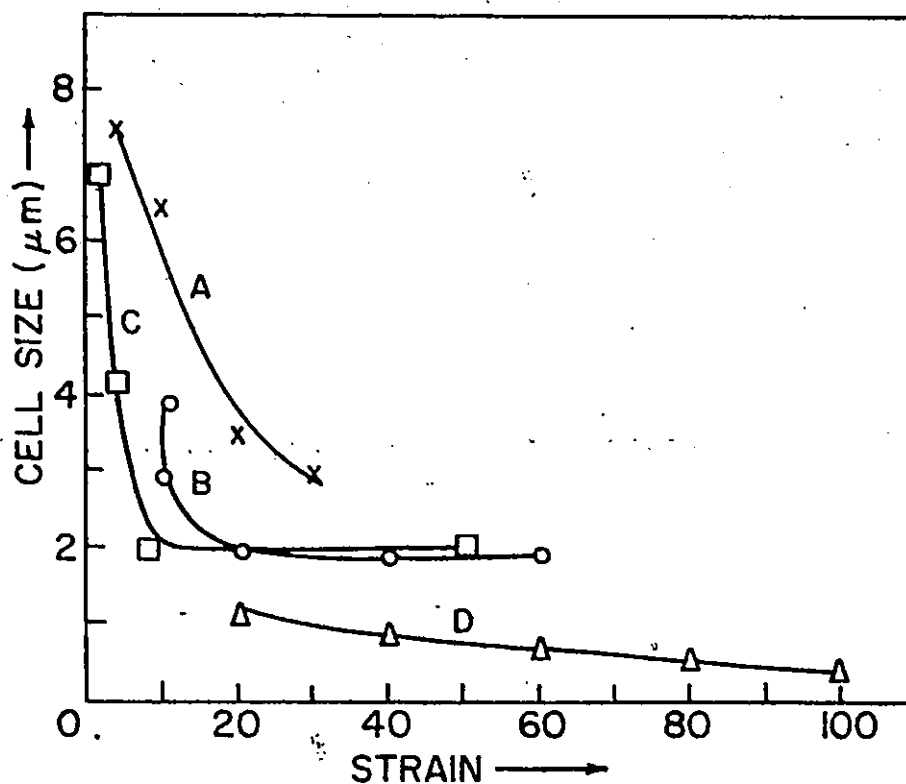
Fig. 2.3   Variation of cell size in aluminum during deformation.

	Deformation Mode	Purity	Reference	Method of Measurement
A	Tension	super pure polycrystals	Swann (1963)	T.E.M.
B	Rolling	99.994% polycrystals	Swann (1963)	T.E.M.
C	Rolling	super pure polycrystals	Hirsch & Kellar (1952)	Microbeam x-ray
D	Wire Drawing	99.998% polycrystals	Hansen (1969)	T.E.M.

Strain is % Elongation in A

% Thickness reduction in B and C

% Area reduction in D
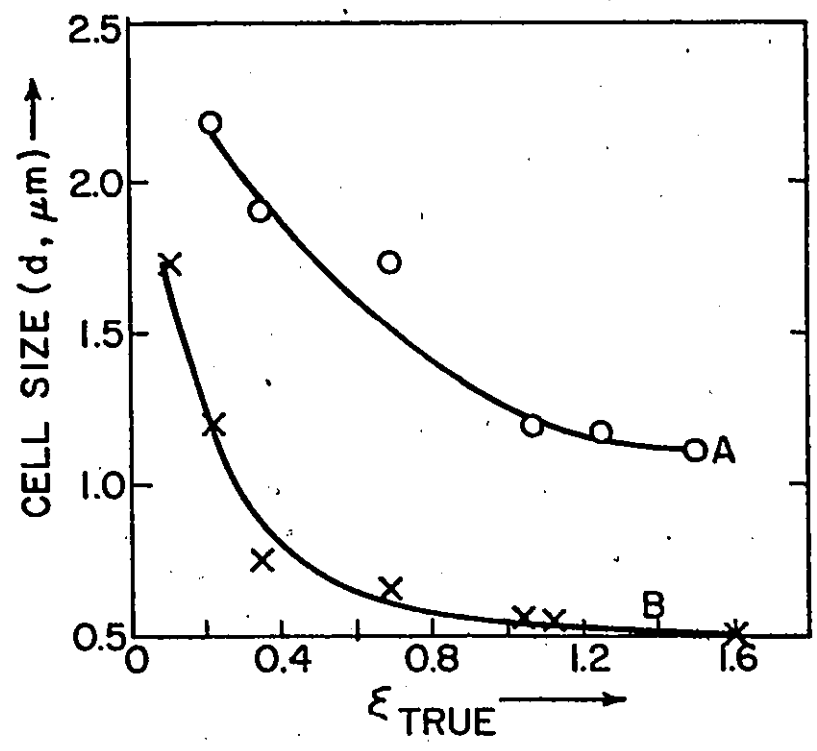
Fig. 2.4   Variation of cell size with true strain in rolling,
measured in the longitudinal section along:

A: rolling direction, and

B: rolling plane normal.

Ref.   Schuh and von Heimendahl (1974)

drawing. This apparent difference could be due to the poorer resolution of the microbeam x-ray work used in the work of Hirsch and Kellar (1952) and because measurements of the cell size were conducted only in the rolling plane as in Swann's data. The importance of determining the cell size in different sections of the deformed material is evident from the data of Schuh and Von Heimendahl (1974) for rolled Al, which is reproduced in Fig. 2.4. The cell sizes measured in the rolling plane and the free plane, perpendicular to the rolling direction appear to vary by almost a factor of two and continue to decrease with increasing strains of up to a true strain of 1.6 whereas the mean cell size appeared to saturate around a true strain of 2.0.

2.3.3.2 Variation of Misorientation With Strain

The average lattice misorientation across cell walls increases with strain. Schuh and Von Heimendahl (1974) report a linear variation up to about 90% thickness reduction in aluminum rolled at room temperature. The average misorientation is about 1.5° ± 1° at 25% thickness reduction strain and increases to ∿ 2.2° ± 1.5° at 90% strain. Along with the mean misorientation, the spread of misorientation during deformation, is of great importance. In severely deformed materials, large misorientations similar to high angle boundaries appear to develop. This has been observed in compressed polycrystalline aluminum by Faivre and Doherty (1979), in copper by Schnell and Grewe (1978) and in low carbon steel by Langford and Cohen (1975). Faivre and Doherty (1979) and Langford and Cohen (1975) also reported increases in the spread in misorientation and average misorientation with increasing deformation. In Fig. 2.5 the results of Langford and Cohen (1975) is reproduced. A
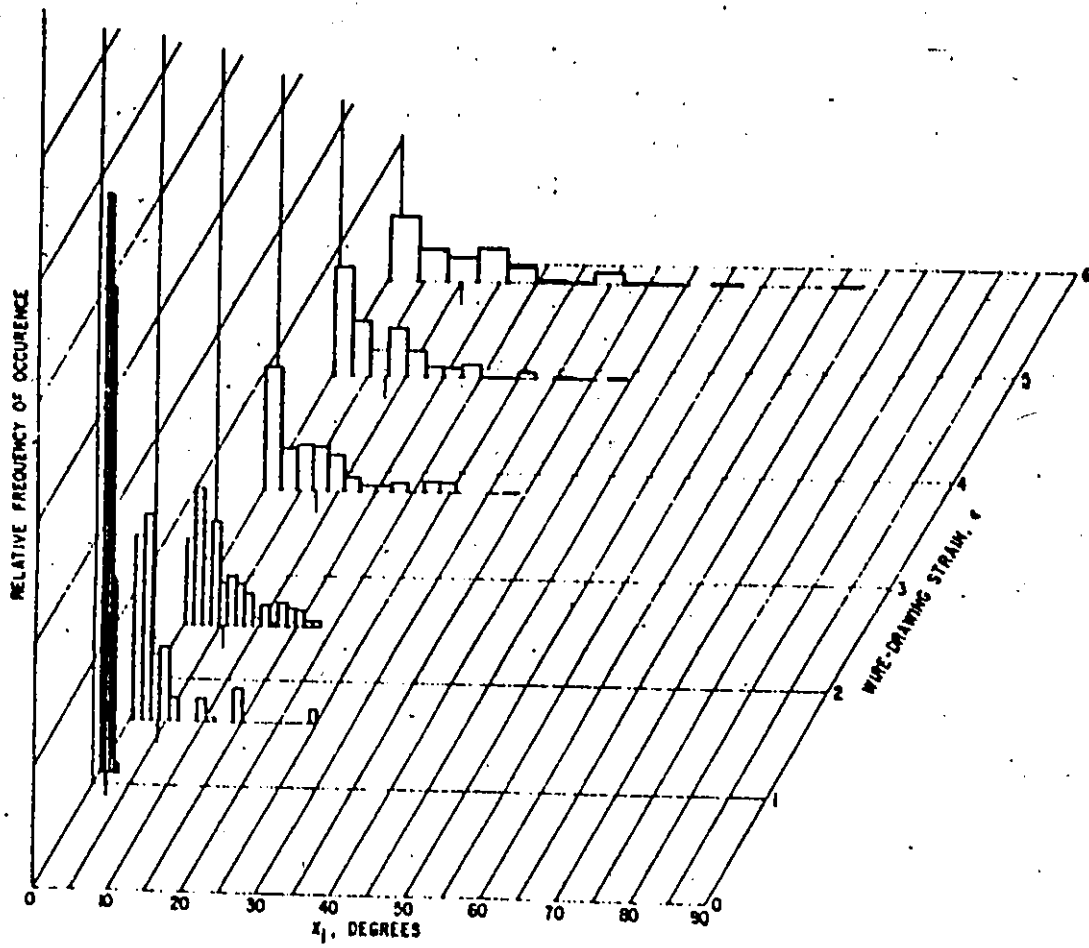
Fig. 2.5 Illustration of the distribution of misorientation as a
function of strain in wire drawing.
Ref. Langford and Cohen (1975)

large number of cells associated with low misorientation are still present, indicating that creation of cell walls could still be occurring. At high strains, it was reported that the original grain boundaries could be recognized. So it is difficult to conclude whether these high angle boundaries were created during deformation or are related to cells in the vicinity of original grain boundaries.

In Faivre and Doherty's work on aluminum, a comparison between optical microscope and T.E.M. observations shows that subgrains bounded by high angle boundaries could occur in the interior of the original grains. It was reported that regions containing cells of similar orientations were separated by a high angle boundary occurring between two individual cells. These high angle boundaries were observed in the as-deformed condition.

As will be discussed later in section 2.4, the presence of cell walls with the character of high angle boundaries in the deformed structure is important because of its influence on the subsequent recovery and recrystallization behaviour. This brings up the importance of the upper tail in the distribution of misorientation. According to Figure 2.5 the fraction of cells belonging to the tail is extremely small. Similar study in compressed aluminum by Faivre and Doherty also showed that less than 1% of the cells in the dislocation substructure have large misorientations of about 20°. Also, the high angle cell walls appear as isolated events in the substructure. Thus it is germane to ask how these highly misoriented cells develop and how they relate to nucleation event in any subsequent recrystallization process.

2.3.3.3 Effect of Deformation Mode

Reanalysis of the data in Fig. 2.3 shows that at the same equivalent strain, large differences in sizes are observed in cells produced by different deformation modes. This could be due either to the differences in strain rates characteristic of the deformation modes or the effect of strain path on the evolution of the substructure. (There being no appreciable differences in the purity, the effect of purity on cell size can be neglected.)

Re-examination of the data of McQueen and Hockett (1970) of dislocation substructure developed in commercial aluminum at various temperatures and strain rates shows that strain rates varying over three orders of magnitude have negligible effect on cell size below a temperature of 0.5 T_m. Unfortunately, though, the dislocation substructure was not observed immediately after deformation.

In contrast, the data of Korbel and Swiatkowski (1972) in aluminum deformed to 8% in tension shows the dependence of cell size on strain rate, varying from nearly 5.9 μm at a strain rate of 6.4×10^{-6}/sec. to about 3.3 μm at a strain rate of 6.88×10/sec.

Sevillano et al. (1979) also report that the influence of the mode of deformation on cell size is negligible, especially at large strains. Data for different materials is reported to fall within a narrow band.

It is difficult to rationalize the data at large strains though, because of the influence of texture development on the nature of operative slip systems, of the effect of dynamic recovery the extent of which is influenced by the purity of the material, its stacking fault energy and temperature of deformation.

2.3.3.4 Influence of Orientation

It has long been observed that crystal orientation influences
its work hardening behaviour (Lücke and Lange, 1952). Of particular
interest are the investigations of Kocks (1960) and Hosford et al. (1960)
who report that [100] oriented crystals of high purity aluminum deformed
at room temperature exhibits a rapid decrease in work hardening rate.
This is in contrast to [111] oriented crystals which continued to work
harden. The difference in behaviour was explained based on differences
in the nature of active slip systems as discussed in Section 2.2 (Kocks,
1960; Hosford et al., 1960; Saeki and Miura, 1977). No detailed inves-
tigation of the nature of the dislocation substructure has been under-
taken.

In copper single crystals oriented for multiple slip, the nature
of the dislocation substructure has been studied in T.E.M. by Göttler
(1973) and Ambrosi et al. (1974). It was reported that the average cell
size is similar in both [100] and [111] oriented crystals though the
dislocation density was higher in [100] crystals. No details are avail-
able about the spread in cell size and misorientation. The work harden-
ing behaviour of [100] and [111] oriented copper crystals at room tem-
perature is not as drastically different as the aluminum crystals,
reported earlier.

Dillamore et al. (1972) reported that both average cell size and
misorientation as well as spread in cell size and misorientation are
dependent on the initial orientation of individual grains in cold-rolled
polycrystalline iron. The average cell size appears to be least and
misorientation is highest in the orientation with highest M, the Taylor

factor. According to Eq. (2.8) the total shear strain, $\Sigma d\gamma_i$ produced in the crystal is inversely proportional to M. The effect of M on $\Sigma d\gamma_i$ on the nature of dislocation substructure reflects possible influence of the number of active slip systems, density of dislocations and the area swept by dislocations. The difference of the scale and nature of dislocation substructure can also be related to the difference in the amounts of energy stored in crystals of different orientations deformed to the same strain level (Smith & Dillamore, 1970; Haessner et al., 1979).

2.3.4 Structural Features Associated with Inhomogeneous Plastic Flow

The macroscopic treatment of deformation discussed in Section 2.1 is based on the assumption that deformation is uniform and homogeneous. Inhomogeneities may arise in deformation due to preferential selection of slip systems in different regions of the specimen, localization of flow, strain gradients introduced by the nature of deformation and external frictional conditions. These aspects have been discussed by Mecking (1978). The presence of structural features like kink bands, bands of secondary slip, deformation bands, microbands, shear bands, twins, etc., are indicative of the inhomogeneity of deformation. The origin, occurrence and substructural details of some of the above features are summarized in Table 2.6. An important aspect of these structural features is their role in the subsequent recrystallization behaviour.

T.E.M. observations of kink bands in single crystals of aluminum have shown that the orientation difference between the matrix and kink bands is accommodated by rectangular subgrains about $1-2$ μm wide and

Table 2.6

Structural features characteristic of inhomogeneity of deformation.

Structural Features	Where They Occur	Special Characteristics	Dimensions	Features seen in TEM and associated misorientations	References
kink bands	in single crystals oriented for single slip	are seen in planes perpendicular to primary slip plane; represent regions of severe lattice curvature; opposite sides of kink bands are made up of dislocations of opposite sign; lattice reorientation about [112] type axis.	can be macroscopic in dimensions; spacing can vary between 50 – 250 μm; nearly 100 μm wide	made of rectangular subgrains; degree of misorientation varies with strain; misorientation is associated within subgrains in transition region	Honeycombe (1951) Karduck et al. (1978)
bands of secondary slip	in single crystals oriented for single slip	in regions where primary slip is absent; associated with localized secondary slip	macrosopic		Honeycombe (1951) Rosi (1954)
deformation bands	in single crystals oriented for multiple and polyslip and in individual grains of polycrystals	represents regions where different sets of slip systems operate separated by transition bands	macroscopic	transition bands few μm wide accommodate orientation difference between deformation bands	Walter & Koch(1963) Hu(1963) Kreisler & Doherty (1979)
microbands	in rolled and drawn crystals	appears among equiaxed cells; on slip planes, elongated subcells	∿ 40 μm long; ∿ 30 μm wide; 0.2 – 0.3 μm thick	not much orientation difference; degree of misorientation depends on strain	Malin & Hatherly (1979) Ahlborn & Sauer(1968)
shear bands	in rolled and extended metals	in noncrystallographic planes; regions of localized slip		degree of misorientation depends on strain	Malin & Hatherly (1979)

44

elongated along the length of the kink band (Karduck et al., 1978).
An orientation difference of about 30° was accommodated within a dis-
tance of 30 - 45 μm,   each subgrain contributing 0.5 - 3° to the total
misorientation.

The difference in orientation between deformation bands (defined
in Table 2.6) is also accommodated by narrow transition bands. T.E.M.
observations in rolled iron-silicon alloys reveal that these transition
bands are made up of elongated subgrains with their long axis parallel
to the deformation band (Walter and Koch, 1963; Hu, 1963). Instead,
Kreisler and Doherty, 1978) conclude that the transition bands present
in aluminum deformed in torsion are made up of equiaxed cells when ob-
served in a section parallel to the torsion axis. The misorientation
across the transition band is cumulative, about 30° being accommodated
within 3 μm containing about five subgrains (Walter and Koch, 1963).

Microbands are another type of microstructural feature character-
istic of inhomogeneous deformation. They are elongated bands, about
0.2 - 0.3 μm thick, 20 - 30 μm wide and up to 40 μm long and occur within
equiaxed cells (Grewen et al., 1978). The degree of misorientation
across the microband boundary appears to depend on the amount of deform-
ation.

The origin of the shear bands is summarized in Table 2.6. They
are composed of elongated subgrains with significant misorientations
(Dillamore and Bush, 1978).

2.3.5 Arrangement of Dislocations in Boundaries

A subgrain wall can be considered in an idealized sense as a general
boundary made up of a network of dislocations. In general it will be

made of several kinds of dislocations and will have a mixed character consisting of both tilt and twist components. According to Read (1953), a general boundary is characterized by five degrees of freedom - the degree of misorientation, the orientation of the boundary given by a unit vector $\underline{n}$ perpendicular to the plane of the boundary and the rotation axis which has three degrees of freedom.

The arrangement of dislocations within a boundary of misorientation θ given by a unit vector $\underline{U}$ along the rotation axis can be determined according to Frank (1950), as:

$$\underline{d} = (\underline{v} \times \underline{U}) \, 2 \sin \frac{\theta}{2}$$

where $\underline{v}$ is an arbitrary straight line lying within the plane of the boundary and $\underline{d}$ is the sum of the Burgers vectors of the dislocations intersecting $\underline{v}$.

Frank's treatment has been extended to determine the various kinds of networks that can be built up by different combinations of glide dislocations. (Amelinckx and Dekeyser, 1958, Ball and Hirsch, 1955). Frank's formulism is based on energy criterion and is applicable to networks with no long range stress field.

However, it must be remembered that cell walls are built up during deformation at low homologous temperature due to accumulation of dislocations, which reflect the overall kinetics of the flow process and its geometrical constraints. The constituent dislocations may be geometrically necessary in order to accommodate lattice compatibility and are stored statistically in relation to the flux of dislocations required for the flow process. Therefore, the resultant assembly of dislocations may not meet the geometrical criterion of the Frank network.

2.3.6 Stability of Cell Walls

In this section, the stability of cell walls with respect to continued deformation along the original strain path and along a different path will be considered.

The experimental evidence discussed earlier concerning the evolution of the structure indicates the stability of cell walls with respect to continued deformation; during deformation both the scale and thickness of the cell walls gradually decrease together with associated increases in misorientation. Also the scale and character of cell walls is affected by the extent of dynamic recovery.

The stability of cell walls when the operative slip system is changed due to a change in the path of deformation can be inferred by observations of changes in macroscopic parameters, e.g., nature of slip plane traces, flow stress, rate of work hardening, and strain rate sensitivity. For crystals deformed in Stages II and III, a lowering of the work hardening rate and increases in flow stress were observed associated with formation of coarse bands of slip (Kocks and Brown, 1966; Jackson and Basinski, 1967). Drops in stress-strain curves were observed during tensile deformation of [100] oriented aluminum single crystals at room temperature, whenever there was a change in the operative slip systems (Saeki and Miura, 1977). Similar softening processes were also observed by periodic decreases in stored energy associated with changes in operative slip systems during the extension of single crystals of brass (Masima and Sachs, 1929).

Changes occurring in the predeveloped dislocation substructure, due to change in deformation path have been observed in copper single crystals by Sharp and Makin (1966). It was observed that during the

initial stages of deformation on the new system, fine slip occurs within

the predeveloped cell structure which penetrated through the existing

structure. As deformation on the new system is continued, localized

slip occurs, locally breaking down predeveloped cell structure, leading

to the creation of softened regions which spread across the crystal, akin

to occurrence of coarse slip bands. Washburn and Murty (1966) propose a

theoretical explanation for the low rate of work hardening and the associ-

ated clustering of slip in coarse slip bands following a change in the

operative slip system.

Much of the above discussion is based on crystals deformed to rela-

tively low strains; i.e., the early part of Stage III. It would be of

great interest to examine whether similar breakdown occurs where the sub-

structure is developed at true strains of 0.5 and above and in crystals

deforming under polyclip mode. Particular questions which then arise

are: Does activity on new slip systems destroy the predeveloped substruc-

ture or does the interaction between the new type of dislocations and pre-

existing cell walls result in regions of increasing misorientation? Such

increased misorientations were observed at intersecting slip bands in MgO

crystals (Argon and Orowan, 1961).

2.3.7 Relation Between Cell Size and Flow Stress

The contribution of the dislocation substructure to strengthening

of metals has been treated by Embury (1971), McElroy and Szkopiak (1972)

and Thompson (1977). An empirical relationship has been established

between the cell size, d and the flow stress σ_f as:

$$\sigma_f = \sigma_o + \alpha \, ubd^{-n} \qquad (2.17)$$

Data available in the literature yields a value of 1 or 1/2 for n. Where the spacing between the dislocations in the cell walls causes strengthening, the dislocations in the cell walls acting like forest dislocations, n takes the value of 1. When strengthening is due to an effect similar to the Hall-Petch effect, the value of $n = 1/2$.

In the above formalisms of the dependence of flow stress on cell size, the treatment is such that the main parameter of the dislocation substructure which contributes to strengthening is the cell size. It has been shown earlier in this section that the misorientation also changes as the cell size changes and this may have an important contribution to the flow stress. The above treatment completely neglects another important contribution to the flow stress - the effect of the strain path on the evolution of the dislocation substructure. Turner (1979) has shown that dislocation substructures produced under different conditions and having similar average cell size exhibit major differences in terms of their subsequent mechanical behaviour.

Thus it is clear that what is of importance is not the value of n in Eq. (2.17), but the understanding of how a given dislocation substructure actually evolves and what are the effects of the nature of evolution of the dislocation substructure on subsequent mechanical and thermal behaviour of the material.

2.4 Recovery and Recrystallization Behaviour of the Deformed Material

As discussed earlier it is important to consider the structural changes which accompany both thermal and dynamic recovery processes. It must be pointed out that dynamic recovery is difficult to investigate because it occurs concomittantly with strain hardening. Thus, in this section, some of the structural changes which occur in the deformed structure on subsequent thermal annealing will be reviewed. Following this, a brief comparison will be made of the structural changes which occur during thermal and dynamic recovery processes.

In addition, the phenomenon of recrystallization will be considered, but with emphasis on the relation between the nature of specific sites developed in the deformed structure and nucleation event in recrystallization. The analysis of the kinetics of recovery and recrystalliz- ation processes and the determination of the associated activation ener- gies will not be considered. They have been treated in detail elsewhere, particularly in "Recovery, Recrystallization and Grain Growth" by Byrne (1965), "Recovery, Recrystallization and Textures" - ASM Seminar (1966), "Recovery and Recrystallization",Ed: Himmel (1963) and "Recrystallization in Metallic Materials",   Ed: Haessner (1978), and "Recrystallization and Grain Growth in Metals" by Cotterill and Mould (1976).

2.4.1 Processes of Thermal and Dynamic Recovery

Thermal recovery in general is described as annealing the deformed material in the temperature regime in which no movement of high angle boundaries occurs and the overall orientation of the material remains unaltered.

The effect of thermal recovery on the mechanical response of the

deformed material is reflected in reductions of up to 20% in flow stress and an increase in the rate of work hardening observed immediately upon subsequent deformation. The recovery processes are divided into two regimes based on whether or not the flow stress (Cherian et al., 1949) and the work hardening rate (Hasegawa and Kocks, 1979) of the recovered material is restored to the level of the unrecovered material by subsequent strain.

Thermal recovery processes are also often characterized by release of a significant part of the energy stored during deformation. The exact fraction of the total stored energy released during recovery, depends upon the nature of the material, the level and mode of deformation. Energy release at various annealing temperatures occurred under sharp peaks for nickel, silver (Bever et al., 1973), copper; whereas in Al no sharp peak was observed prior to recrystallization (Gottstein, 1974).

The experimental evidence indicates that during recovery a variety of local rearrangements of the deformed structure can occur, including the removal of free dislocations from the interior of the cells, annihilation of dipoles, refining of cell walls with respect to their thickness and arrangement of dislocations they contain. No significant change occurs in the average cell size and misorientation in the early part of the recovery process; coarsening of the subgrains takes place only after continued recovery (Bailey and Hirsch, 1955; Boyd et al., 1976; Hasegawa and Kocks, 1979).

The changes affected by thermal recovery also depend on the crystal structure of the material, the initial orientation of the crystal, the

temperature, level and mode of deformation, because these factors determine the detailed dislocation substructure in the as-deformed material. It has been observed that stress-strain behaviour of zinc single crystals could be restored to the level of the undeformed material by thermal recovery, by controlling the deformation such that slip occurred only on the basal system. When the deformation was not homogeneous and some bending in the sample was introduced, similar restoration of the initial flow stress was no longer possible (Li et al., 1953). It was observed by von Drunen and Saimoto (1971) that crystals deformed such that slip occurred on many slip systems with no severe lattice curvature did not recrystallize easily. They deformed [100] oriented copper single crystals into Stages II and III and annealed the crystals at temperatures up to 1000°C without observing any recrystallization.

The recovery process discussed so far occurs in the unloaded condition and can be considered as "static" in nature because it occurs without deformation. The degree of recovery depends on the time and temperature for which the sample is annealed. In contrast to this, "dynamic" recovery occurs during deformation; the resulting softening events result in a progressive reduction in the work hardening rate in crystals deformed beyond Stage II. The initiation of dynamic recovery is best identified by departures from linearity in the plots of $\tau\theta$ (the rate of dislocation storage, θ being the rate of work hardening) vs. τ (the flow stress in shear) (Lücke and Mecking, 1973).

To incorporate the softening effects of dynamic recovery with the usual work hardening behaviour one has to consider the net density of

dislocations stored at a given instance, $d\rho_{net} = d\rho_{stored} - d\rho_{recovered}$, the arrangement of these dislocations and be able to separate out the influence of strain, strain rate, temperature, strain path, etc., on the evolution of the dislocation substructure. During a given strain increment work hardening occurs by the immobilization and accumulation of some of the mobile dislocations. During the same increment of strain dynamic recovery events are also triggered; every site in the deformed structure where a moving dislocation (which contributes a finite amount to the strain increment) meets the stored dislocations can be considered as a potential site for a recovery event.

The parameters which are usually used to describe the effect of the recovery processes are the flow stress and the rate of work hardening. In addition consideration of the strain rate sensitivity, and the magnitude of the Bauschinger effect, measured immediately after the recovery event and compared with the value of the unrecovered material, are also of importance.

The variations in flow stress and work hardening rate resulting from thermal and dynamic recovery are illustrated in Fig. 2.6. Thermal recovery results in a reduction in the flow stress and increase in the rate of work hardening, immediately upon restraining. In contrast, the effects of dynamic recovery are manifest in reduced rate of work hardening compared to the unrecovered material.

Effect of thermal recovery on the Bauschinger effect has been investigated in copper by Kishi (1969). Copper prestrained to 50% was annealed for 30 minutes at various temperatures, up to 0.6 T_m. It was observed that τ_F, the flow stress in the forward direction, decreased

Static Recovery   Dynamic Recovery
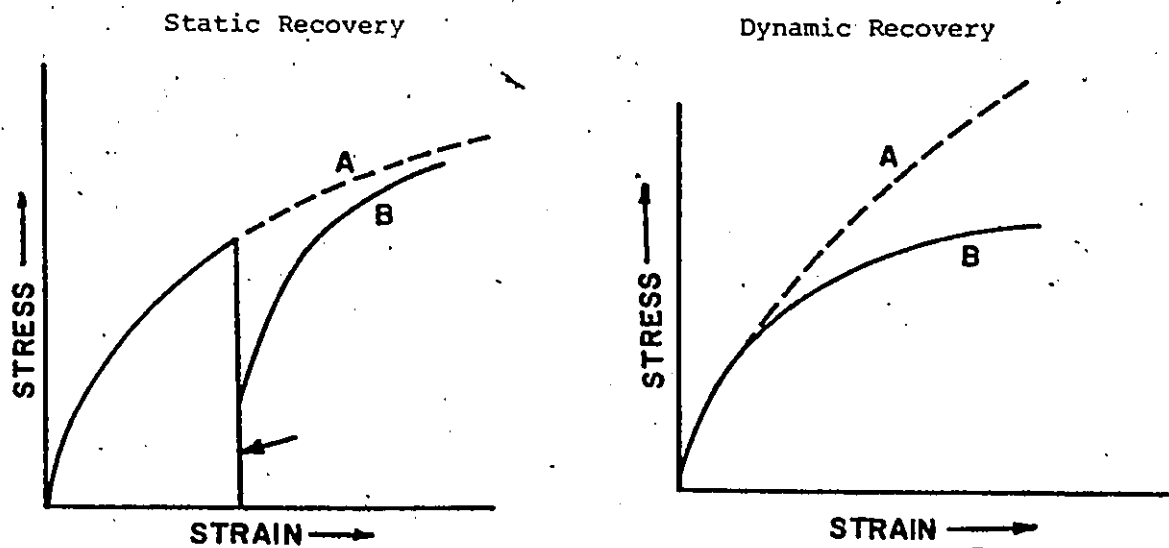
Fig. 2.6   Schematic illustration of the effects of static and
           dynamic recovery on mechanical properties.

A   without thermal recovery   A   without dynamic recovery

B   after subjecting to   B   due to combined effects
    thermal recovery   of work hardening and
                                      dynamic recovery

Flow stress immediately   Flow stress increases and
after recovery has decreased; d_σ/d_ϵ decreases continuously
d_σ/d_ϵ has increased compared   during dynamic recovery
to prerecovery values.   superposed with work
                                  hardening.

slowly after annealing in the recovery range, and at a rapid rate when annealed in the recrystallization range. In contrast, $|\tau_R|$, the absolute magnitude of the yield stress in reverse flow increased due to thermal recovery and decreased up to the level of τ_F after annealing in the recrystallization range. This indicates that if the stored dislocation is "polarized" then thermal recovery is effective in removing the dislocations which otherwise would have given rise to strain during reverse deformation. Hasegawa et al. (1976) report that the Bauschinger effect in polycrystalline aluminum decreases with increasing deformation temperature. In these tests the effects of both dynamic and thermal recovery are superimposed.

The influence of dynamic recovery on the Bauschinger parameter in aluminum is not clearly known. Buckley and Entwistle (1956) studied the effect of prestrain on the Bauschinger effect in single crystals of aluminum, but the investigations were confined to within Stage II. One of the problems of studying the effect of dynamic recovery on Bauschinger effect is the possible amount of prestrain, which is limited by the nature of the tests.

Similarity between the effect of dynamic and thermal recovery is indicated in their effect on the release of the energy stored. With increasing level of prestrain, the fraction of the total stored energy released during thermal recovery decreases from about 10.8% at a prestrain of 0.1 to about 3% at 0.33 (Gordon, 1955).

This can be explained on the basis that the extent of dynamic recovery is greater in the material deformed to large strains and therefore the amount of energy that can be released, without major changes

such as recrystallization, is reduced.

Dynamic and thermal recovery processes have similar influence on recrystallization behaviour. Thermal recovery in aluminum deformed to low strains retards the recrystallization behaviour, but the same kind of thermal recovery, conducted on aluminum deformed to large strains where extensive dynamic recovery has occurred, has little effect of subsequent recrystallization behaviour (Kaspar and Pluhar, 1975).

Hasegawa and Kocks (1979) show substructural evidence in aluminum single crystals compressed along [111] axis to indicate that similar structural changes occur during the thermal recovery of a sample deformed to low strains and identical samples deformed to larger strains but without thermal recovery.

The cellular arrangements of the dislocation substructure, present in the as-deformed condition at approximately 4% strain, was found to undergo conversion into subgrains in the early stages of thermal recovery at 453°K. Only after prolonged annealing up to 30 hours at 453°K did subgrain coarsening occur. Increasing the strain results in decreasing the annealing time required to start the coarsening process. Subgrains in a sample deformed to 20% strain start coarsening after only 30 minutes at 453°K.

In much of the experimental work relating to effects of thermal recovery, emphasis has been to understand the kinetics of the process and to observe the changes in the overall features of the deformed structure. Though the range of thermal recovery is divided into different regimes based on stored energy release measurements, depending on the type of defects - point defects, dislocations - that are removed, not much is

known yet about what kind of dislocations apart from dipoles are removed. It is also not known whether similar structural rearrangements occur during both thermal and dynamic recovery. Determination of the strain rate sensitivity parameter and examination of the Cottrell-Stokes Law may yield some additional evidence in regard to this problem. Increase in strain rate sensitivity can be associated with a breakdown of Cottrell-Stokes Law.

Increase in the strain rate sensitivity (defined as $\frac{\delta\sigma}{\delta\ln\dot\epsilon}$) has been observed in Stage III hardening of aluminum single crystals (Kocks et al., 1966) indicating that the nature of the obstacles changes when extensive dynamic recovery occurs. Kocks et al. (op cit) conclude that the strain rate sensitivity of the asymptotic flow stress (Kocks, 1968) is more sensitive to dynamic recovery. In contrast, Roberts (1976) reported no variation in the strain rate sensitivity in pure polycrystalline aluminum deformed at room temperature. This shows that extreme care must be exercised in interpreting the variation of strain rate sensitivity during different stages of deformation. The change in the strain rate sensitivity is, at the most 20%, and the corresponding change in flow stress may go undetected. In evaluating the strain rate sensitivity parameter based on the asymptotic flow stress change, the strain rate dependence of the rate of work hardening itself must be considered.

No clear data is available about the effect of thermal recovery on strain rate sensitivity. Basinski (1959) reported that there was no difference in the magnitude of strain rate sensitivity of aluminum, measured at 78°K before and after thermal recovery for 15 minutes at

100°C. No difference in the strain rate sensitivity measured at room temperature was observed by Chandra (1979) in polycrystalline aluminum, before and after thermal recovery at 180°C for 3 hours. These latter strain rate cycling experiments were conducted well past the transient stage observed during restraining after thermal recovery. To determine the effect of thermal recovery on strain rate sensitivity, the strain rate cycling experiments must be conducted within the transient. Otherwise, the data obtained may not be representative of the change brought about by thermal recovery. This is obvious from the small change in the flow stress caused by thermal recovery compared to the prerecovery flow stress.

2.4.2 The Deformed Structure as Nuclei for Recrystallization

Recrystallization is characterized by the removal of the deformed structure due to migration of high angle boundaries. Though the energy stored during deformation is the driving force for the process to occur, local variations in the deformed structure are the essential features which influence the actual nucleation event in recrystallization. The probability of detecting a subgrain which is a potential site for recrystallization is of the order of 1 in 10^8, equal to the ratio of the volume of a typical subgrain of diameter 1 μm to the volume of a typical recrystallized grain of 100 μm (Doherty, 1974). Experimental evidence from single phase, single crystals shows that recrystallization occurs at structural features such as kink bands, transition bands, microbands, shear bands, deformation twins etc. These features, described in Section 2.3, represent regions of higher misorientation in the deformed structure.

Large misorientation is a prerequisite for a subgrain to act as

nucleus for recrystallization, because the mobility of the subgrain

boundaries is a function of misorientation (Viswanathan and Bauer, 1973).

It has been observed that boundaries need to be misoriented by 15 - 20°

prior to the initiation of recrystallization (Inokuti and Doherty, 1978;

Humphreys, 1979).

Experimental evidence suggests that the nucleus for recrystalliza-

tion is preformed during deformation and is not created during the sub-

sequent annealing process. This has been concluded based on a consider-

ation of the orientation relationship between the recrystallized and

deformed material.   Faivre and Doherty (1979),

Bellier and Doherty (1977) observed that the orientation of the recry-

stallized material is contained within the orientation spread of the

deformed material. The question is how the high angle boundaries which

represent the potential nucleus are created during deformation.

Various models which have been proposed have been reviewed by

Cahn (1966, 1970), Doherty and Cahn (1972). Experimental support is

available for the following mechanisms:

(1). The strain induced boundary movement proposed and observed at pre-

existing grain boundaries in polycrystals by Beck and Sperry (1950)

in aluminum and Bailey and Hirsch (1960) in copper, aluminum,

silver and gold has also been observed in aluminum by Bellier and

Doherty (1977).

(2) Subgrain coalescence and rotation proposed by Hu (1963), Li (1962,

1966) and Sandström (1977) has been observed within the transition

bands in metals deformed to moderate strains by

Dillamore (1972) and Sandström (1978).

(3) Subgrain growth suggested by Beck (1949) and Cahn (1950) has also

been observed, in the transition bands of Fe-Si alloys rolled to

large strains (Walter and Koch, 1966).

Subgrain coalescence is observed in most of the metals deformed

to low and moderate strains, prior to the start of recrystallization.

This occurs as a means of building up the necessary lattice misorienta-

tion. As a consequence, the subgrain size tends to increase and it has

often been reported in the literature that a larger than average sub-

grain size is also a prerequisite characteristic of a potential nucleus.

It was concluded, based on classical nucleation theories that a subgrain

of average size bounded by high angle boundaries, would shrink because

of the higher energy associated with the boundaries. (Bellier, 1971;

Doherty and Cahn, 1972). Such a conclusion is difficult to accept as

the boundaries accommodating large misorientations are created during

deformation, due to storing of dislocations; and is not a process of

fluctuations typical of the classical nucleation process. At low and

moderate strains the subgrain coarsening and growth processes are a

means of accumulating the necessary misorientation.

At large strains where the local lattice deformation is severe

enough, recrystallization is known to occur without being preceded by

any coalescence process. At these strain levels, the preference for

nucleation at pre-existing grain boundaries in polycrystals is lost and

recrystallization can occur at sites of large misorientation in the in-

terior of the grain. This suggests that at large strains high angle

boundaries must have developed during deformation. Experimental obser-

vations of such high angle boundaries have been discussed in Section 2.3. The actual mechanism of the formation of these high angle boundaries is not yet clear. Dynamic recrystallization is one of the possibilities. It has been reported at strains beyond 1.0 during room temperature deformation in polycrystalline copper (Cairns et al., 1971), copper-aluminum alloys (Ratsuzek and Karp, 1976) and in bicrystals of aluminum (Serpoul and Driver, 1979). Observations of the deformed structure in T.E.M., indicated that the interior of the recrystallized grains contained very little dislocation content (Cairns et al., op cit). It is therefore difficult to unequivocally conclude whether the nature of recrystallization was dynamic or static. The dislocation substructure observed by Faivre and Doherty (1979) does not differ in the highly misoriented regions from the rest of the substructure.

If the high angle boundaries are created by any such process it would mean that the distribution of misorientations in the deformed structure resembles a schematic illustration of Fig. 2.6. Instead, the experimental evidence of Langford and Cohen (1969) and Faivre and Doherty (1979), discussed in Section 2.3, approximate to a distribution of Fig. 2.7. The question is how a distribution similar to A gets evolved into a B-type distribution. Some possibilities are:

(1) local differences in operative slip systems, leading to large local misorientations, a phenomenon similar to formation of deformation bands, but occurring on a micro scale;

(2) accumulation of dislocations to accommodate flow around non-deformable regions (Humphrey, 1979); and,

(3) interaction between groups of dislocations as at intersecting slip bands (Argon and Orowan, 1961).
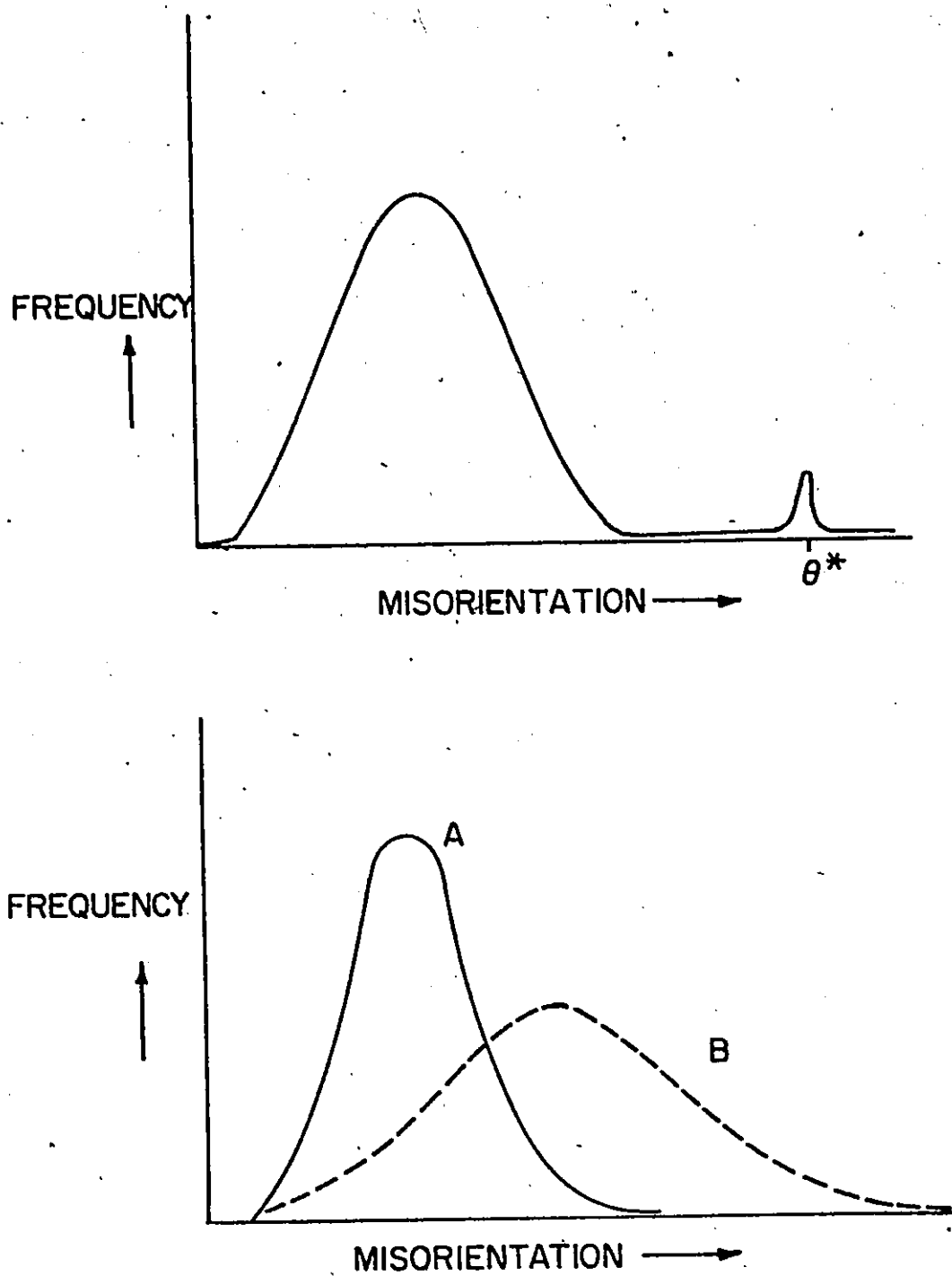
Fig. 2.7   Frequency distribution of misorientation in
the substructure

CHAPTER 3

EXPERIMENTAL TECHNIQUES

In this section, a review is given of the method used to grow the single crystals, and their structural and compositional character- ization. In addition, the procedure used to deform the crystals in the channel die and the various experimental techniques used to study the nature of the dislocation substructure developed as a result of deforma- tion, are described.

3.1 Material and Purity

Single crystals prepared from two different batches of aluminum were used in this investigation. The nominal purity of the material for both the batches was 99.99%.

The crystal of orientation $(1\bar{1}1)$ $[\bar{1}12]$ was obtained in the form of a grown and oriented crystal, courtesy of Dr. U.F. Kocks of Argonne National Laboratory. The aluminum used to grow the original crystal was of 99.99^+ purity.

The crystal of orientation $(1\bar{1}1)$ $[\bar{1}23]$ was grown during the course of this study. Aluminum for this crystal was supplied by Alcan, Kingston, Ontario. In Table 2.1, the compositional analysis of the crystal in the as-grown condition is given.

In the following section, the technique used to grow the $(1\bar{1}1)$ $[\bar{1}23]$ crystal is described.

63

Table 3.1

Composition of (1$\bar{1}$1)[$\bar{1}$23] crystal in the as-grown condition.

Chief Impurities	Fe	Si	Cu	Mg
Level of Impurity in wt.%	0.001	0.004	0.002	< 0.001

3.2 Growth of the Single Crystal

Single crystals were grown from the melt, based on the Bridgmann (1925) Technique. Split cylindrical graphite molds were used to house the crystal. To minimise contamination, high purity Argon gas atmosphere was used. Attempts were also made to use the soft mold technique of Noggle (1953) using aluminum oxide powder as molding material. However, the Bridgmann technique produced crystals with superior surface finish and was therefore preferred.

3.2.1 Description of Crystal Growth Technique

Figure 3.1 shows the apparatus used for growing the single crystals. An electrical resistance furnace was counterbalanced and moved along a vertical axis with the aid of a motor. A speed reduction gear box controlled the speed of movement of the furnace. The furnace was coaxial with an Inconel tube, and open at both ends. An inlet for the Argon gas and a Chromel-Alumel thermocouple were fixed at the bottom end of the Inconel tube. The outlet for Argon gas was provided at the top. The bottom fitting also served as the base on which the graphite mold rested. Cold water was passed through a copper coil wound around the bottom end of the Inconel tube. The lower portion of the graphite mold was thus cooled.

Figure 3.2 illustrates the split cylindrical graphite molds, with rectangular inner cross section, which was used to grow the single crystal. One end of the inside of the mold was tapered to a point so that solidification of the molten aluminum could start at this point. The inner surface of the mold was polished using 600 grade emery and

Fig. 3.1   Apparatus for growing single crystals.
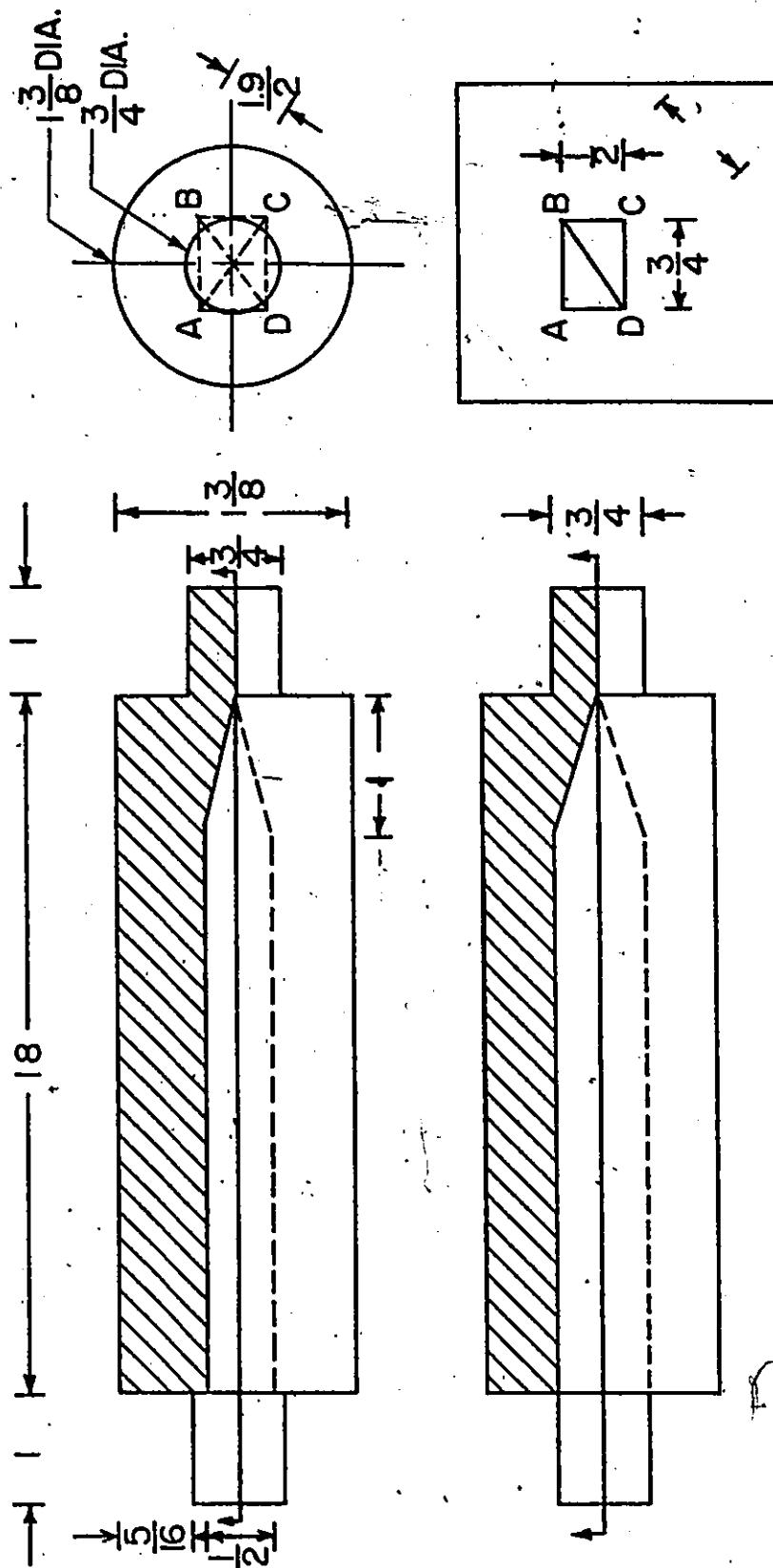
Fig. 3.2 Illustration of the split graphite molds used to grow the single crystals.

soft kleenex tissue so that the surface of the mold was smooth and free

of crevices. The mold stood upright in the tube, with the tapered end

near the lower end of the Inconel tube. The two split ends of the mold

were closed by retaining rings at both ends. Asbestos paper was wrapped

around the entire mold to prevent the leakage of the molten metal. The

top of the Chromel-Alumel thermocouple inserted through the bottom ring

of the mold was adjusted to be close to the tapered end of the mold. The

temperature recorded was close to that of the metal in that region.

3.2.2 Procedure for Growing Single Crystals

After inserting an aluminum block of rectangular cross section

inside the mold, the two halves of the mold were secured firmly together

and the mold was introduced into the Inconel tube. Both ends of the

Inconel tube were closed and Argon gas was pumped in through the lower

inlet. At this stage, the furnace was near the bottom end of the Inco-

nel tube. After flushing the inside of the tube for approximately two

hours with Argon gas, the power to the furnace was switched on. When

the thermocouple which was inside the mold measured ∿750°C, the motor

connected to the furnace was switched on. The furnace was driven up at

the rate of ∿0.8"/hr. A temperature gradient of ∿13°C/cm was maintained

by water cooling the bottom end of the Inconel tube. The furnace took

about 20 hours to travel the entire length of the graphite mold. During

this time, the inflow of Argon gas was maintained at a steady rate. When

the furnace had travelled well beyond the length of the mold, the flow

of Argon gas was stopped, the power to the furnace was switched off, and

the mold was removed. The preparation of samples for deformation from

the as-grown crystal, is described in Section 3.4.

3.3 Characterization of the Single Crystals

The characterization of the crystals involved macroetching the crystal to check for the occurrence of possible stray surface grains and grown-in substructures, as well as determination of the orientation of the crystal by back reflection Laue x-ray technique.

3.3.1 Procedure for Macroetching

The crystal was macroetched after it was taken out of the mold. The etchant used for pure aluminum samples was as recommended in the A.S.M. Metals Handbook, Vol. 8, Ed. 8. The composition is given in Table 3.2. The etchant was freshly prepared prior to use, and was cooled in running water. The crystal was dipped in the etchant for a few seconds, and washed in distilled water. Care was taken to ensure that the specimen did not get heated during etching.

3.3.2 Back Reflection Laue X-Ray Technique

The initial orientations of the single crystal specimens were determined using the back reflection Laue x-ray technique. The orientation of the three orthogonal faces was determined using white x-rays from a tungsten tube operating at 50 kV and 12 MA. The exposure time was ∼1/2 hour. Using the Laue photograph and a proper Wulff net, the orientation of each face could be fixed to an accuracy of ∼1°. In Figure 3.3, typical Laue photographs for "stable" and "unstable" crystals are shown. The orientation of the compression face of the "unstable" crystal is about 1° away from exact [111] orientation.
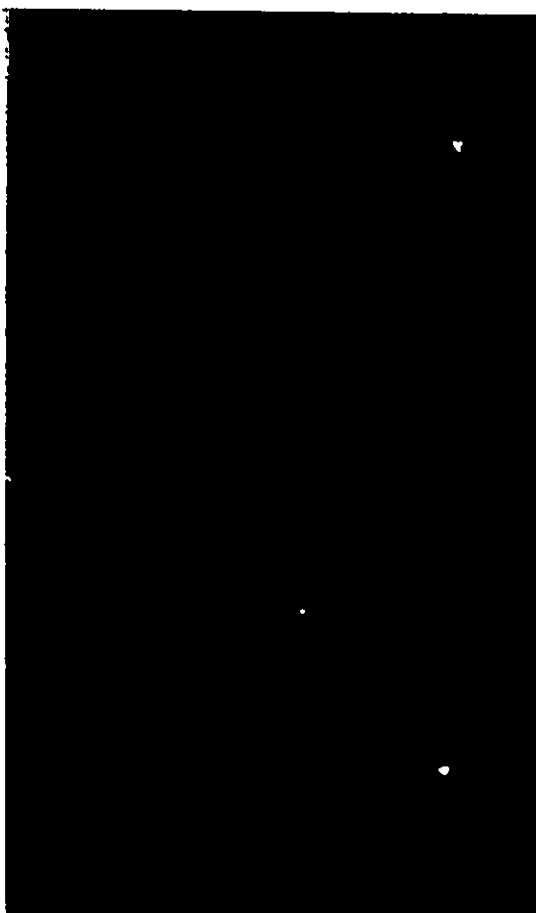
Fig. 3.3   Back reflection Laue x-ray photographs
of the compression face of:

(a) "stable" and,

(b) "unstable" crystals

taken prior to deformation.

3.3.3 Nomenclature of the Crystals Studied

In the present investigation, the nature of the substructure developed at large strains in differently orientated crystals is described. The orientations of the crystals studied are:

1) (100) [$\bar{1}12$] – "stable"

2) ($1\bar{1}1$) [$\bar{1}23$] – "unstable".

For each crystal, the Miller indices within the first brackets denote the plane on which compression was carried out. The Miller indices within the second brackets denote the direction of free flow, i.e., the channel axis, as shown in Figure 3.5. The orientations given refer to the initial orientations. The (110) [$\bar{1}12$] crystal will be referred to as "stable" crystal throughout because the orientation of this crystal did not change during deformation.

Similarly, the ($1\bar{1}1$) [$\bar{1}23$] crystal will be referred to as the "unstable" crystal because its orientation did change during the course of deformation.

The present investigation was aimed at comparing the dislocation substructure which develops at similar plastic strains in the "stable" and "unstable" crystals, and at correlating the nature of the substructure with the macroscopic observations of the slip systems active during deformation and the measured shape change.

3.4 Details of Deformation Procedure

Plastic deformation was imparted by compressing the crystal to large plastic strains in a channel die as shown in Figure 3.4. To determine the mechanical response of the crystal after a given amount of

deformation in the channel die, subsequent uniaxial compression tests were performed.

3.4.1 Preparation of the Samples

Four rectangular samples of approximate initial dimensions. 1 x 1.12 x 1 cm (length x width x thickness) were spark machined from each crystal. Figure 3.4 illustrates the virgin crystals and the axis relative to the growth direction, along which the samples were cut. Appropriate Miller indices are shown, defining the initial orientation of each of the faces. Their positioning in the die has been shown in Figure 3.4.

After spark machining, the samples were prepared by polishing the surfaces on 600 grade emery paper. They were then annealed for 24 hours at 475°C in a box furnace and furnace cooled. Prior to deformation, the samples were electropolished in a solution of methylalcohol and 20% nitric acid. Electropolishing results in a surface on which friction is reduced and from which the traces of slip planes formed during deformation can be recorded. The linear dimensions of the crystal were measured to an accuracy of 0.005 mm using a tool maker's microscope.

3.4.2 Deformation in the Channel Die

3.4.2.1 Description of the Channel Die

Figure 3.5 is a schematic illustration of the channel die and the plunger. The design is similar to the one used by Chin et al (1966). Both the die and the plunger were made of tool steel. The plunger was attached to the crosshead of a Tinius Olsen machine. The tolerance

━━━━▶ DIRECTION OF GROWTH

UNSTABLE CRYSTAL

$(1\bar{1}1)$

$(54\bar{1})$

$(\bar{1}23)$

1.27 cm

X

Z

Y

"STABLE" CRYSTAL

(110)

$(\bar{1}12)$

$(\bar{1}\bar{1}1)$

⊢1.27⊣
cm

X

Y

Z
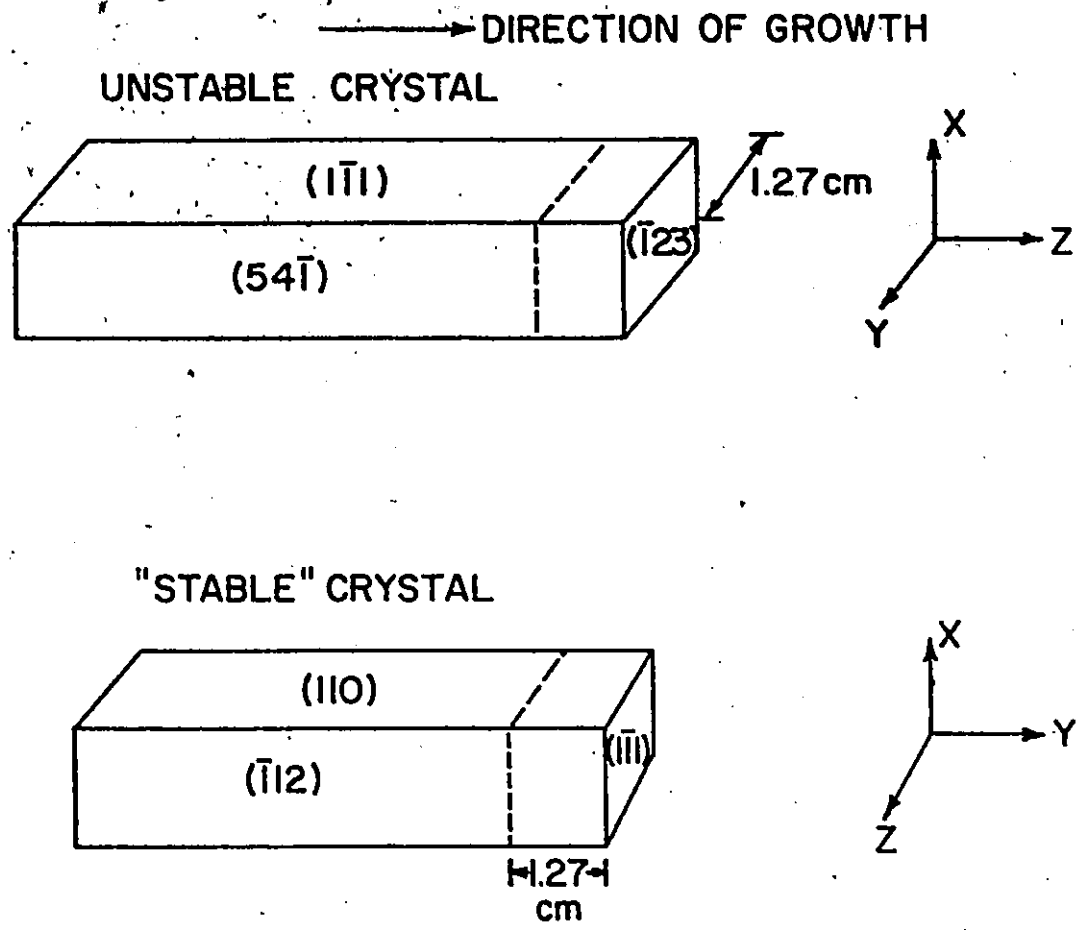
Fig. 3.4   Illustration of the as-grown crystals
with direction of growth along the
long axis. x, y and z are defined
in Fig. 3.5.
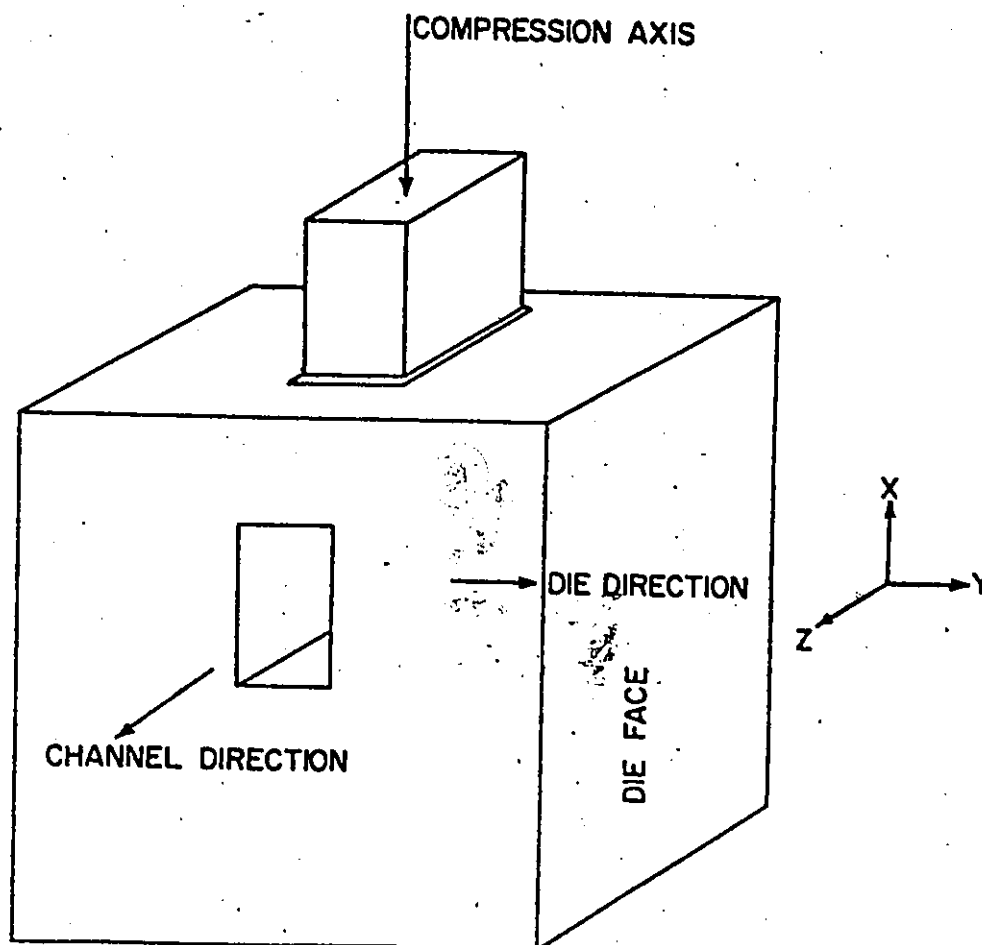
Fig. 3.5   Schematic illustration of the channel die
            and the plunger.

   x: compression axis

   y: direction normal to die walls referred
        to as die direction

   z: channel direction

between the plunger and the die was ±0.0025 mm, to provide a good sliding fit.

3.4.2.2 Lubrication in the Channel Die

To minimise frictional forces developed between the faces of the crystal and the surfaces of the channel and plunger, teflon tapes of thickness ~0.06 mm and polythene sheets of thickness ~0.15 mm were used. This combination of lubricants was chosen based on a preliminary study of the deformation of polycrystalline pure Aluminum samples of identical initial dimensions.

The teflon lubricating sheets become thin after deformation. Hence, the tests were stopped at about every 3-5% thickness reduction. The lubricants were renewed before continuing the deformation.

3.4.2.3 Details of Compression in the Channel Die

The deformation was carried out at room temperature with a crosshead speed of ~0.05"/min.

Samples prepared as described in Section 3.4.1 were compressed to true strains of approximately 0.1, 0.2, 0.5 and 1.0. Deformation was carried out in steps of ~3-5% thickness reduction. After each deformation step, the shape of the crystal was characterized by measuring the linear dimensions of each edge, along with the angle subtended between the edges on each of the faces of the crystal.

Using a tool maker's microscope, the linear dimensions were measured to an accuracy of ±0.005 mm and the angle was measured to within ±6 minutes of arc. This enabled evaluation of the normal strains to an accuracy of 0.5% and of shear strains to an accuracy of 0.08%.

Laue back reflection x-ray technique, described in Section 3.3.2, was used to determine the orientation of the faces of the "stable" crystal after deformation. The orientation of the faces of the "unstable" crystal was determined using the selected area diffraction technique in the transmission electron microscope. This is because of the development of asterism due to deformation, as shown in Figure 4.2.

After the measurements were made, the sample was polished on 600 grade emery paper and electropolished before further deformation. After a given strain increment the slip plane traces were recorded from the faces of the deformed crystal. The details of the technique used to record and analyse the slip plane traces are given in Section 3.6.1.

After deforming the crystal to predetermined total strain levels in the channel die, samples were spark cut from these for uniaxial compression tests and for transmission electron microscope studies. For the transmission electron microscope work, slices were spark cut parallel to the three orthogonal faces - the compression, die and free faces. and thin foils were prepared from these.

3.4.3 Uniaxial Compression Deformation

Uniaxial compression tests were performed in an Instron machine at room temperature, using a crosshead speed of 0.002"/min. The axis of compression was maintained to be the same as in the channel die. The yield stress of each sample was determined at 0.2% offset strain. This was taken to be the flow stress of the sample corresponding to the amount of deformation carried out previously in the channel die.

3.5 Techniques Used to Study the Dislocation Substructure

The main experimental techniques utilised in the present inves-
tigation were optical microscopy to study the slip plane traces formed
on the surface of the crystal, and transmission electron microscopy to
study the nature of the dislocation substructure. The transmission
electron microscope was preferred as the experimental tool to study
the dislocation substructure as it enables direct examination of areas
in the submicron range, and because of the availability of diffraction
technique to study the orientation relationships.

3.5.1 Optical Microscopy – Study of Traces of
Slip Planes Formed on the Surface

The deformation was carried out in small strain intervals,
according to the procedure described in Section 3.4.4.   The traces
recorded at the end of a given strain increment correspond to the slip
systems actually active during that strain increment. This technique
enables one to check whether the same set of slip systems are active
throughout the entire deformation. The use of teflon tapes as lubri-
cating agents enables recording of the traces of slip planes from all
the surfaces of the crystal.

When the traces form on all three faces, the slip planes
which cause the traces can be determined unambiguously (Barrett and
Massalski, 1966). The scale of the slip plane traces was measured
with respect to their length and spacing. The spacing was measured
to an accuracy of ∿0.5 mm at 600 X. This corresponds to a true spacing
of ∿1 μm, which is nearly the available resolution of the technique.

3.5.2 Electron Optical Work - Transmission Electron Microscopy

T.E.M. observations were made using a Phillips E.M. 300 transmission electron microscope. The nature of the dislocation substructure developed during deformation, the scale of the substructure, the orientation difference across the cell walls were studied in samples deformed to true strains of, approximately 0.1, 0.2, 0.5 and 1.0. Where the dislocations making up the cell walls could be resolved, their Burger vectors were identified.

3.5.2.1 Preparation of Samples

Slices ∿0.25 - 0.5 mm in thickness were spark cut parallel to the three orthogonal faces using molybdenum wire of 0.003 mm diameter. Approximately 1 mm thick slices parallel to the external surface were removed from each face. All the transmission studies were done on slices cut from beyond this region. This helped in the elimination of possible extraneous structure developed at the surface.

To eliminate the damage introduced due to spark cutting, the slices were initially polished on 600 grade emery.

Discs 3 mm in diameter were prepared from these slices, and were electropolished in a Tenupol (an automated jet electropolishing unit). Ethanol - 20.1% perchloric acid solution was used as the electrolyte.

The electrolyte in the Tenupol was cooled to between -20°C and -25°C by circulating liquid nitrogen. A voltage of 15-20 volts was applied. A current of 20-40 MA passed across the disc sample. Where a small perforation occurred in the disc, the sample was thin enough for study in the transmission electron microscope.

After removal from the jet polishing unit, the discs were washed

dislocations in the boundary was low. As the density of dislocations in
the boundary increases, the separation between dislocations decreases.
In a simple tile boundary made up of dislocations of one particular
Burger's vector b,d, the spacing between individual dislocations·is re-
lated to the θ misorientation across the wall (Read,1953) according to
the relation

$$d = \frac{b}{\theta}.$$

In Table 3.3   the separation between dislocations in walls of
different misorientations is given.

The practical resolution in the Phillips E.M.300 being ∿ 50 A,
it is difficult to resolve dislocations in boundaries across which the
misorientation is much more than 1°. Resolution of the images of in-
dividual dislocations is essential to determine their Burgers vectors.
The Burgers vectors were assigned when the images of the same disloc-
ations vanished for at least two different g reflections, according
to the g·b = 0 criterion (Hirsch et al., 1965).

The planes in which the cell walls lie were determined by iden-
tifying the direction of intersection of the cell walls in the various
faces. The direction of the cell walls in a given foil was identified
by comparing the micrograph with its corresponding selected area dif-
fraction pattern. The rotation which occurs between the image and the
selected area diffraction pattern (Hirsch et al., 1965) was calibrated.

3.5.2.3   Consistency in Transferring Data From the Crystal to T.E.M.

To correlate the data of the dislocation substructure as in-
vestigated by the T.E.M. with the slip plane traces studied by optical

in absolute alcohol and cleaned by dipping for ten minutes in a special

solution of chromic oxide and phosphoric acid.   The samples

were washed in distilled water and finally in ethyl alcohol. This en-

abled the storage of the samples in air for long periods without any

problem of oxidation.

3.5.2.2 Details of Investigation Carried Out in T.E.M.

Low magnification micrographs taken in Phillips E.M.300 trans-

mission electron microscope were used to determine the scale of the dis-

location substructure. The scale of the substructure was measured in

terms of the width and length of the cells. The cell size was not uni-

form.

Selected area diffraction photographs were taken from different

regions of a given foil. Diffraction patterns were taken when the

goniometer stage was adjusted at 0° tilt. The orientations of the com-

pression, free and die faces of the crystal were arranged to be anti-

parallel to the beam direction of these diffraction patterns.

The general orientation of the foil under study was taken to be

as given by the spot pattern taken of a large number of cells from dif-

ferent foils for a given face. Misorientations across a given cell

boundary were measured from comparing the Kikuchi Line patterns from

adjacent cells. The accuracy of these methods is discussed in Section

3.6.

Burgers vectors of the individual dislocations constituting

the cell walls were identified by imaging the cell walls at large mag-

nifications, and under two beam conditions. The resolution of indivi-

dual dislocations were possible only at low strains when the density of

Table 3.2

Composition of the macroetchant used for pure aluminum.

Contents	Concentration	Amount in ml
HCl	37.1%	50
HNO_3	70.1%	15
HF	48.0%	3
$FeCL_3$	supersaturated solution in HCl	5

Table 3.3

The spacing, $d(\overset{o}{A})$, between individual dislocations in a simple tilt boundary as a function of θ, the angle of misorientation across the tilt boundary. $b_{Al} = 2.86$ $\overset{o}{A}$

θ(deg)	1	5	10
$d(\overset{o}{A})$	163	32	0.5

microscopy, it is essential to view both the data in the same sense of direction. When the sample was inserted into the electron microscope, care was taken to ensure that the foil normal coincided with the outward normal of the crystal face from which the foil was prepared. Also, the electron micrographs were printed with the emulsion side up. The 3 mm disc samples were prepared so that the edges of the crystal could be easily identified. This enabled the orienting of a given micrograph with respect to the external axes of deformation.

3.6 Accuracy of Measurements

3.6.1 Measurements of Orientation - Available Techniques and Possible Accuracy

X-ray methods are the most widely used in the determination of orientation. Johnson (1969) used Laue back reflection method - an accuracy of ±0.25° was reported. The regular Laue technique described in Section 3.3.2 suffers from two major disadvantages:

1) the size of the collimator beam, which decides the size of the x-ray spot and thus makes the study a very local event,

and 2) the effect of deformation on the sharpness of laue spots, even when the area studied is small.

As a result of deformation, asterism develops and often the original Laue spots are completely lost. Instead, arcs of Debye-Scherrer rings may develop. At levels of deformation where this occurs, the Laue back reflection x-ray method is quite inappropriate in determining the orientation of the crystal.

The orientation can also be determined using pole figures plotted

using a texture goniometer (Barrett, 1952). Unlike the Laue technique, this information is averaged over the entire surface of the crystal, but the effect of deformation results in spreading the intensity at each pole; particularly in crystals of unstable orientation. Precise location of the centre of these spreads is difficult because the spread is not symmetrical. The accuracy possible is, at best, a few degrees. In both these methods, considerable care is necessary in the alignment of the crystal with the x-ray source.

Basinski and Basinski (1969) also used an x-ray method for orientation determination. They used a single crystal x-ray diffractometer. Cu K_β radiation was chosen to avoid confusion between Cu K_{α_1} and Cu K_{α_2} radiations. The alignment of the crystal surface with respect to the x-ray source was checked optically by fitting glass mirrors on the surface of the crystal. Three different reflections were used, and the angles measured with these were used to determine the orientation of a given face. Basinski and Basinski report the following accuracy in their measurements: the angle measured by the diffractometer was reproducible to within ±0.02° for the virgin crystal with ±0.05° error due to surface irregularity. In the deformed crystal, an accuracy of ±0.05° was reported. When the surface of the deformed crystal was not smooth, the error of measurement was estimated to be between ±0.1 to ±0.15°. The significance of these measurements is that Basinski and Basinski find that 90% of the shape change is caused by primary slip alone, contrary to Johnson's results (1969).

Yet another technique of determining orientation is to use electrons diffraction method. The selected area diffraction technique

available in a transmission electron microscope is such a method (Hirsch et al., 1965). The diffraction pattern can be of two types: spot pattern or line pattern, or both, depending on the thickness of the sample being studied. The accuracy of determining the orientation from spot pattern is, at best, within ± 5°. The shift in the position of the Kikuchi lines can be analyzed to an accuracy of ± 0.5 mm, based on which an accuracy of ± 0.05° is possible in the orientation determination.

A serious disadvantage of this method is the volume of the material from which the information is obtained. The accuracy possible from the Kikuchi line pattern cannot be well utilized. Distinct patterns can be obtained only from regions of 1 μm in diamter. The sensitivity of the position of the Kikuchi Lines to orientation itself is the chief advantage of using Kikuchi patterns for the determination of orientation from larger areas of a deformed sample. The misorientation across the dislocation substructure which is the characteristic of the deformed condition gives rise to a smeared out Kikuchi pattern. Errors are also introduced due to elastic bending of the sample.

When taken from a large area, the sharpness of the spots in the spot pattern is also affected by the degree of misorientation in that area.

CHAPTER 4

ANALYSIS OF SHAPE CHANGE AND PREDICTION OF
ACTIVE SLIP SYSTEMS - RESULTS OF PRESENT WORK

In this chapter, the deformation of the crystals of "stable" and "unstable" orientations between strain levels of 0.1 and 1.0 in a channel die is considered. The shape change undergone by each crystal at different strain levels and the observed pattern of slip plane traces are reported. The results are compared with predictions of active slip systems based on the formalism of Bishop-Hill and the yield subsurface analysis.

4.1 Details of Deformation Conditions in the Channel Die

4.1.1 Possible Shape Change

The approximation of the mode of deformation in the channel die of Figure 3.5 to plane strain conditions is not strictly accurate (Chin et al., 1966). More general shape changes with finite shear strains which are possible are schematically shown in Figure 4.1. The solid lines represent the initial shape of the crystal and the dotted lines indicate a possible shape change. Definitions of the strain components are also given in Figure 4.1. In the channel die, the actual shape change undergone by the crystal depends on its initial orientation and the clearance between the crystal and the die at the time of assembly.

The plunger and the platform of the die illustrated in Figure 3.5, prohibit the possibility of producing ϵ_{xy}, the plastic shear strain on the free face. The magnitude of the plastic strain component of $d\epsilon_{yy}$
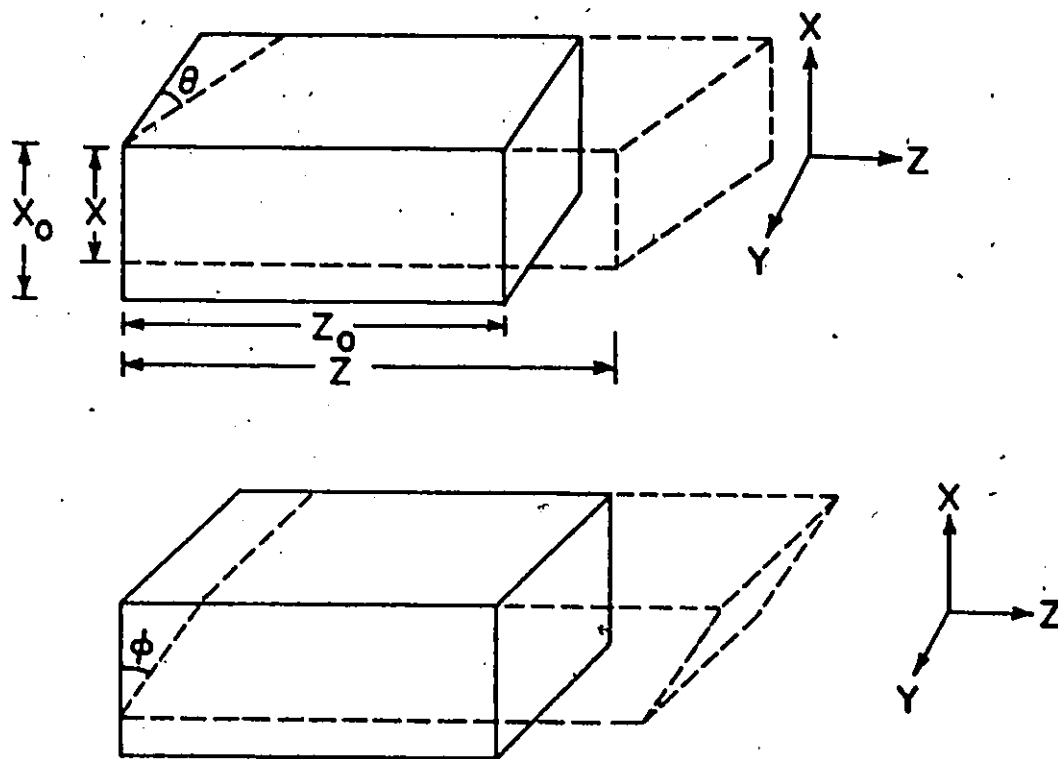
Fig. 4.1   General shape changes possible in the channel die.

$$\epsilon_{xx} = \ln \frac{x}{x_o} \; ; \qquad \epsilon_{zz} = \ln \frac{z}{z_o} \; ; \qquad \epsilon_{yz} = 1/2 \tan \theta$$

$$\epsilon_{zx} = 1/2 \tan \phi$$

x: compression direction

y: die face normal

z: channel direction

depends on how well the crystal fits into the die at the beginning of deformation. The magnitude of the other components $d\epsilon_{xx}$, $d\epsilon_{zz}$, $d\epsilon_{yz}$ and $d\epsilon_{xz}$ depends on the degree of deformation and the ratio of activity on each active slip system.

4.1.2 Stress Components Acting During Deformation

There are two types of stresses acting on the crystal being deformed in a channel die. (The effect of friction is neglected here.) These are termed primary and reaction stresses. The compressive stress σ_{xx} applied on the crystal is the primary stress. At zero strain, the crystal does not feel the presence of the die walls. When the applied stress σ_{xx} rises to the level required to satisfy the yield criterion of Eq. (2.8), a particular set of slip systems will be activated. In general, these contribute to the strain components $d\epsilon_{yy}$ and $d\epsilon_{xy}$. The die geometry will restrict these strain components and reaction stresses. σ_{yy} and σ_{xy} are built up within the crystal. This results in either suppressing activity on some of the slip systems or adjusting the activity on each of the operative slip systems, so that the shape change conforms to that allowed by the geometry of the die configuration. Thus, the only stress components that act on a crystal being deformed, in a channel die, in the absence of friction, are the primary stress σ_{xx} and reaction stresses σ_{yy} and σ_{xy}. The magnitude of reaction stresses developed depend on the orientation of the crystal being deformed and on the level of deformation, as has been shown by the measurements of the stress components by Chin et al. (1971). In the present investigations, the magnitudes of the reaction stresses were not measured.

4.2 Experimental Results

In this section, the results of the shape change, orientation and nature of slip plane traces observed on the surfaces at compressive strain levels of 0.1, 0.2, 0.5 and 1.0 for the "stable" and "unstable" crystals are given. The shape change is measured according to the strain components defined in Figure 4.1. The orientation of the faces was determined either by back reflection Laue X-ray method or by the use of selected area diffraction (SAD) technique in a transmission electron microscope, as described in Chapter 3. The method suggested by Barrett (1951) was followed in identifying the active slip planes based on the observed slip plane traces.

The experimental results for the "stable" and "unstable" crystals are summarized in Tables 4.1(a) and 4.1(b), respectively. In Figures 4.2(a-d), the back reflection Laue x-ray patterns for the compression faces of the "stable" and "unstable" crystals taken after deformation, are given. The orientations of the stable crystal can be determined based on this technique up to strain of ≃ 0.5 even though asterism develops. The orientations at a strain of 1.0 for the "stable" crystal, and at all strain levels between 0.1 and 1.0 for the "unstable" crystal can only be determined by the SAD technique as described in Chapter 3. Particularly for the "unstable" crystal, asterism leads to development of pronounced arcs early in the deformation and back reflection Laue X-ray method becomes quite unsuitable. Accuracy of the determination of the orientation by these techniques has been discussed in Chapter 3.

Table 4.1(a)

Experimental data for "stable" crystal orientation of the faces at the end of deformation.

Level of Compressive Strain	Shape Change $-\varepsilon_{xx}\ \varepsilon_{xy}\ \varepsilon_{xz}$ / $\varepsilon_{yx}\ \varepsilon_{yy}\ \varepsilon_{yz}$ / $\varepsilon_{zx}\ \varepsilon_{zy}\ \varepsilon_{zz}$			Compression Face Normal	Die Face Normal	Channel Direction	Slip Plane Traces Observed		
							Compression Face	Die Face	Free Face
0.1	-0.094	0.0	0.0	*110	$\bar{1}\bar{1}\bar{1}$	$\bar{1}12$	111, 11$\bar{1}$	111, 11$\bar{1}$	111, 11$\bar{1}$
	0.0	0.001	-0.031						
	0.0	-0.031	0.093						
0.2	-0.203	0.0	0.0	*110	$\bar{1}\bar{1}\bar{1}$	$\bar{1}12$	111, 11$\bar{1}$	111, 11$\bar{1}$	111, 11$\bar{1}$
	0.0	0.04	-0.088						
	0.0	-0.088	0.163						
0.5	-0.474	0.0	0.017	*110	$\bar{1}\bar{1}\bar{1}$	$\bar{1}12$	111, 11$\bar{1}$	111, 11$\bar{1}$	111, 11$\bar{1}$
	0.0	0.04	-0.21						
	0.017	-0.21	0.434						
1.0	-1.0	0.0	0.052	†110	$\bar{1}\bar{1}\bar{1}$	$\bar{1}12$	111, 11$\bar{1}$	111, 11$\bar{1}$	111, 11$\bar{1}$
	0.0	0.021	-0.28						
	0.052	-0.28	0.979						

* Orientation determined by back reflection Laue X-ray technique.

† Orientation determined by S.A.D. technique in T.E.M.

Table 4.1(b)

Experimental data for "unstable" crystal

Level of Compressive Strain	Shape Change ε_{xx} ε_{xy} ε_{xz}	ε_{yx} ε_{yy} ε_{yz}	ε_{zx} ε_{zy} ε_{zz}	Compression Initial	Compression Final	Die(D) Initial	Die(D) Final	Free(F) Initial	Free(F) Final	Slip Compression Face	Slip Die Face	Slip Free Face
0.1	−0.116	0.0	0.0	1̄1̄1 *	11̄1 †	541̄ *	110 †	1̄23 *	1̄12 †	111 *	(1̄11, 111)	111, 1̄11
	0.0	0.0	0.026									
	0.0	0.026	0.116									
0.2	−0.229	0.0	0.008	1̄1̄1	11̄1	541̄	110	1̄23	1̄12	11̄1	11̄1, (1̄1̄1 / 111)	11̄1, 1̄11
	0.0	0.04	0.061									
	0.008	0.061	0.189									
0.5	−0.487	0.0	0.06	1̄1̄1	1̄1̄1	541̄	110 **	1̄23	1̄12	1̄1̄1	1̄1̄1, 111	1̄1̄1, 111
	0.0	0.04	0.135									
	0.06	0.135	0.447									
1.0	−1.08	0.0	0.0	1̄1̄1	11̄1	541̄	110	1̄23	1̄12 ††	–	–	–
#	0.0	0.01	0.202									
	0.0	0.202	1.07									

* Orientations determined by back reflection Laue X-ray method.

† Orientations determined by S.A.D. technique in T.E.M.

** Within 10° of 110.

†† Orientation of channel direction(C) as opposed to free direction.

Shape change is approximate. Deformation bands were observed on the surface.

(c)　　　　　　　　　　　　　　　　(d)
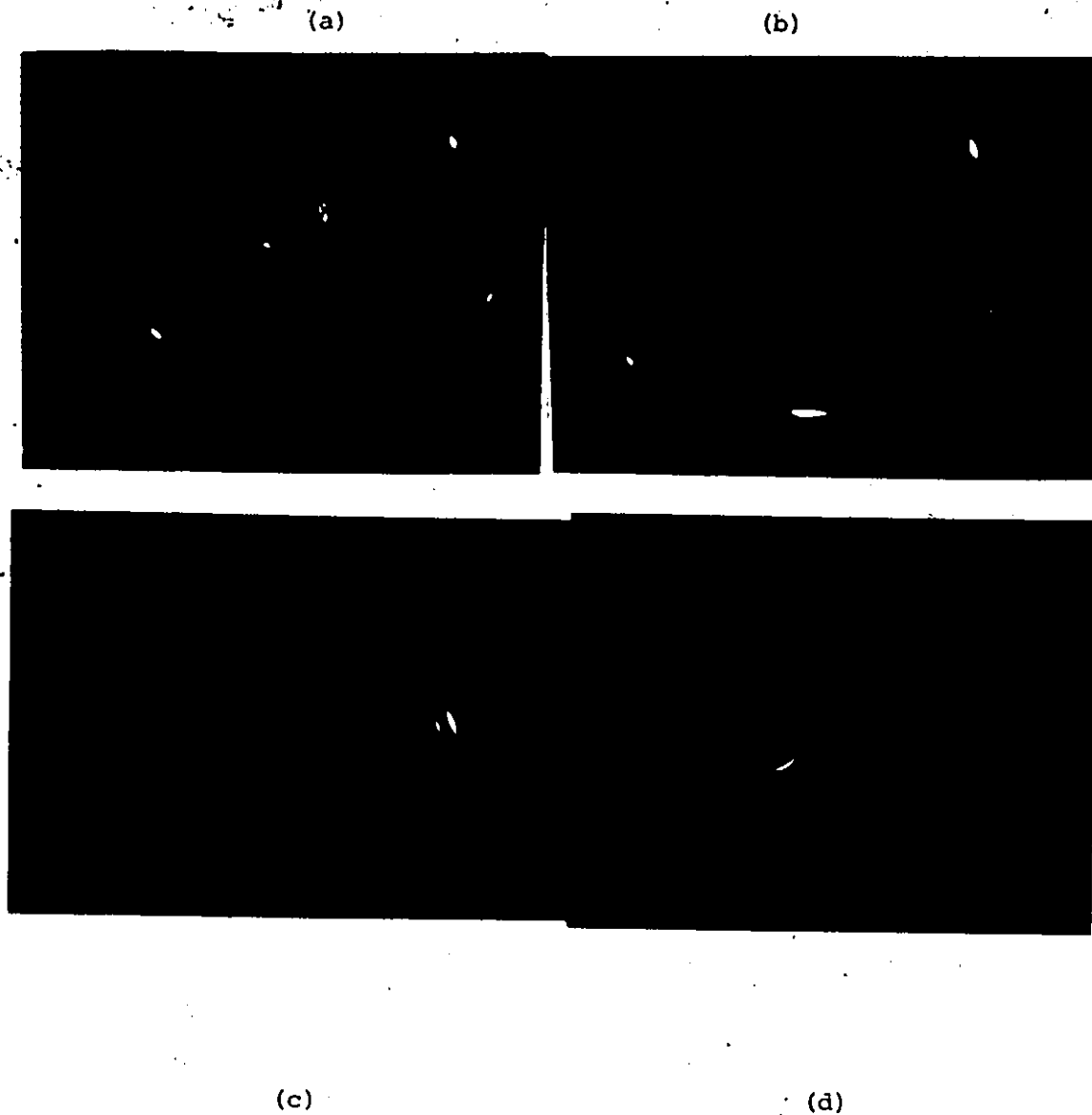
Fig. 4.2(a-d)　　Back reflection Laue x-ray photographs of the
　　　　　　　　compression face of the "stable crystal　(a-b)
　　　　　　　　and "unstable" crystal (c-d) at strains
　　　　　　　　(a)　0.1;　(b) 0.5;　(c) 0.1;　(d) 0.2

4.2.1 Nature of Slip Plane Traces

The slip plane traces observed on the surfaces of the deformed

crystals after incremental straining at true strains 0.1 and 0.5 are

shown along with schematic illustrations of the distribution of {111}

<110> slip systems, in Figures 4.3 and 4.4, respectively, for the

"stable" and "unstable" crystals. The traces on the "stable" crystal

are caused by slip on (111) and (11$\bar{1}$) planes, the distribution being

homogeneous over the entire surface of the crystal. The traces are

long, straight and fine. The slip plane traces observed at true strains of

0.2, 0.5 and 1.0 on the "stable" crystal are shown in Figure 4.5. It is

seen that throughout the deformation slip occurs on the (111) and (11$\bar{1}$)

slip planes, although the nature of the slip plane traces becomes coarse

at large strains. Analysis of the slip plane traces shows that nature

of active slip systems changes during deformation in the "unstable"

crystals. Traces observed after incremental straining at strain 0.1 to

0.5 are shown in Figure 4.6. The distribution of slip is not homogeneous

over the entire surface of the crystal, as can be observed from the

clustering of slip lines on the die face at a strain of 0.1 and on the

free face after 0.2% strain as shown in Figure 4.6. Distribution of

slip is inhomogeneous both sequentially with respect to strain (Figures

4.4 and 4.6(a)) and spatially at a given level of strain (Figure 4.7).

The slip plane traces observed at strain of 1.0 for the "unstable"

crystal, shown in Figure 4.8, appears to be very inhomogeneous. Very

coarse slip is observed on the compression face, bands in which the

nature and distribution of traces vary are seen on the die face, whereas

no such feature is observed on the free face. At this strain level it

Fig. 4.3(b) Schematic representation of traces of primary slip planes (1̄1̄1)(1̄11̄)(11̄1̄) in the three ortho-gonal faces of (110)[112̄] crystal.

Fig. 4.3(a) 110 stereographic projection for (110)[1̄1̄2] crystal repre-senting primary (heavy arrows) and cross slip (dotted arrows) systems.
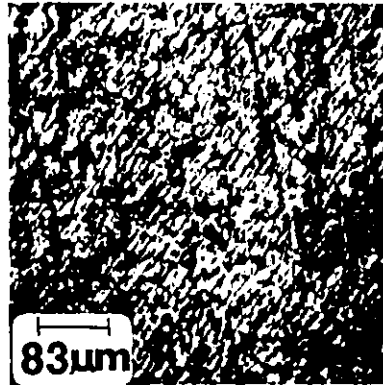
(1)
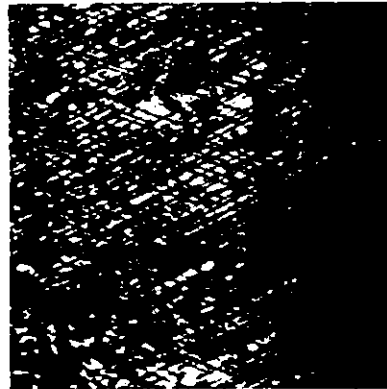
(2)
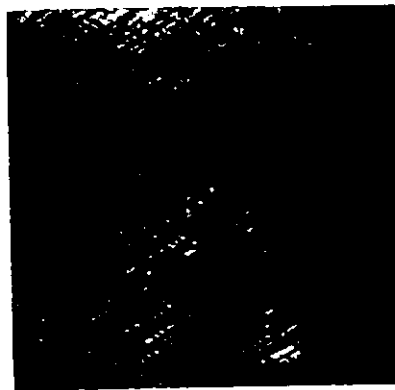
(3)

Fig. 4.3(c)   Slip plane traces observed at strain of 0.1 on
             (1) the compression face (2) free face and,
             (3) die faces showing traces of (1̄1̄1) (1̄11) planes.
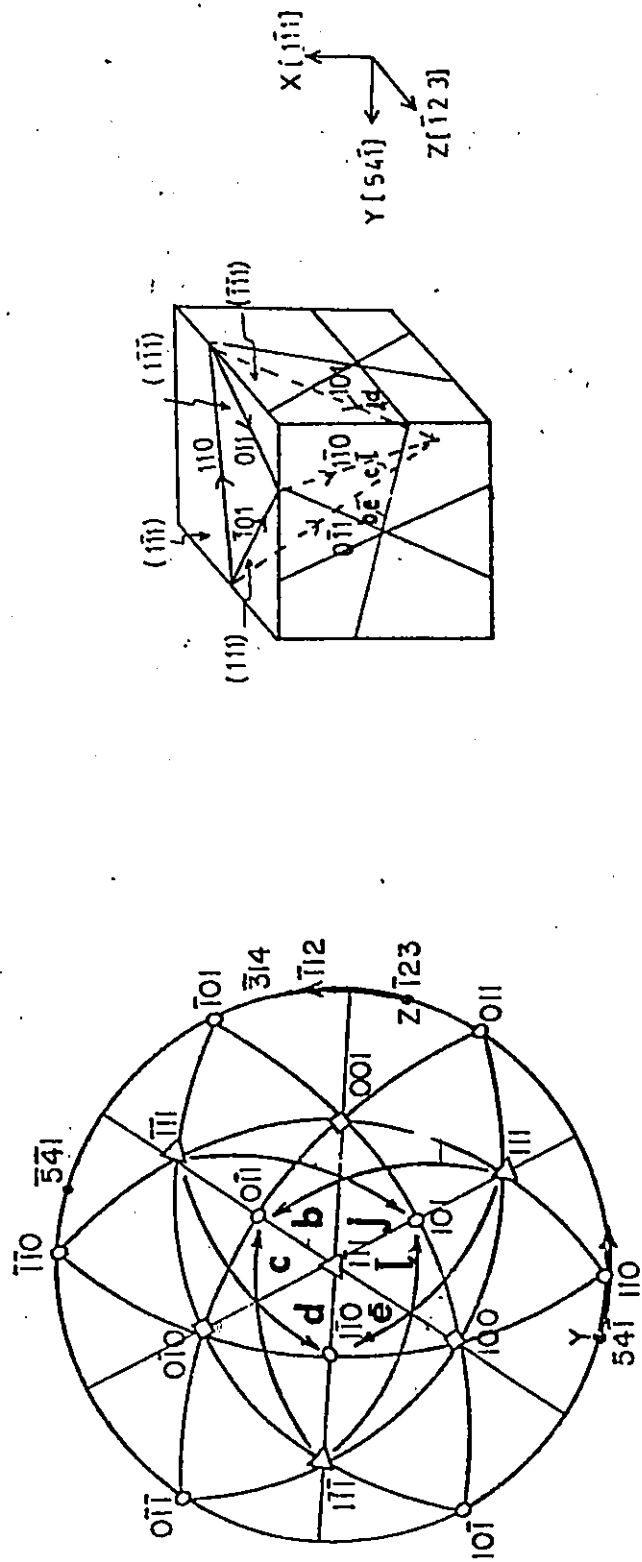
Fig. 4.4 (a-b) (a) ($\bar{1}$11) standard stereographic projection and
               (b) schematic illustration of the primary slip plane traces in
                    the "unstable" crystal.
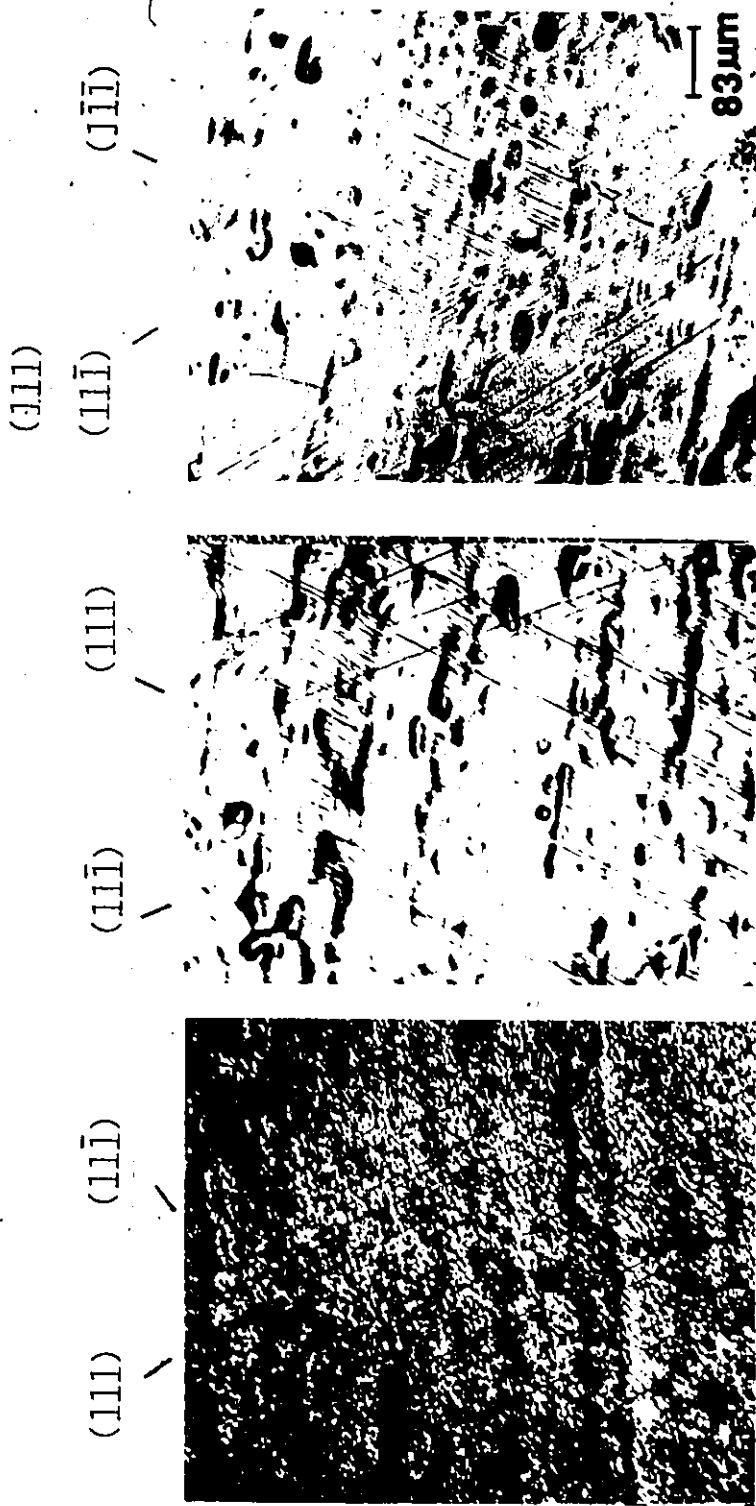
Fig. 4.4(c) Slip plane traces observed at strain of 0.05 on (1) compression face, (2) free face, and (3) die face.
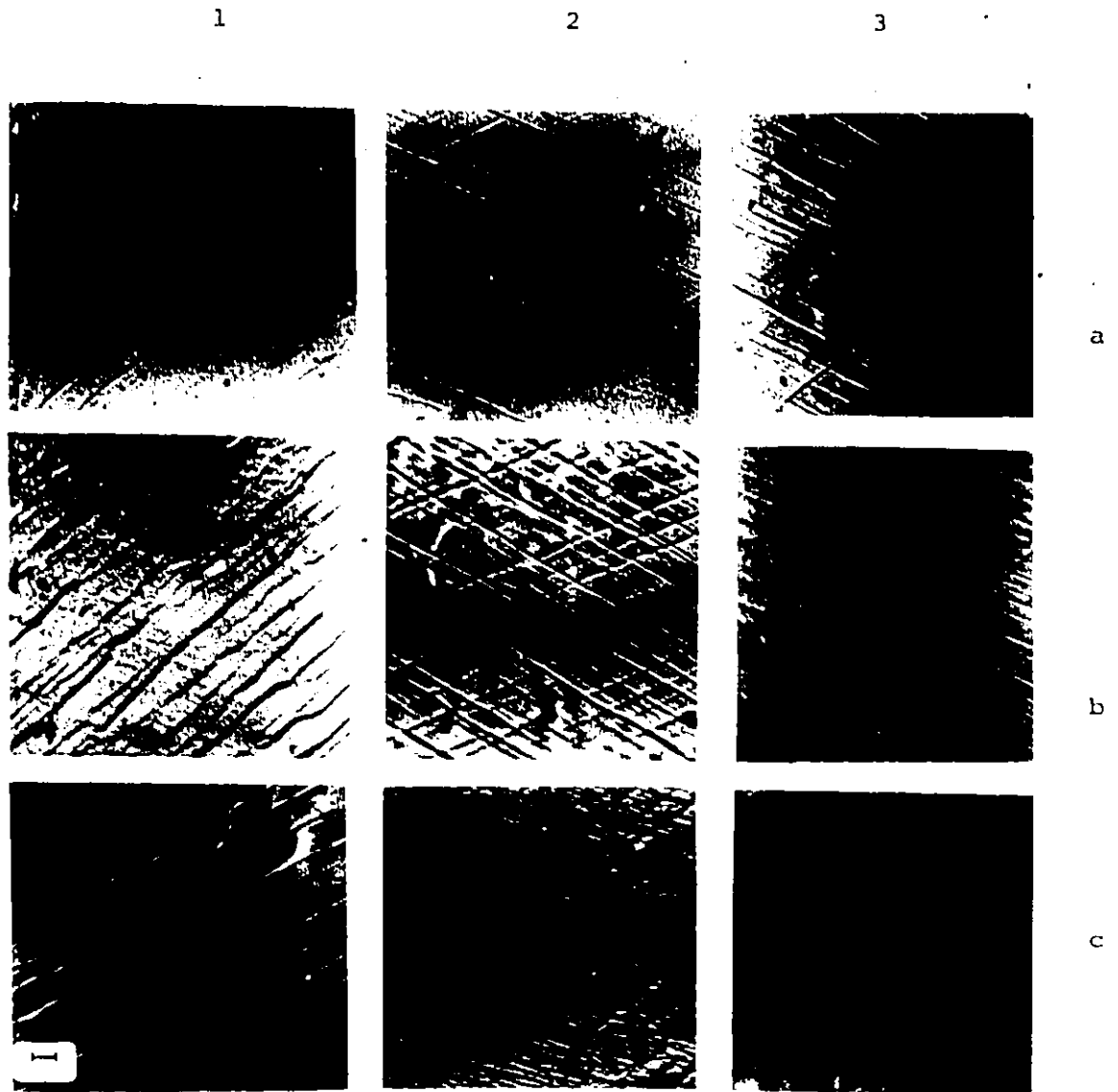
Fig. 4.5 Slip plane traces observed on the (1) compression face, (2) free face and (3) die faces of the "stable" crystal after incremental straining at strain of (a) 0.2; (b) 0.5; (c) 1.0. Traces are identified in Table 4.1(b).
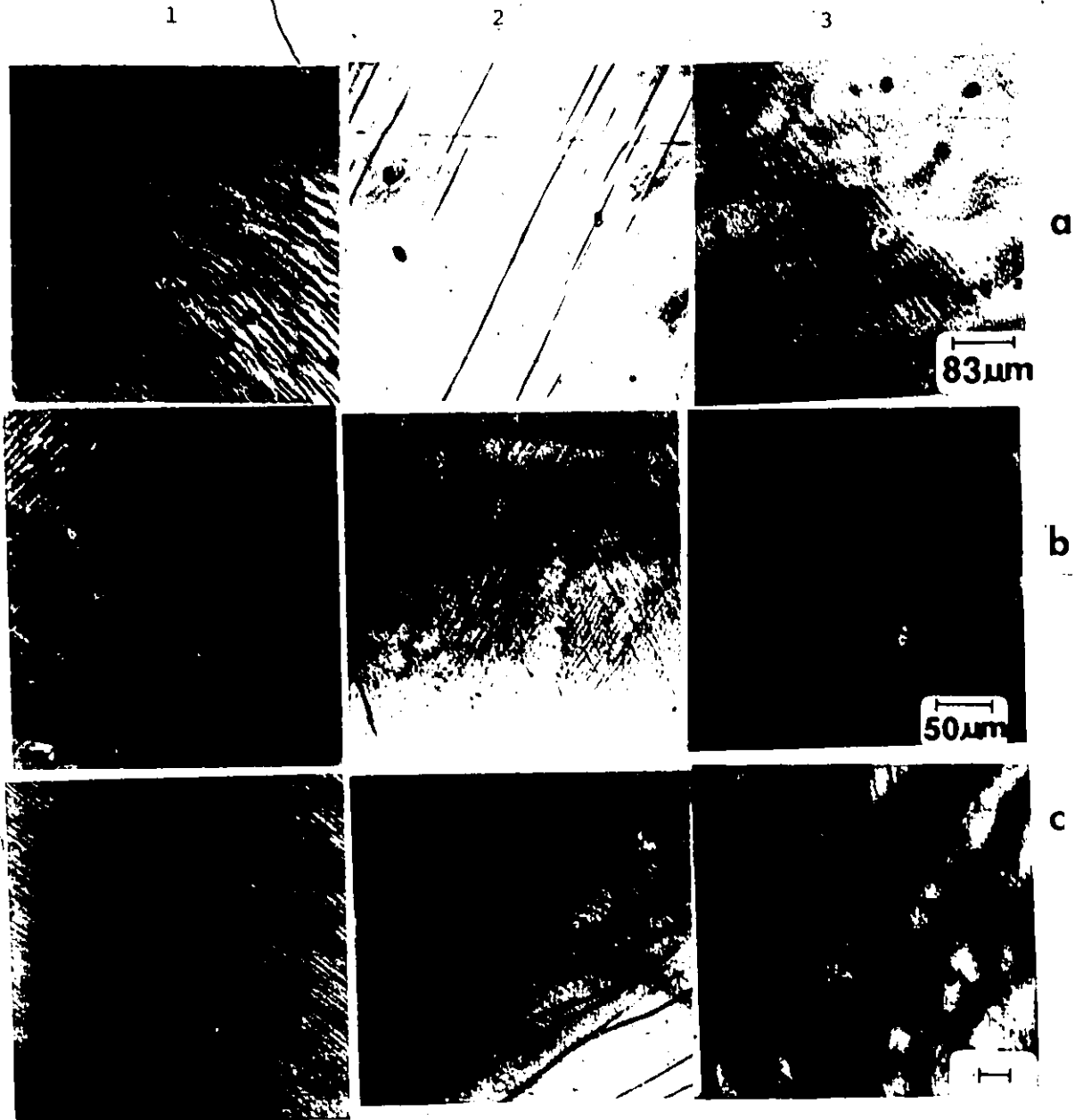
Fig. 4.6   Slip plane traces observed on (1) compression, (2) free
and (3) die faces of the "unstable" crystal after incre-
mental straining at strain (a) 0.1;   (b) 0.2;   (c) 0.5.

Fig. 4.7   Inhomogeneity in the spatial distribution of slip
            plane traces observed on the die face at strain 0.04.
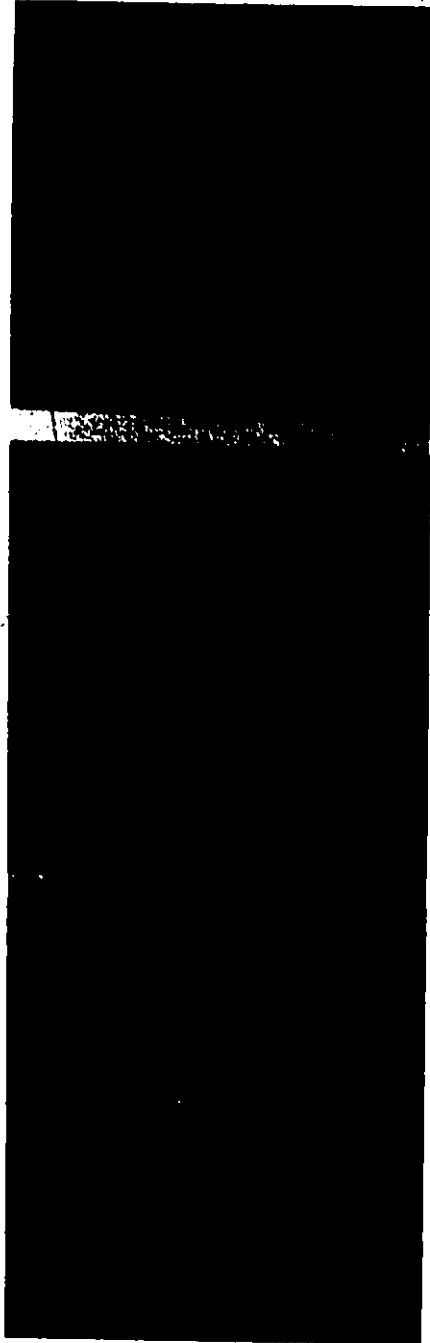
(1)   (2)   (3)

Fig. 4.8   Slip plane traces observed at strain ∿ 1.0 showing (1) coarse slip bands on compression face and (2) deformation bands on die face. (3) is free face. Micron marker on (1) is along the channel direction.

is difficult to unequivocally correlate the nature of the slip plane traces to the orientation of the faces as determined by the selected area diffraction technique.

The differences in the nature and homogeneity of the distribution of slip plane traces in the "stable" and "unstable" crystal are of. importance in considering the applicability of the methods of predicting active slip systems, and this will be discussed later in this section. The consideration of inhomogeneity is also important based on the effect it. has on the nature of the dislocation substructure, developed within the crystal.

The variation of the scale of the slip plane traces during deformation observed on the free face of the "unstable" and "stable" crystals are given in Figures 4.9(a-d), respectively. The data is given in terms of the range of the length and spacing of the slip plane traces at each level of strain.

4.3 Application of the Bishop-Hill Theory

In this section the results of Bishop-Hill analysis used to predict the slip systems active during the deformation of "stable" and "unstable" crystals are presented based on the method described in Chapter 2. The shape change undergone by the crystals given in Tables 4.1(a) and 4.1(b), refer to the components of $d\varepsilon_{ij}$ in the crystal axes coordinate system, which are in turn transformed to components in the cubic coordinate system. The values of the external work done at the 56 polyslip corners are calculated based on Eq. (2.15). The polyslip corner which maximises the external work contains the possible combination of active slip systems. The results of the application of the Bishop-Hill analysis at strain levels between 0.1 to 1.0 for the
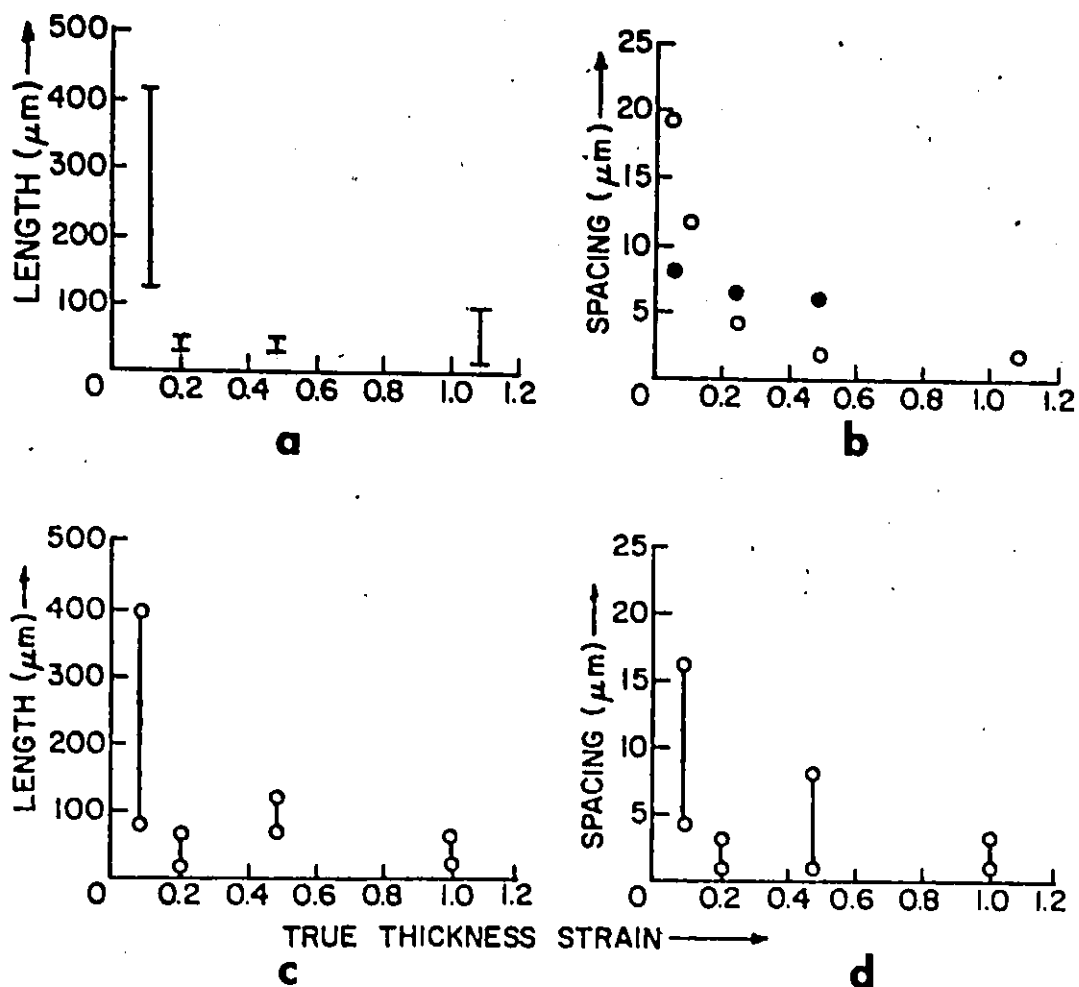
Fig. 4.9 Variation in the length and spacing of the slip plane
traces observed on the free face of the "unstable"
crystal (a-b) and "stable" crystal (c-d) during deform-
ation. The data indicates the range measured at each
level of strain. The different symbols in (b) repre-
sent two types of traces. Only average values are
given in (b).

"stable" and "unstable" crystals are given in Tables 4.2(a) and 4.2(b), respectively. The tables contain information of the polyslip corner selected, and the combination of slip systems at that corner, predicted for the exact shape change measured. The Taylor factor, M, calculated based on Eq. (2.9) (neglecting the width strain) and dw, the amount of work done by the external stresses in achieving the given shape change, are also included. The work is given in terms of arbitrary units of $\sqrt{6}\tau$ where τ is the resolved shear stress. The work done at different levels of strain for the "unstable" crystal is calculated based on the initial orientation of the crystal. This is meaningful for the low strain (0.1) deformation but not accurate for the larger strains.

4.4 Prediction of Active Slip Systems Based on Yield Subsurface Approach

To construct the three-dimensional yield subsurface in stress space along σ_{xx}, σ_{yy} and σ_{xy} axes based on Eq. (2.13), the corresponding m values must be known. The complete m matrices derived based on Eq. (2.4) for the twelve $\{111\}$ <110> type slip systems in fcc lattice are given for the "stable" and "unstable" crystals in Tables 4.3(a) and 4.4(a), respectively. In Tables 4.3(b) and 4.4(b), the respective m components relevant to deformation in the channel die are given.

As discussed in Chapter 2, only slip systems with the largest values for m_{xx} will be activated by the primary compressive stress σ_{xx}. The strain components that are possible due to activity on these slip systems, depend on the sign of the other m components. The yield subsurfaces constructed based on the method described in Chapter 2, for the "stable" and "unstable" crystals are given in Figures 4.10(a) and 4.10(b), respectively. To complete the view of the yield subsurface, other slip systems which are not activated by the primary stress are

Table 4.2(a)

Results of Bishop-Hill analysis for the "stable" crystal.

Level of Compressive Strain	Polyslip Corner Selected	Taylor Factor M	Magnitude of Work Done ($\sqrt{6}\tau$)	Slip Systems Contained in the Corner
0.1[†]	C*$\bar{3}$	2.5123	0.236	a $\bar{b}$ $\bar{d}$ e g $\bar{h}$ $\bar{j}$ $\bar{k}$
0.2[†]	A*$\bar{3}$	2.473	0.502	a $\bar{b}$ $\bar{d}$ e g $\bar{h}$ $\bar{j}$ $\bar{k}$
0.4[††]	A*$\bar{3}$	2.586	1.226	a $\bar{b}$ $\bar{d}$ e g $\bar{h}$ $\bar{j}$ $\bar{k}$
1.0[††]	C*$\bar{3}$	2.636	2.635	a $\bar{b}$ $\bar{d}$ e g $\bar{h}$ $\bar{j}$ $\bar{k}$

[†] Actual shape change with $d\varepsilon_{xz} = d\varepsilon_{xy} = 0$

[††] Actual shape change with $d\varepsilon_{xy} = 0$

Table 4.2(b)

Results of Bishop-Hill analysis for the "unstable" crystal.

Level of Compressive Strain	Polyslip Corner Selected	Taylor Factor M	Magnitude of Work Done ($\sqrt{6}\tau$)	Slip Systems Contained in the Corner
0.1*	c*1	3.732	0.373	b c ē f̄ h ī k̄ l̄
0.1†	c*1	4.185	0.485	b c ē f̄ h ī k̄ l̄
0.2††	c*1	3.796	0.869	b c ē f̄ h ī k̄ l̄
0.5††	c*1	3.988	1.942	b c ē f̄ h ī k̄ l̄
1.0†	c*1	3.911	4.224	b c ē f̄ h ī k̄ l̄

*   Ideal plane strain $d\varepsilon_{yy} = d\varepsilon_{yz} = d\varepsilon_{zx} = d\varepsilon_{xy} = 0$

†   Actual shape change $d\varepsilon_{xz} = d\varepsilon_{xy} = 0$

††   Actual shape change $d\varepsilon_{xy} = 0$

Table 4.3(a)

Complete m matrix for the twelve {111} <110> type slip systems of the "stable" crystal.

Slip System	m_{xx} $\frac{1}{\sqrt{6}}$	m_{yy} $\frac{1}{3\sqrt{6}}$	m_{zz} $\frac{1}{6\sqrt{6}}$	$m_{yz} + m_{zy}$ $\frac{1}{6\sqrt{3}}$	$m_{zx} + m_{xz}$ $\frac{1}{6\sqrt{2}}$	$m_{xy} + m_{yx}$ $\frac{1}{6}$	$m_{yz} - m_{zy}$ $\frac{1}{6\sqrt{3}}$	$m_{zx} - m_{xz}$ $\frac{1}{6\sqrt{2}}$	$m_{xy} - m_{yx}$ $\frac{1}{6}$
a	1	0	-6	3	4	1	3	-8	-1
b	1	-2	-2	5	0	-3	-3	-4	-5
c	0	-2	4	2	-4	-4	-6	4	-4
d	0	-2	4	-7	-4	-1	9	-4	1
e	0	2	-4	7	-4	-1	-9	-4	1
f	0	0	0	0	-4	-2	0	-4	1
g	0	0	0	-9	0	-3	-9	0	3
h	0	0	0	9	0	-3	9	0	3
i	0	0	0	0	0	-6	0	0	6
j	1	-2	-2	5	0	3	-3	4	5
k	1	0	-6	3	-4	-1	3	8	1
l	0	2	-4	-2	-4	-4	6	4	-4

Table 4.3(b)

Relevant m components for deformation of "stable" crystal in channel die.

slip System	m_{xx} $\frac{1}{\sqrt{6}}$	m_{yy} $\frac{1}{6\sqrt{6}}$	$m_{xy} + m_{yx}$ $\frac{1}{6}$
$\bar{a}$	-1	0	-1
$\bar{b}$	-1	2	3
$\bar{j}$	-1	2	-3
$\bar{k}$	-1	0	1

Primary compressive stress along [110] activates slip systems $\bar{a}$, $\bar{b}$, $\bar{j}$ and $\bar{k}$. Hence the sign difference of the M components compared to Table 4.3(a).

Table 4.4(a)

Complete m matrix for the twelve {111} <110> type slip systems of the "unstable" crystal.

Slip System	m_{xx} $\frac{1}{3\sqrt{6}}$	m_{yy} $\frac{1}{42\sqrt{6}}$	m_{zz} $\frac{1}{14\sqrt{6}}$	$m_{yz}+m_{zy}$ $\frac{1}{14\sqrt{18}}$	$m_{2x}+m_{xz}$ $\frac{1}{\sqrt{42}\sqrt{6}}$	$m_{xy}+m_{yx}$ $\frac{1}{3\sqrt{84}}$	$m_{yz}-m_{zy}$ $\frac{1}{14\sqrt{18}}$	$m_{zx}-m_{xz}$ $\frac{1}{\sqrt{42}\sqrt{6}}$	$m_{xy}-m_{yx}$ $\frac{1}{3\sqrt{84}}$
a	0	30	-10	44	-5	-3	56	5	3
b	-2	40	-4	12	-6	16	28	-2	-24
c	-2	10	6	-32	-1	19	-28	-7	-21
d	-2	10	6	-32	11	1	28	13	9
e	2	8	-12	-20	-10	8	28	-14	0
f	0	18	-6	-52	1	9	56	-1	9
g	0	0	0	0	15	9	0	-15	9
h	0	0	0	0	-12	18	0	12	18
i	0	0	0	0	3	27	0	-3	27
j	-2	40	-4	12	-9	-11	-28	-7	21
k	0	48	-16	-8	-4	6	-56	4	6
l	2	8	-12	-20	5	17	-28	11	-15

Table 4.4(b)

Relevant m components for deformation of "unstable" crystal in channel die.

Slip System	m_{xx} $\frac{1}{3\sqrt{6}}$	m_{yy} $\frac{1}{42\sqrt{6}}$	$m_{xy}+m_{yx}$ $\frac{1}{3\sqrt{84}}$
b	-2	40	16
c	-2	10	19
d	-2	10	1
ē	-2	-8	-8
j	-2	40	-11
ī	-2	-8	-17

Primary compressive stress along [1̄1̄1] activates slip systems b, c, d, ē, j and ī. Hence the negative signs of the m components compared to Table 4.4(a).

Fig. 4.10 Yield subsurface for (a) the "stable" crystal
and (b) the "unstable" crystal.

included. The results of the "yield subsurface" analysis for the "stable" and "unstable" crystals are given in Table 4.5.

4.5 Applicability of the Bishop-Hill Method and the Yield Subsurface Analysis for Deformation in the Channel Die

The applicability of each method is discussed primarily for low strain deformation by comparing the predictions of the set of active slip systems, the expected nature of slip plane traces with the measured shape change, and observed slip plane traces. Extension to large strain deformations will be discussed.

The data of slip plane traces and the shape change observed for the "stable" and "unstable" crystals (Tables 4.1(a) and 4.1(b)) correlate well with the predictions based on yield subsurface (Table 4.5) but not of Bishop-Hill (Tables 4.2(a) and 4.2(b)).

The predictions of possible slip systems in the yield subsurface analysis is based on the primary compression stress, based on an approach similar to the Schmid approach. But the analysis extends further than being a simple generalized Schmid law, because a selection of these slip systems which are actually active, is made based on the deformation conditions imposed by the geometry of the channel die. This is apparent by considering the set of slip systems predicted for the "stable" crystal. According to the Schmid law all the four slip systems $\bar{a}$, $\bar{b}$, $\bar{j}$ and $\bar{k}$ should be active.   Equal activity on slip systems $\bar{j}$ and $\bar{b}$ will cause considerable width strain $d\epsilon_{yy}$, which is not allowed by the die walls in the channel die. Activity on the slip systems $\bar{b}$ and $\bar{j}$ is possible only till the crystal expands up to the die walls. Any further expansion along the die wall normal, will give rise to the reaction stress σ_{yy}, compressive in nature. This will result

Table 4.5

Results of yield subsurface analysis for
"stable" and "unstable" crystals.

Crystal	Possible active slip systems	Possible slip plane traces
"Stable"	$\bar{a}$* $\bar{b}$ $\bar{j}$ $\bar{k}$*	(111), (11$\bar{1}$)
"Unstable"	b c d $\bar{e}$ j $\bar{l}$	(111), (11$\bar{1}$), ($\bar{1}$11)

* Major slip systems - the amount of activity on
these is far greater than the other two.

in suppression of activity on the slip systems $\bar{b}$ and $\bar{j}$ (negative values of m_{yy} in Table 4.3(b) must be considered for a compressive σ_{yy} stress). As the m_{yy} values for $\bar{a}$ and $\bar{k}$ are zero, reaction stress σ_{yy} will not affect activity on $\bar{a}$ and $\bar{k}$. According to Table 4.3(a), the other slip systems which have non-zero m_{yy} values are c, d, e and 1. But these will not be activated unless the magnitude of stress σ_{yy} exceeds that of σ_{xx}, an unlikely situation in the present investigations. Thus, major activity must occur on the slip systems $\bar{a}$ and $\bar{k}$, with a small amount of activity on $\bar{b}$ and $\bar{j}$. The yield subsurface shown in Figure 4.10(a) also leads to similar conclusions.

Examination of the yield subsurface of Figure 4.10(b) for the "unstable" crystal indicates that equal activity on the slip systems b, c, d, $\bar{e}$, j and $\bar{1}$ (predicted according to Schmid approach) will lead to considerable $d\varepsilon_{yy}$ strain (actually $d\varepsilon_{yy} = d\varepsilon_{zz} = -1/2\ d\varepsilon_{xx}$, $d\varepsilon_{xz} = d\varepsilon_{yz} = d\varepsilon_{xy} = 0$) and does not correspond to the shape change imposed in the channel die. The buildup of the reaction stress σ_{yy} will result in activating only subsets of the above six slip systems, and adjusting the ratios on each so that the shape change undergone by the crystal conforms to the imposed shape change.

Examining the predictions based on the Bishop-Hill analysis, the curious features to be noted according to Tables 4.2(a) and 4.2(b) are the following:

(1) For the "stable" crystal different polyslip corners are selected (based on the principle of maximum work and for initial crystal orientation) and at different strain levels, whereas for the "unstable" crystal, the same polyslip corner is selected throughout the deformation.

(a)   The set of possibly active slip systems predicted for both orientations contains slip systems on which the resolved shear stress values due to the primary compressive stress should be zero.

These aspects will be examined in detail for the deformation of the "stable" crystal. The polyslip corner in the Bishop-Hill method is selected based on the principle of maximum work. The sensitivity of the magnitude of the work done to shape change, will be examined for two assumed shape changes:

(1)   ideal plane strain deformation (a shape change often assumed for deformation in the channel die), and,

(2)   deformation in which a finite ϵ_{yz} shear is allowed.

Shape change (2) is calculated based on the predictions of the yield subsurface analysis – assuming equal activity on only slip systems $\bar{a}$ and $\bar{k}$. Magnitude of $d\epsilon_{xy}$ is assumed to be zero. Amounts of activity on $\bar{a}$ and $\bar{k}$ are calculated using the equation $d\epsilon_{ij} = \sum m_{ij}^{s} dr^{s}$ (Eq. 2.6), the corresponding m matrix (Table 4.3(b)). With $d\epsilon_{xy} = 0$ and $d\epsilon_{xy} = -0.094$ (corresponding to the low strain deformation). Using these values of shears on $\bar{a}$ and $\bar{k}$, the other components of strain, $d\epsilon_{xz}$, $d\epsilon_{yz}$, $d\epsilon_{yy}$ and $d\epsilon_{zz}$ are calculated, according to Eq. (2.6). The derived shape change (equal activity on $\bar{a}$ and $\bar{k}$ will result in only $d\epsilon_{yz}$ and $d\epsilon_{zz}$ being finite) is fed into the Bishop-Hill analysis and the polyslip corners predicted accordingly are given in Table 4.6. The data for ideal plane strain deformation is also included.

According to the data in Table 4.6, for the case of ideal plane strain, the work done is much larger than when a finite amount of ϵ_{yz} shear is allowed. This indicates that it is more difficult to achieve plane strain deformation for the orientation of the "stable" crystal.

Table 4.6

Results of Bishop-Hill analysis for some assumed shape changes.

Type of Deformation	Shape Change			Polyslip Corner Selected	Work done at the Corner ($\sqrt{6}\tau$)	% Difference in Work	Common Slip Systems
Ideal plane strain	-0.094	0.0	0.0	C* $\bar{3}$	0.3265		$\bar{a}$ $\bar{g}$ h $\bar{k}$
	0.0	0.0	0.0	B* $\bar{2}$	0.3264	0.03	
	0.0	0.0	0.094				
Allowing shear strain components (except $d\varepsilon_{xy}$)	-0.094	0.0	0.0	C* $\bar{3}$	0.2307		
	0.0	0.0	-0.033	D* 11	0.2301		
	0.0	-0.033	+0.094	D* $\bar{7}$	0.2304	0.2	$\bar{a}$ $\bar{k}$
				D* $\bar{1}$	0.2304		
				B* $\bar{2}$	0.2307		

This explains the surprising observation that slip systems $\bar{g}$ and h on which the magnitude of resolved shear stress is zero, are predicted to be active for the ideal plane strain shape change. When a finite ε_{yz} is allowed, only slip systems $\bar{a}$ and $\bar{k}$ are predicted. For deformation to be ideal plane strain in nature, this shear must be suppressed. Thus, a stress component σ_{yz} has to be somehow activated, which could cause activity on slip systems $\bar{g}$ and h. The m_{yz} values for these two slip systems are positive according to Table 4.2(a). Activity on $\bar{g}$ and h will result in positive ε_{yz} component and will counterbalance the nega- tive ε_{yz} component due to activity on slip systems $\bar{a}$ and $\bar{k}$, thus causing ideal plane strain deformation. In fact, Chin et al. (1966) observed traces belonging to $(1\bar{1}1)$ slip plane (slip plane of $\bar{g}$ and h) in a similar experiment in a channel die where the ε_{yz} shear was intentionally suppressed.

These two shape changes (ideal plane strain, and with finite ε_{yz}) were discussed in detail, in order to highlight the fact that the Bishop-Hill analysis is extremely sensitive to shape change. This explains the selection of different corners at different strain levels for the "stable" crystal (Table 4.2(a)). Theoretically, in the channel die, only three strain components – the imposed thickness strain $d\varepsilon_{xx} \neq 0$ and $d\varepsilon_{yy} = d\varepsilon_{xy} = 0$ – are prescribed. The other three are free to occur and thus slip could be accommodated by activity on only three slip systems. In the Bishop-Hill analysis fewer than six or eight slip systems will be predicted only if the same amount of (maximum) work is done at more than one polyslip corner. As the analysis is extremely sensitive to shape change, consideration of corners at which the magni- tude of work done approximates to the maximum work may yield a better

prediction of possible slip systems.

Based on this assumption, the predictions of the Bishop-Hill analysis for the actual shape change measured at strain ~ 0.1 are re-examined. The data given in Table 4.7 considers all the polyslip corners at which the magnitude of work done differs by 2%.[ ] It is seen that four different polyslip corners are selected and the slip systems common to these are $\bar{a}$ and $\bar{k}$.

$\bar{a}$ and $\bar{k}$ are the primary slip systems predicted according to the yield subsurface analysis. According to the corresponding m matrix (Table 4.3(b)) for the "stable" crystal activity on only $\bar{a}$ and $\bar{k}$ does not cause any width strain, $d\epsilon_{yy}$. To account for $d\epsilon_{yy}$, activity on $\bar{b}$ and $\bar{j}$ is necessary. Thus, the prediction according to Table 4.7 for the actual shape change measured at strain 0.1 is still an approximation, but a better one than the prediction according to Table 4.2(a).

The predictions at larger strains will be examined based on the data in Table 4.8 in which the polyslip corners, at which the magnitude of the work done is maximum along with the corners where the magnitude of work done is closest to the magnitude of maximum work done at the given strain for the "stable" crystals, are given.

Permitting a difference of 2% in the amount of work done, the common slip systems at corners $A*\bar{3}$ and $C*\bar{3}$ for the "stable" crystal deformed to strain 0.2 are $\bar{a}$, $\bar{b}$, $\bar{j}$ and $\bar{k}$. At larger strain, the difference between the magnitudes of maximum work done and the nearest one is larger. The set of slip systems common to these corners, contain slip systems, h, d and g, the traces of which were not observed on the surface. Also, the slip system $\bar{k}$ which is a major slip system, is not contained within the set of common slip systems. It is true that the Bishop-Hill

Table 4.7

Results of Bishop-Hill analysis for the actually measured shape change at $d\varepsilon_{xx} \sim 0.1$ for the "stable" crystal.

Measured Shape Change			Polyslip Corner Selected	Work done at the corner ($\sqrt{6}\tau$)	% Difference in work	Common Slip Systems
-0.094	0.0		$C^*\bar{3}$	0.2362		
0.0	0.001	-0.031	$B^*\bar{2}$	0.232	2	
0.0	-0.031	0.094	$D^*\bar{7}$	0.231		$\bar{a}\ \bar{k}$
			$D^*\bar{1}$	0.231		

Table 4.8

Detailed results of Bishop-Hill analysis for "stable" crystal.

Measured Shape Change			Polyslip Corner Selected	Work Done at the Corner ($\sqrt{6}\tau$)	% Difference in Work	Common Slip Systems
-0.203	0.0	0.0	A*3̄	0.5019	2	ā b̄ j̄ k̄
0.0	0.04	-0.088	C*3̄	0.4923		
0.0	0.088	0.163				
-0.474	0.0	0.017	A*3̄	1.226	7.3	ā d e g j̄ k̄
0.0	0.04	-0.21	E*1			
-0.017	-0.21	0.434				
-1.0	0.0	0.052	C*3̄	2.636	3.6	ā h k̄
0.0	0.021	-0.28	D*7̄	2.54		
0.052	-0.28	0.979	B*2̄	2.558		

analysis only predicts a possible set of slip systems. Not all the predicted systems need be active.

These results indicate that the predictions of a possible set of slip systems based on the Bishop-Hill analysis are sensitive to accuracy of the measurement of shape change. Even an error of 0.3° in the angle measured for shear strain calculations leads to a difference of ∿ 2% in the magnitude of the maximum work done.

The problem becomes more critical at large strains where friction effects influence the uniformity of shape change. In principle, even a difference of 2% in the magnitude of work done is large. For the ideal plane strain deformation given in Table 4.7, the difference is about 0.03%.

Comparison of the results for the "unstable" crystal indicates major differences between the predictions of the yield subsurface analysis and the Bishop-Hill method. In Table 4.9 data for "unstable" crystal derived on similar basis like in Table 4.8 for the "stable" crystal, are given. The analysis is considered for the shape change imposed for the crystal of initial orientation. The results given in Tables 4.2(b) and 4.9 could be affected by the orientation change undergone by the crystal. Orientation changes were observed by SAD technique even at the end of a strain of 0.1. As discussed earlier, inaccuracy of ± 5° is possible for orientation determination by SAD technique. This itself could lead to possible errors in the selection of polyslip corner. In order to investigate this aspect, the following procedure is adopted. Because the change in orientation was observed at a strain of 0.1, the shape change at strain of 0.2 was arbitrarily considered to have been accomplished in two steps. The first step is based on the initial orientation of the

Table 4.9

Detailed results of Bishop-Hill analysis for "unstable" crystal.

Measured Shape Change			Polyslip Corner Selected	Work Done at the Corner ($\sqrt{6}\tau$)	% Difference in Work	Common Slip Systems
-0.116	0.0	0.0	C^*1	0.485	12	b c̄ ē ī
0.0	0.0	0.026	B^*3	0.426		
0.0	0.026	0.116				
-0.229	0.0	-0.008	C^*1	0.869	2.6	b c̄ ē ī
0.0	0.04	0.061	B^*3	0.841		
0.008	0.061	0.189				
-0.487	0.0	0.06	C^*1	1.942	8	b c̄ ē ī
0.0	0.02	0.135	B^*3	1.78		
0.06	0.135	0.467				
-1.08	0.0	0.0	C^*1	4.224	8.7	b c̄ ē ī
0.0	0.01	0.202	B^*3			
0.0	0.202	1.07				

crystal and considers a shape change measured at strain $\sim$ 0.1. The next step is based on the orientation $(1\bar{1}1)$ $[\bar{1}12]$ (the orientations given at strain 0.1 in Table 4.1(b)) and the corresponding polyslip corner selected for the shape change at strain of 0.1 is derived. The results given in Table 4.10 indicate no major differences in the corners selected whether the deformation is considered to occur in one step based on the initial orientation or is divided into two steps. It must be remembered here that such a subdivision of strain is very arbitrary. The results are also inaccurate because it is not known at what stage the orientation changes occur and because of the inaccuracy inherent in the SAD technqiue used for determination of the orientation.

Assumptions inherent to the yield surface analysis are uniformity of flow, uniform expansion of the yield surface and that the same strain path is maintained throughout the deformation. The analysis also neglects the influence of internal stress, which could give rise to considerable secondary slip. The role of secondary slip has been discussed in Chapter 2.

The complications present in the experimental studies of determination of yield surfaces and the changes introduced by deformation on the size and shape of subsequent yield surfaces have been discussed by Martin (1975). Detailed treatment of the validity of the assumption about uniform expansion of the yield surface is not within the scope of this work. Perhaps the most questionable assumption is about the continuity of the same strain path during deformation, because this path in fact is determined by the nature of operative slip systems and relative activity on each. If either of these features change during deformation, then the initial strain path will no longer be maintained. This

121

Table 4.10

Results of Bishop-Hill analysis for the "unstable" crystal incorporating possible change in orientation.

Strain Level 0.2	Shape Change Accomplished	Initial Orientation Corresponding to the Shape Change	Polyslip Corner Selected	Work Done at the Corner ($\sqrt{6}\tau$)
(1) ~ 0.2	in single step	$(1\bar{1}1)[\bar{1}23]$	C^*_1	0.869
			B^*_3	0.841
(2) ~ 0.2	in two steps:			
	(a) strain ~ 0.1	$(1\bar{1}1)[\bar{1}23]$	C^*_1	0.434
	+		B^*_3	0.426
	(b) strain ~ 0.1	$(1\bar{1}1)[\bar{1}12]$	C^*_1	0.426
			B^*_3	0.415

aspect of maintaining the same strain path throughout deformation is crucial for the case of the "unstable" crystal. To understand the deformation of the "unstable" crystal and to predict the operative slip systems, shape measurements and orientation determination at much smaller intervals of strain than attempted in the present study, are essential. Theoretically, a complete analysis is possible for the "unstable" crystal, by evaluation of the corresponding m matrices at different stages of strain.

Even with all the inherent assumptions discussed earlier, it has been shown here that the yield subsurface analysis adequately explains the deformation behaviour of the crystal of "stable" orientation in the present investigation.

CHAPTER 5

NATURE OF DISLOCATION SUBSTRUCTURE

In this chapter, the results of the detailed investigations con-
ducted by transmission electron microscopy to study the nature of the
dislocation substructure developed at strain levels of 0.1, 0.2, 0.5 and
1.0 in the "stable" and "unstable" crystals will be discussed. The data
obtained from three sections of the crystal – the compression face, free
face and the die face will be presented. The similarities and differ-
ences between the dislocation substructures developed in the "stable"
and "unstable" crystals at various strain levels will be described.

In considering the evolution of the dislocation substructure it
is necessary to ascertain its geometric arrangement with respect to the
operative slip systems. In the present study, the correlation between
the directions of cell walls and the traces of the operative slip systems
was examined. In studying the evolution of the dislocation substructure
as a function of imposed strain, attention was given to the arrangement
of dislocations, i.e., whether they are arranged in tangles or in cell
walls which extend into three dimensions and also to the conversion of
these cell walls into subgrains. The variation in the scale and misori-
entation of the substructure with imposed strain was examined. A des-
cription of the dislocations consituting the cell walls was obtained
from the determination of their Burgers vectors.

The nomenclature adopted to distinguish crystals of "stable" and

"unstable" orientations, deformed to various strain levels are given

in Table 5.1 along with the primary planes causing traces on the surface

of the deformed crystals. The term "primary slip plane" is used to des-

cribe those slip planes which cause prominent traces on the surfaces of

the crystals.

5.1 Nature of the Dislocation Substructure Observed in the "Stable" Crystal

Dislocation substructure viewed from all the three faces was

analyzed but emphasis will be given to the data from the compression

face, as it adequately describes all the features of the dislocation

substructure developed in the "stable" crystal.

In Figs. 5.1 (a-c) the substructure viewed in the three sections

of the FC1 crystal is shown. An important feature of the substructure

as viewed in the compression face is the equiaxed cell structure.

Analysis of stereo pairs of the substructure indicated that most of the

substructure is in the form of tangles but in places the beginning of

three-dimensional arrangements can be recognized. One feature to be

noted is the presence of well-developed walls of projected width of

1 μm (indicated at A) aligned along the trace of the primary slip

plances. (These walls will be referred to as major walls to distinguish

them from the rest of the substructure, which will be referred to as

minor cells and minor cell walls, indicated at B.)

It is worth recalling (Fig. 4.3) that both the primary slip

planes (111) and (11$\bar{1}$) intersect along a common direction in the com-

pression face of the "stable" crystal. The average separation between

these major walls approximately   corresponds to the minimum

spacing between the slip plane traces observed on the surface. The projected

Table 5.1

Nomenclature adopted to describe "stable" and
"unstable" crystals deformed to various strain levels.

Approximate True Strain Level	"Stable" Crystal	"Unstable" Crystal
0.1	FC1	HC1
0.2	FC2	HC2
0.5	FC4	HC4
1.0	FC6	HC6
Primary slip plane traces	$1\bar{1}\bar{1}$, $\bar{1}\bar{1}1$	111, $11\bar{1}$, $\bar{1}11$

Fig. 5.1(a) Dislocation substructure as viewed in the compression face
of the "stable" crystal at strain 0.1. Major cell walls
are shown at A and minor cell walls are shown at B. Micron
marker is along the channel direction. Traces of primary
slip planes are shown.
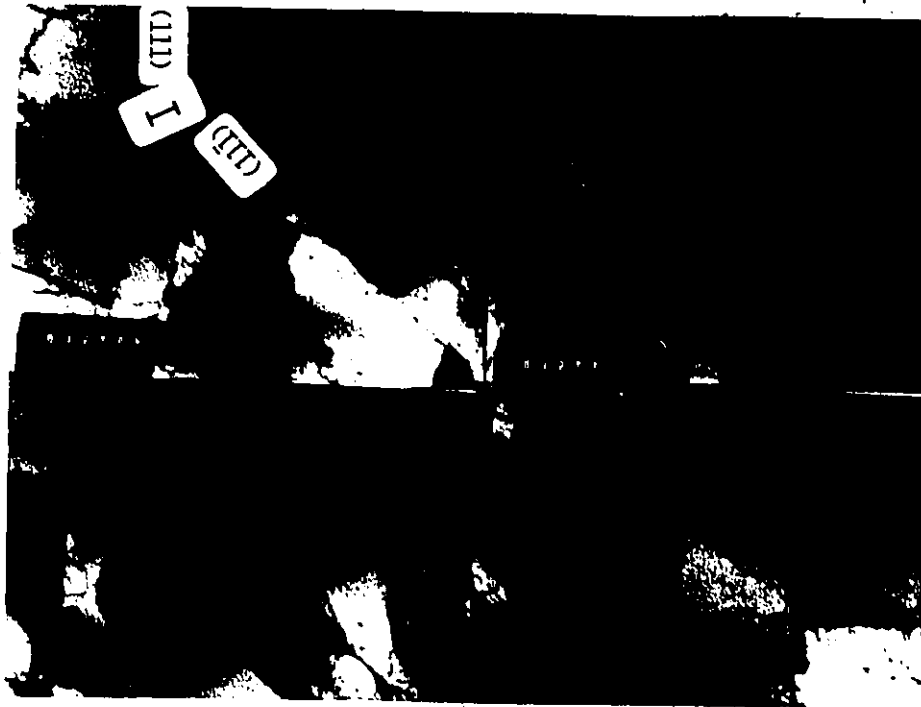
5.1(b)
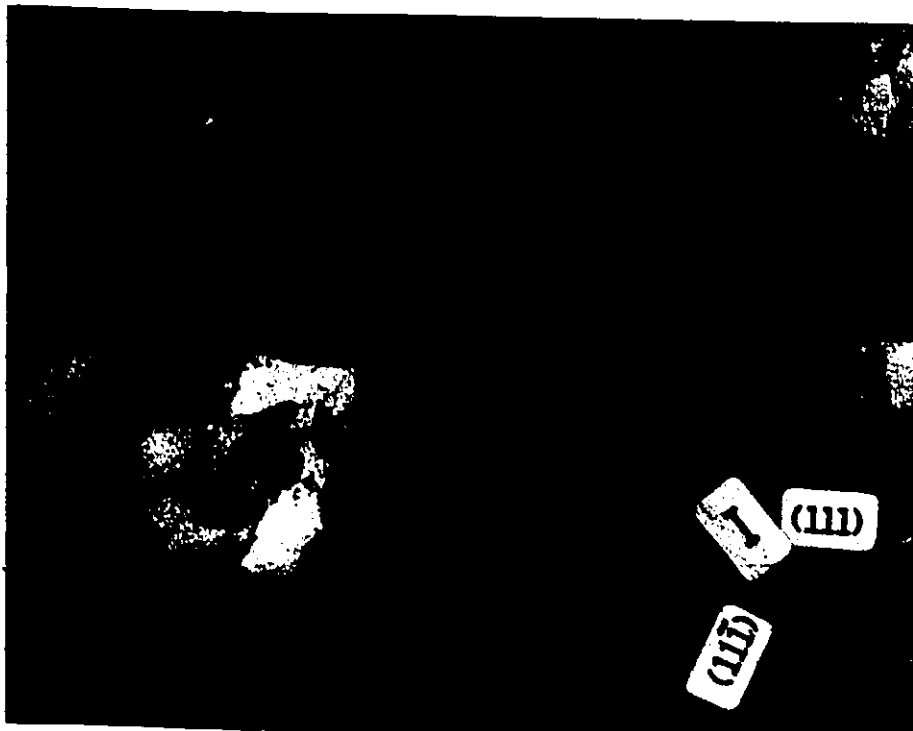
5.1(c)

Fig. 5.1(b-c)   Dislocation substructure as viewed in (b) free face
and (c) die face of the "stable" crystal at strain
0.1.   Micron marker is along the compression direc-
tion.   Traces of primary slip planes are shown.

width of these walls indicates that the constituent dislocations lie on the primary slip planes. However, the majority of the minor cell walls do not follow the slip plane trace direction. There are some prominent walls (indicated at B) which appear to be threading between the slip planes. A high density of dislocation loops and dipoles is also observed.

The arrangement of dislocations in the free face and die face also indicates the tangled nature of the cell walls, which appear to be aligned mostly along the traces of primary slip planes.

The small variation in contrast across the minor cell walls indicates that little misorientation is built up at this strain level. Fig. 5.2 shows representative diffraction micrographs indicating the nature of Kikuchi line patterns taken from within a number of minor cells and across major walls. The range of misorientation and the scale of the substructure will be considered later.

The Burgers vectors of the dislocations making up the cell walls were determined using foils cut parallel to the compression face. The values of the diffraction vectors which were used and the magnitudes of $\underline{g} \cdot \underline{b}$ for all the six <110> type Burgers vectors are given in Table 5.2. In Fig. 5.3(a), a schematic illustration of the location of the primary slip systems in the compression plane is given. The dislocations observed under various $\underline{g}$ reflections are shown in Fig. 5.3(b). Dislocations with Burgers vectors [011], [$\bar{1}$01], [101] and [1$\bar{1}$0] are identified. The first four are the Burgers vectors of primary dislocations belonging to the slip systems predicted to be active according to the yield subsurface analysis, described in Chapter 4. Dislocations with Burgers vector [1$\bar{1}$0] may have formed due to reaction between coplanar
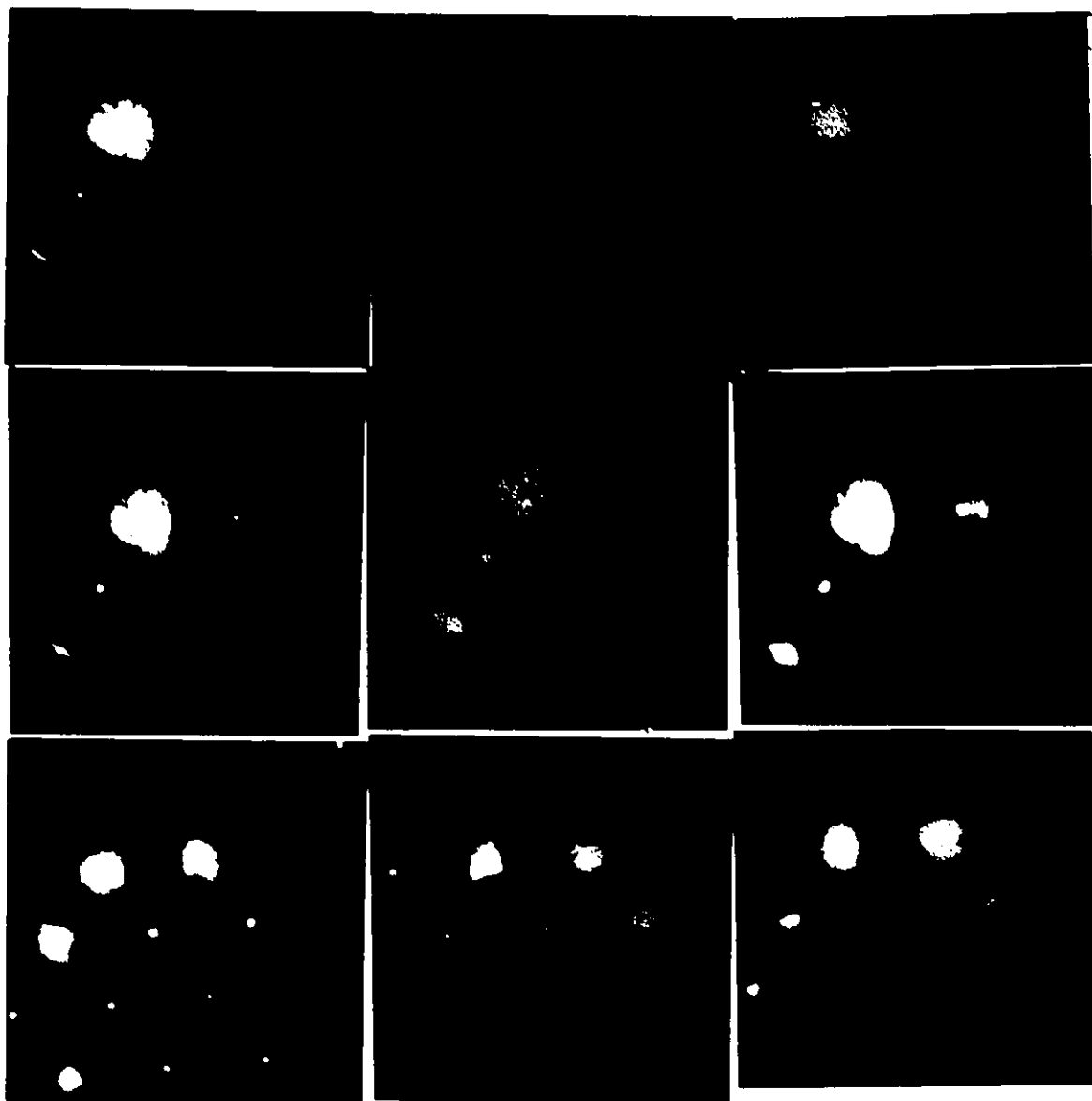
Fig. 5.2 Diffraction patterns taken from within minor cells (a-f) and across major cell walls (g-l).

Table 5.2

Values of $\underline{g} \cdot \underline{b}$ for {110} type Burgers vectors

	$\underline{b}$ 1̄10	01̄0	1̄01	101	011	11̄0
$\underline{g}$						
001	0	0	1	1	1	0
11̄1	2	1	0	2	0	2
1̄11	− 2	− 1	2	0	2	− 2
11̄0	2	1	− 1	1	− 1	2
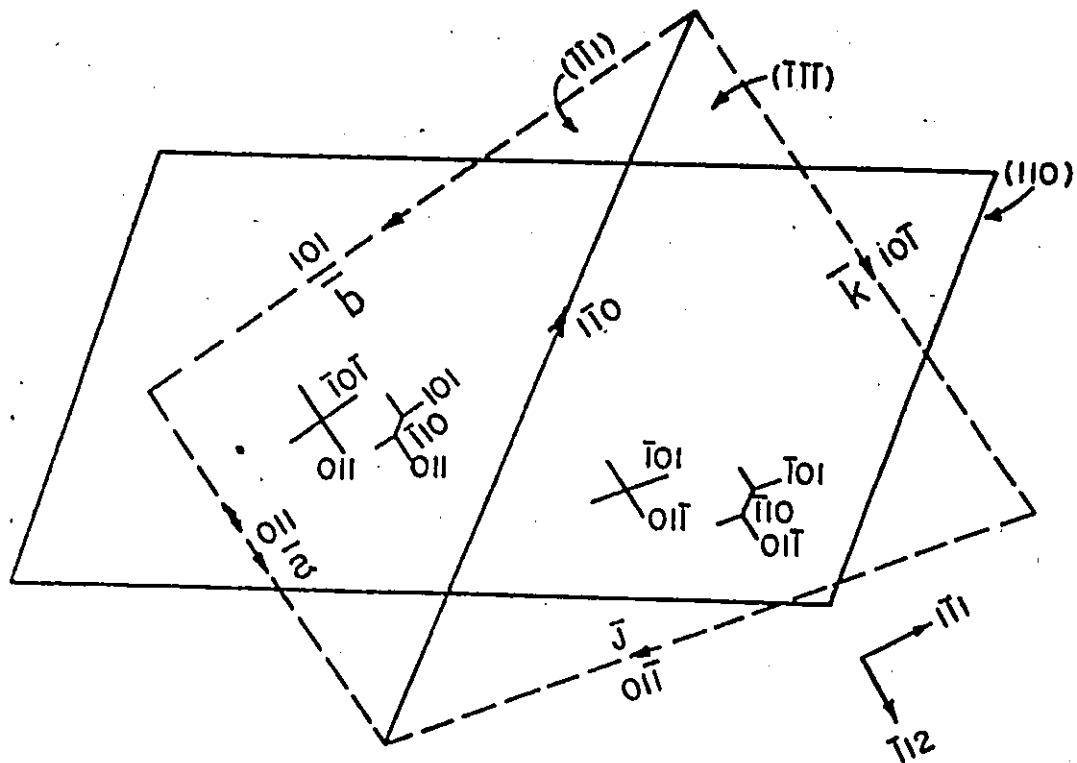
Fig. 5.3(a)   Location of primary slip systems with respect to the
              compression plane (110) and the possible boundaries
              of coplanar dislocations in the ($\bar{1}\bar{1}\bar{1}$) and ($\bar{1}\bar{1}1$) primary
              slip planes.

Fig. 5.3(b)　　Analysis of the nature of dislocations making up a minor cell wall viewed in the compression face of the FC1 crystal.　Primary dislocations with Burgers vector [011] are seen at A, [10$\bar{1}$] at B, [01$\bar{1}$] and [101] at C and reaction dislocation with Burgers vector [1$\bar{1}$0] at D.

dislocations.

The nature of the dislocation substructures as viewed in the compression, free and die faces of the FC2 crystals are shown in Fig. 5.4 (a-c). The first important feature in the micrographs belonging to the FC2 crystal is the absence of the arrangement of dislocations in equi-axed cells. Instead, the dislocations are arranged in major walls. In all three faces, alignment of the dislocation walls along the traces of primary slip planes is observed. A considerable number of dislocation loops and dipoles can still be recognized. The commencement or rearrangement of the dislocations into simpler configurations can be detected at A in all three faces (Fig. 5.4(a-c)). The increase in contrast across the dislocation walls indicates increase in misorientation compared to that in the FC1 crystal.

In the substructures developed at larger strains (≥ 0.5), the cell interiors become progressively cleaner. Most of the dislocations are arranged in major walls; the walls are no longer diffuse, similar to those at lower strains. Instead they are thin and can be termed subgrain walls. The general direction of these walls does not follow the traces of primary slip planes, but the alignment with the externally imposed pattern of flow increases with increasing strain. The scale of the dislocation substructure gets progressively refined and the misorientation across the boundaries increases with increasing strain. These features can be seen in Figs. 5.5(a-c) and 5.6(a-c) which represent the nature of the dislocation substructure in the three faces of the FC4 and FC6 crystals.
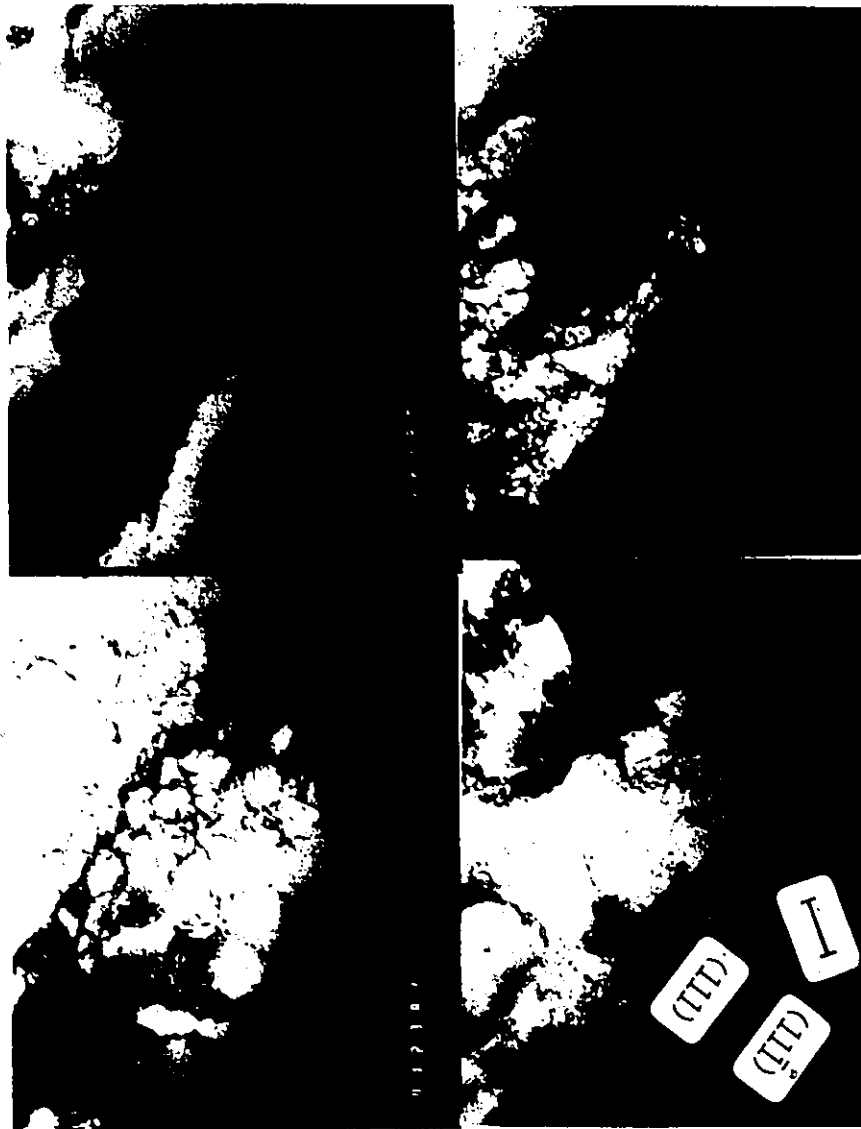
Fig. 5.4 (a)   Dislocation substructure as viewed in the compression
face of the "stable" crystal at strain 0.2.   Simple
configurations shown at A.   Micron marker is along
channel direction.   Traces of primary slip planes
are shown.
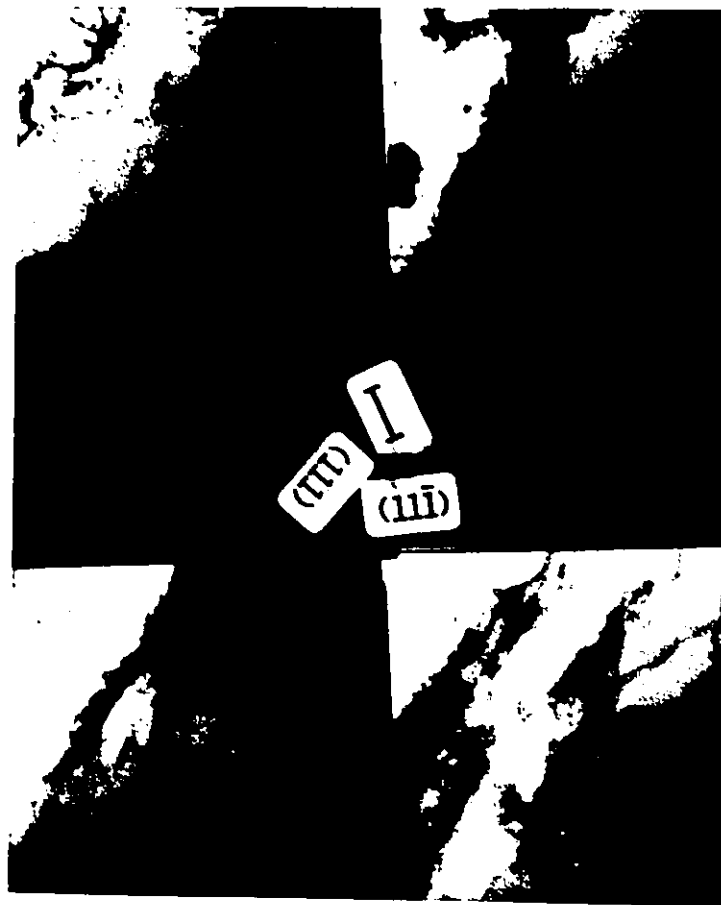
Fig. 5.4(b)   Dislocation substructure as viewed in the free face of
the "stable" crystal at strain 0.2.   Simple configura-
tions shown at A.   Micron marker is along the compres-
sion axis.   Traces of primary slip planes are shown.

.Fig. 5.4(c)   Dislocation substructure as viewed in the die face of
              the "stable" crystal at strain 0.2.   Simple configura-
              tions shown at A.   Micron marker is along the compres-
              sion axis.   Traces of primary slip planes are shown.

Fig. 5.5(a) Dislocation substructure as viewed in the compression
face of the "stable" crystal at strain ∿ 0.5. Micron
marker along the free direction. Traces of primary
slip planes are shown.

Fig. 5.5(b)   Dislocation substructure as viewed in the free face of
the "stable" crystal at strain ∿ 0.5.   Micron marker
along the compression axis.   Traces of primary slip
planes are shown.

Fig. 5.5(c)   Dislocation substructure as viewed in the die face of
the "stable" crystal at strain ∿ 0.5.   Micron marker
along the compression axis.   Traces of primary slip
planes are shown.

Fig. 5.6(a)   Dislocation substructure as viewed in the compression
              face of the "stable" crystal at strain ∿ 1.0.   Micron
              marker along the channel direction.   Traces of primary
              slip planes are shown.

5.6(b)

5.6(c)
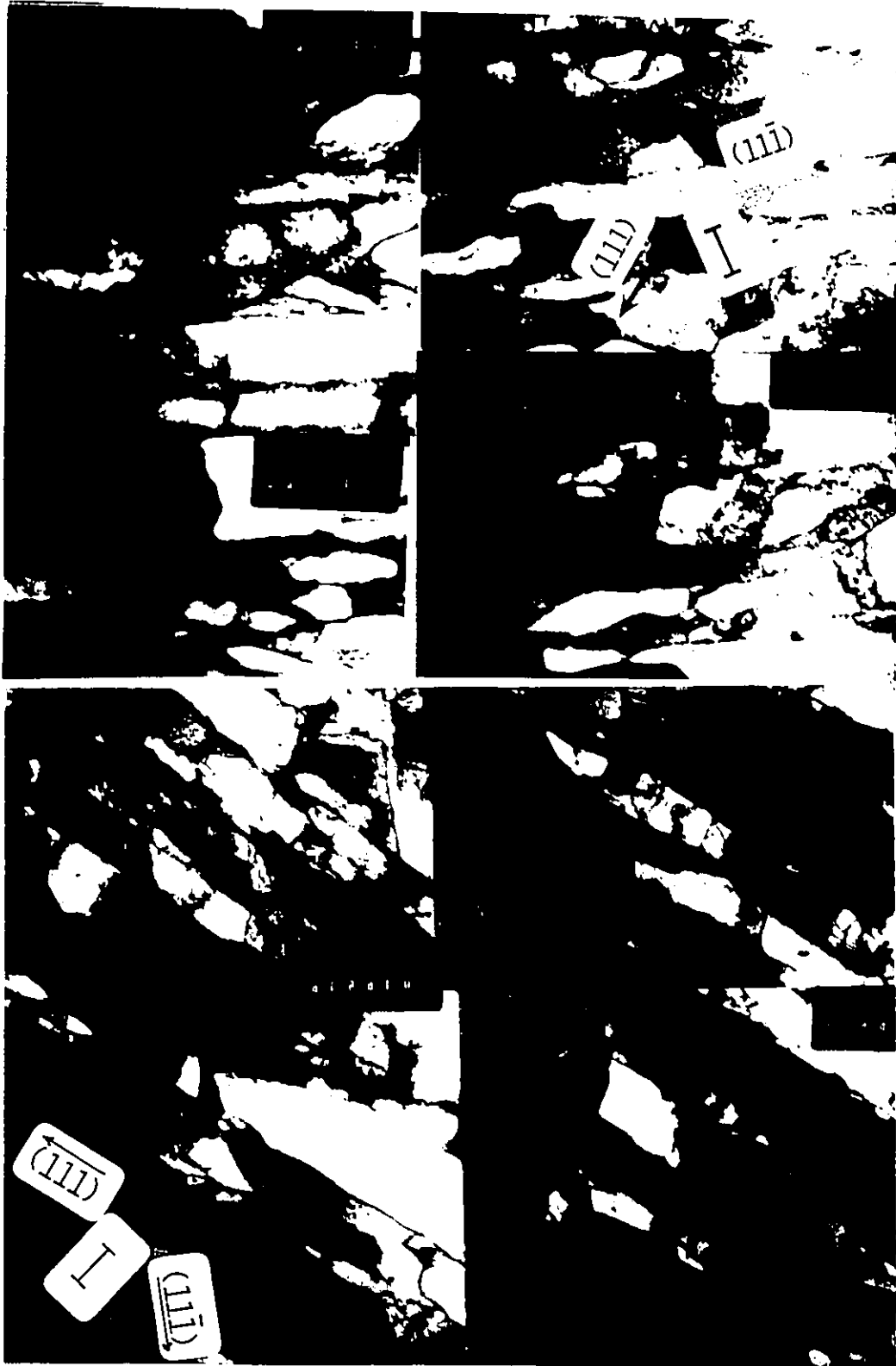
Fig. 5.6(b-c)   Dislocation substructure as viewed in (b) free and
(c) die faces of the "stable" crystal at strain
$\sim$ 1.0.   Micron marker along the compression axis.
Traces of primary slip planes are shown.

5.1.1 Variation of the Average Scale of the Dislocation Substructure and Misorientation with Strain in the "Stable" Crystal

The variation in the scale of the major walls and the smaller cells during deformation is given in Figs. 5.7 and 5.8, respectively. Data is given for compression and die faces. The scale is characterized by the length of the walls and the separation between them. The actual length of the major walls could not be determined because it extended beyond the observable thin areas of the thin foils. Therefore, only the separation between the walls is given in Fig. 5.7. The scale of the smaller cells present in between these major walls is given in terms of both their length and separation. The range of spacings measured at each level of strain is given.

The separation between major walls appears to reach a constant level beyond strain of 0.5 but the scale of the smaller cells continues to decrease over the strain range measured. Comparison with the scale of slip plane traces given in Chapter 4 indicates that the length of the slip bands is much larger than the size of the small cells, but at strain of 1.0, the separation between the slip bands is approximately equal to the separation between the cell walls.

The plot of misorientation across the major walls given as a function of strain in Fig. 5.9 shows that the degree of misorientation built up in the "stable" crystal is not large. The misorientation varies between $0.1 - 0.5°$ at a strain of 0.1 and between $0.5 - 2°$ at a strain of 1.0.

5.2 Nature of the Dislocation Substructure in the "Unstable" Crystal

The dislocation substructure developed in the HCl crystals as viewed from the compression, free and die faces is shown in Figs. 5.10
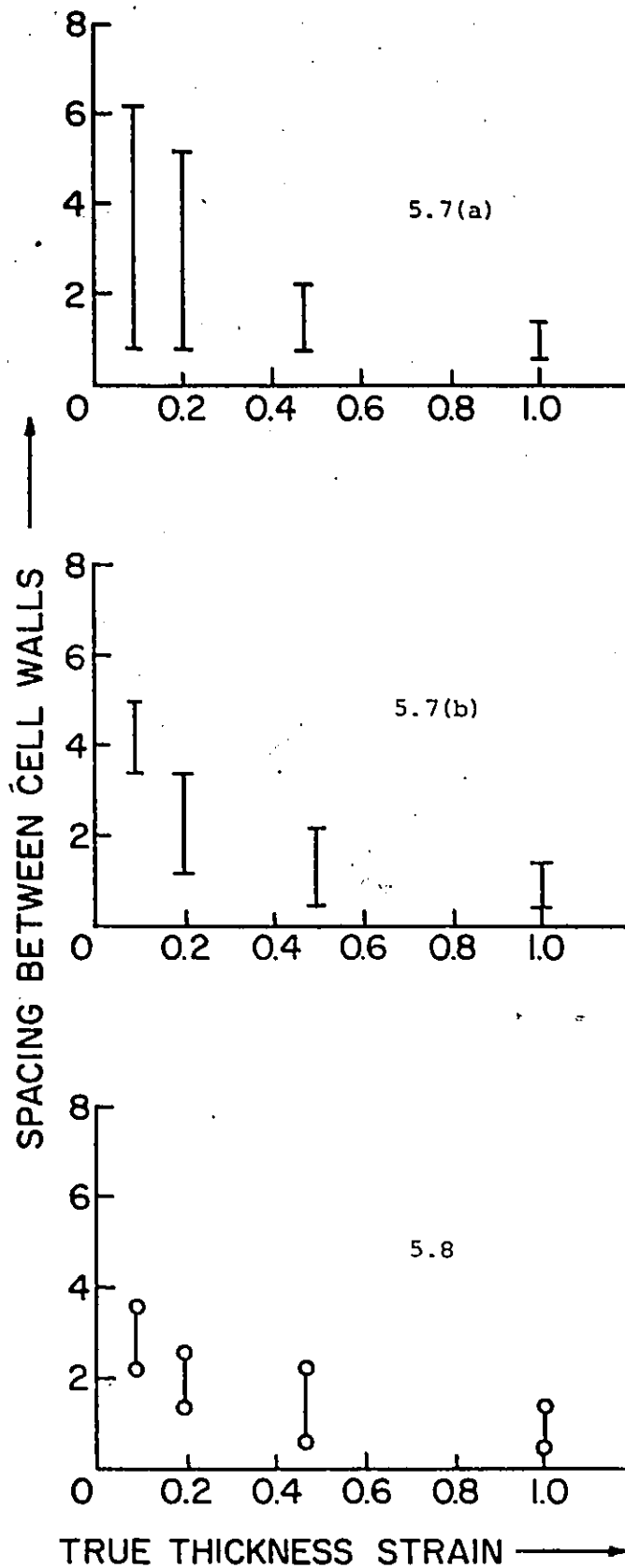
Figs. 5.7 and 5.8 Variation of the spacing between cell walls with strain. Fig. 5.7(a) refers to major walls on the compression face and Fig. 5.7(b) refers to major walls on die face. In Fig. 5.8, the spacing between smaller cell walls in the die face is given. Data at each level of strain refers to the range of spacing measured.
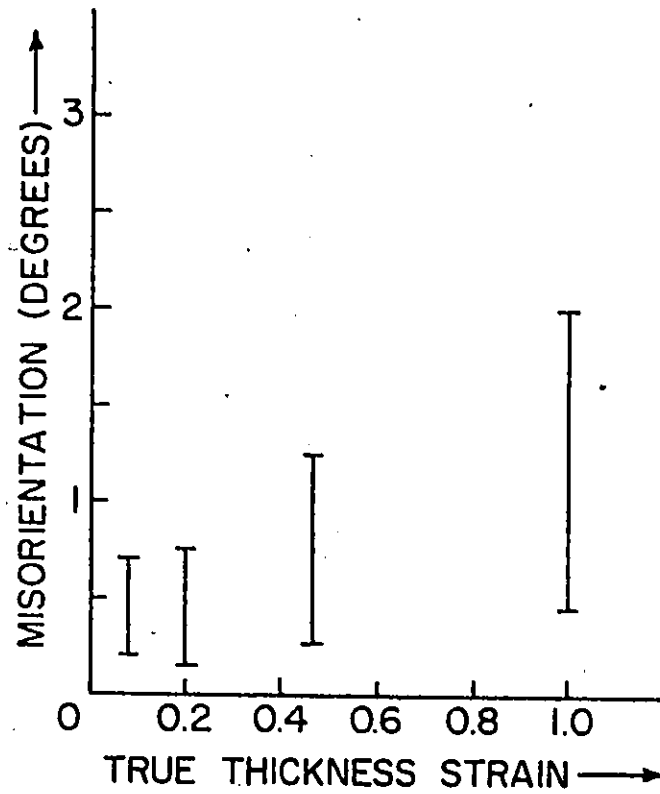
Fig. 5.9   Range of misorientations measured at different strain
levels in the "stable" crystal.

(a-c), respectively. It consists of a number of dislocation loops and
dislocations arranged into cell walls. However, the appearance of the
substructure depends on the direction of observation. The distribution
in the compression face is irregular, whereas in the die face the sub-
structure appears to be composed of neatly arranged walls. The most
striking feature of the dislocation substructure observed in the die
face shown in a magnified view in Fig. 5.11, is concerned with two dif-
ferent kinds of walls - viz.- thin walls (shown at A) in which the indi-
vidual dislocations cannot be distinguished, across which there are
marked changes in contrast and diffuse walls (shown at B) which occur
within the area bounded by these thin walls. In the diffuse walls, the
dislocations are arranged in a tangled form, individual dislocations can
be recognized, and the contrast does not vary very much across the walls.
The thin walls will be referred to as subgrain boundaries and the diffuse
walls as cell walls. The subgrain walls follow two major directions, the
traces of slip planes. Most of the cell walls are parallel to the sub-
grain walls and are also aligned along the slip plane traces. The mis-
orientation across the subgrain and cell walls is determined by studying
the variation in the Kikuchi line patterns.

The
range of misorientation present and the scale of the substructure will
be considered later.

When the dislocation substructure is viewed in the compression
face, some cell walls can be recognized to be aligned along the slip
plane traces, but in general there is no definite correlation between
the cell walls and the slip plane traces.

With increasing deformation it is observed that tangles of dislo-

Fig. 10(a-b)   Dislocation substructure viewed in the (a) compression
and (b) free faces of the "unstable" crystal at strain
0.1.   Micron marker is along the free direction in (a)
and compression axis in (b).   Traces of primary slip
planes are shown.

Fig. 10(c)   Dislocation substructure viewed in the (c) die face
of the "unstable" crystal at strain 0.1.   Micron marker
is along the compression axis.   Traces of primary slip
planes are shown.

Fig. 5.11 Nature of dislocation substructure developed at strain 0.1.
Thin walls at A are subgrain walls and diffuse walls at B
are cell walls. Magnified view of the substructure viewed
in the die face of the "unstable" crystal.

cations get converted into subgrains which constitute the major portion of the substructure. This can be seen in the micrographs from the compression, die and free faces of the HC2 and HC4 crystals (Figs. 5.12 (a-c) and 5.13 (a-c), respectively). In the compression face, the arrangements of the subgrain walls seem to be irregular, with no definite correlation with the slip plane traces. The subgrain interior is remarkably clear. In the compression face there is a wide variation in the subgrain size, almost by a factor of ten. The formation of subgrains is more obvious from the die and free face sections. Arrangement of dislocations in simpler configurations can be recognized as at A. In the free face the walls in general follow the slip plane traces. The variation in misorientation developed and the scale of the substructure with strain will be considered later.

Simple networks lying on slip planes chacterize the nature of the dislocation substructure. A magnified view of one such network is shown in Fig. 5.14. The network lies along the trace of primary slip plane. The misorientation across the network is less than 1°. With increasing misorientation, the nature of subgrain walls becomes more complicated. To study the configuration of dislocations in such walls, weak beam imaging technique was attempted. Fig. 5.15 represents a subgrain wall developed at strain 0.5 and imaged under weak beam conditions. Fig. 5.16 shows the same boundary imaged under dark field conditions. In general it was difficult to obtain good weak beam images. Proper diffraction conditions could not be obtained due to variation in orientation across the walls and the scale over which this misorientation occurs. This also made it difficult to determine the Burgers vectors present.

5.12(a)

5.12(b)

Fig. 5.12(a-b)   Dislocation substructure viewed in the (a) compression
and (b) free faces of the "unstable" crystal at strain
0.2.   Micron marker is along the free direction in (a)
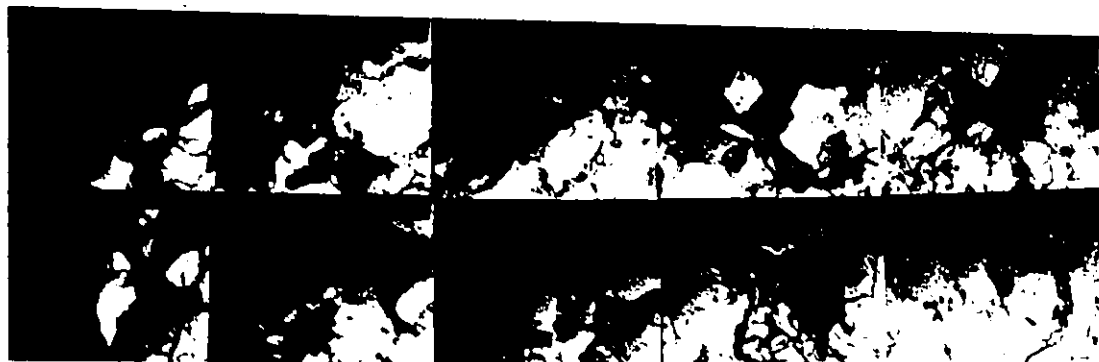and the compression axis in (b).   Traces of primary slip
planes are shown.

Fig. 5.12(c)   Dislocation substructure viewed in the die face of the
"unstable" crystal at strain 0.2.   Traces of primary
slip planes are shown.   Micron marker is along the
compression axis.
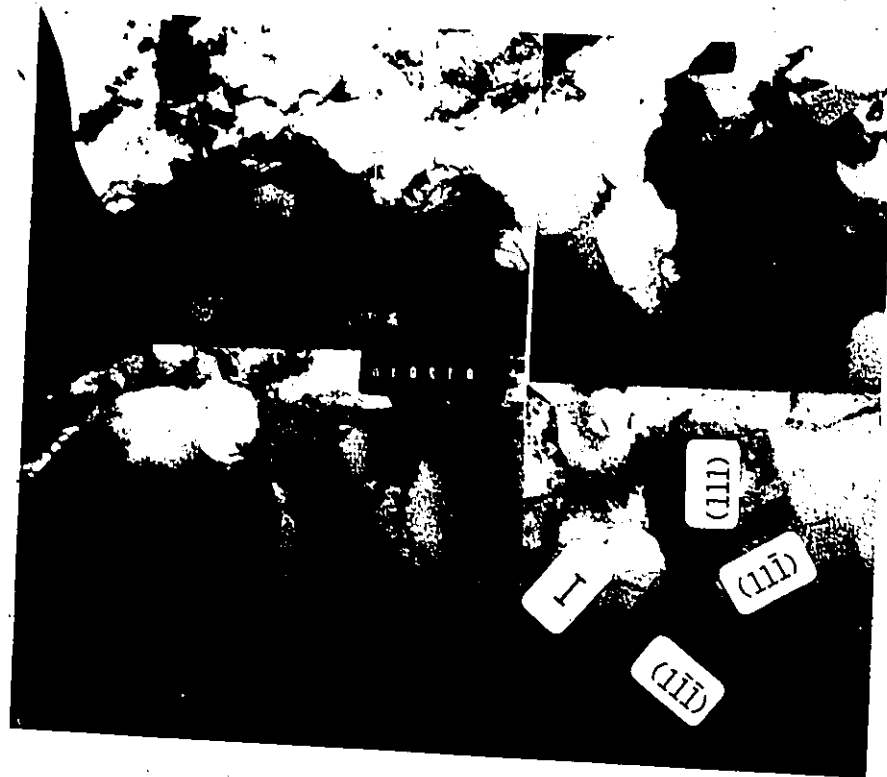
5.13(a)
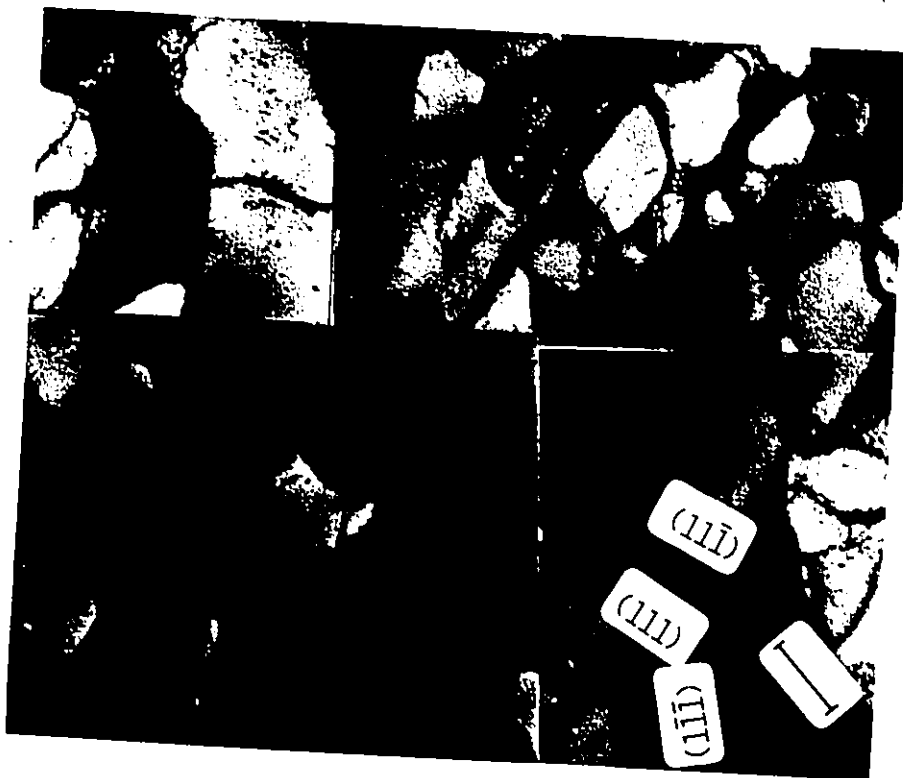
5.13(b)

Fig. 5.13(a-b)   Dislocation substructure viewed in the (a) compression
and (b) die faces of the "unstable" crystal at strain
0.5, showing well-defined subgrain walls. A wide
range of cell sizes is observed in the compression
face. Micron marker is along the free direction in
(a) and along the compression axis in (b).

Fig. 5.13(c) Dislocation substructure consiting of subgrains viewed
in the free face of the "unstable" crystal at strain
∿ 0.5. Micron marker is along the compression axis.
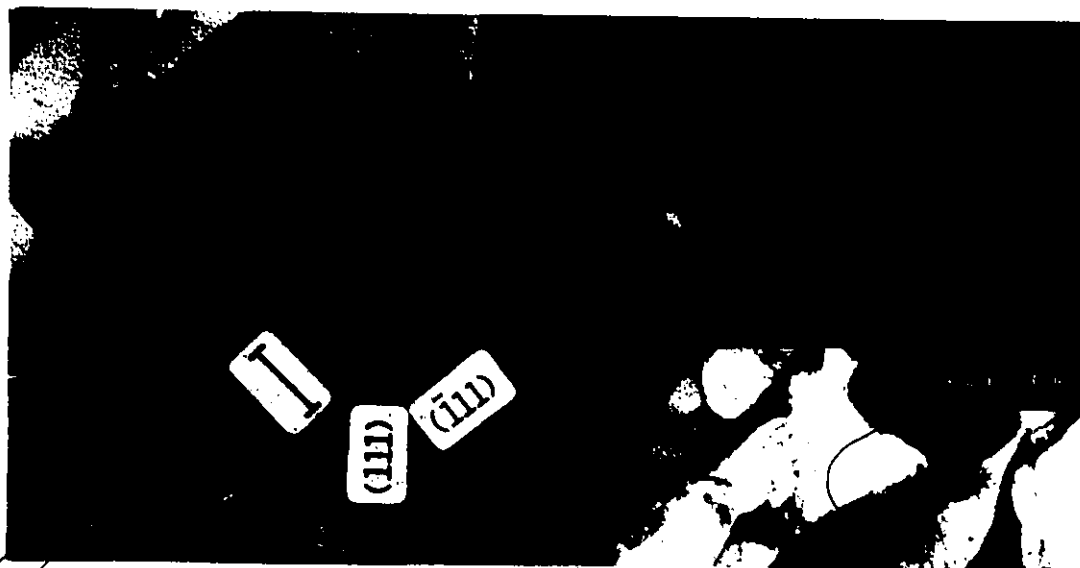Traces of primary slip planes are shown.
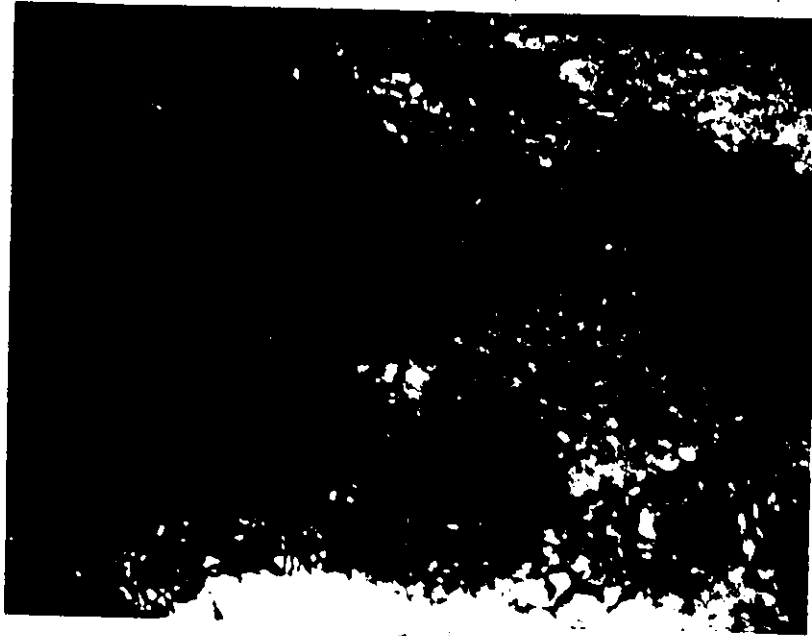
Fig. 5.14 Detailed view of the substructure developed at strain
0.2 illustrating formation of simple networks of dis-
locations.

5.15

5.16
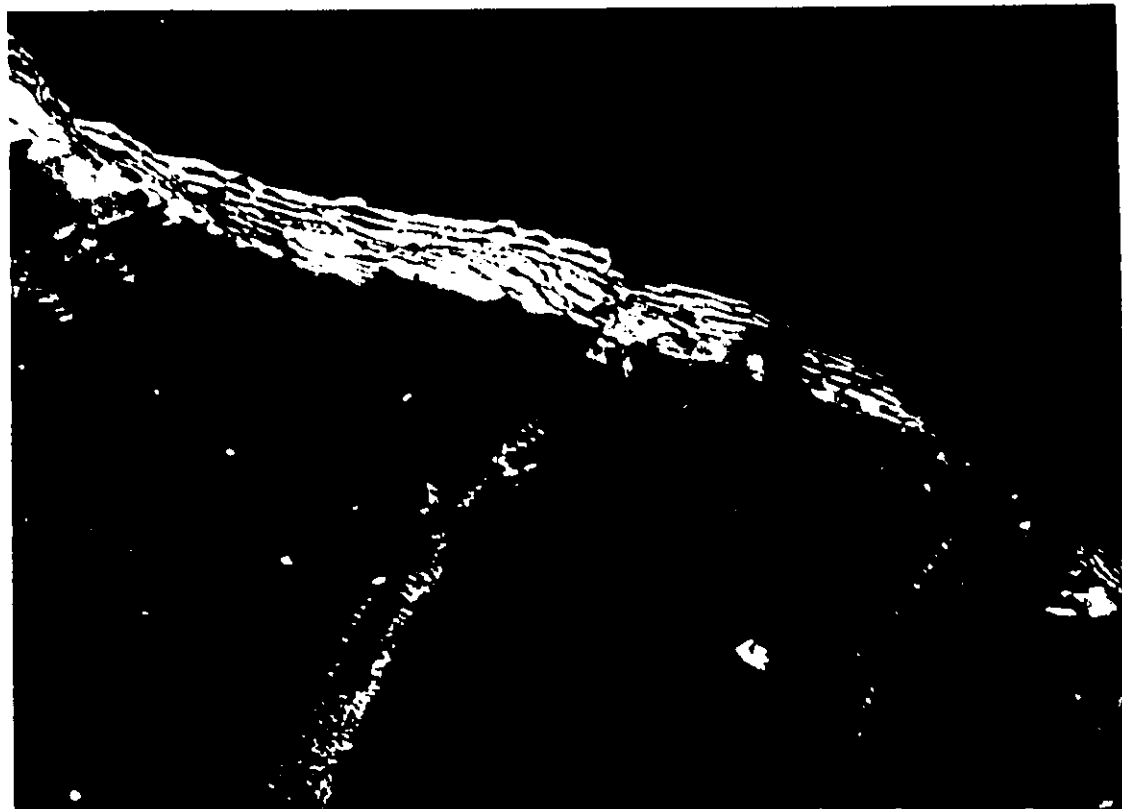
Figs. 5.15 Subgrain walls developed at strain 0.5 imaged under weak
and 5.16 beam conditions. The same wall imaged in dark field is
shown in Fig. 5.16.

The nature of the dislocation substructure developed at a strain of 1.0 in the "unstable" crystal is similar to the substructure developed at an equivalent strain level in the "stable" crystal, with respect to the scale and alignment of subgrain walls following the externally imposed pattern of flow. The micrographs taken from the compression, free and die faces of the HC6 crystal, shown in Fig. 5.17 (a-c) illustrate this aspect. The substructure is made up of long, subgrain walls with smaller cells present within the subgrains.

The width of the subgrains undergoes major reductions and becomes comparable to that of the smaller cells. This indicates that the cells are becoming progressively elongated parallel to the subgrain walls and that the majority of the dislocations are becoming incorporated into sub-grain walls.

5.2.1 Variation of the Scale of the Dislocation Substructure With Strain in the "Unstable" Crystal

The scale of the dislocation substructure is measured based on the length and width of the cells. These parameters are measured separately for subgrains and the smaller cells making up the subgrain interior. The length is measured along the long direction of the subgrain walls (corresponding to directions of slip plane traces up to strain of 0.5) and the width is measured along a perpendicular direction. The observed range in the length and width for the subgrains and cells are shown for the die and free faces in Fig. 5.18 (a-b). The length of the major walls (subgrains) appears to be almost constant at all strain levels. The data given for the length of subgrain walls is an approximation because of the reasons discussed earlier in section 5.1.
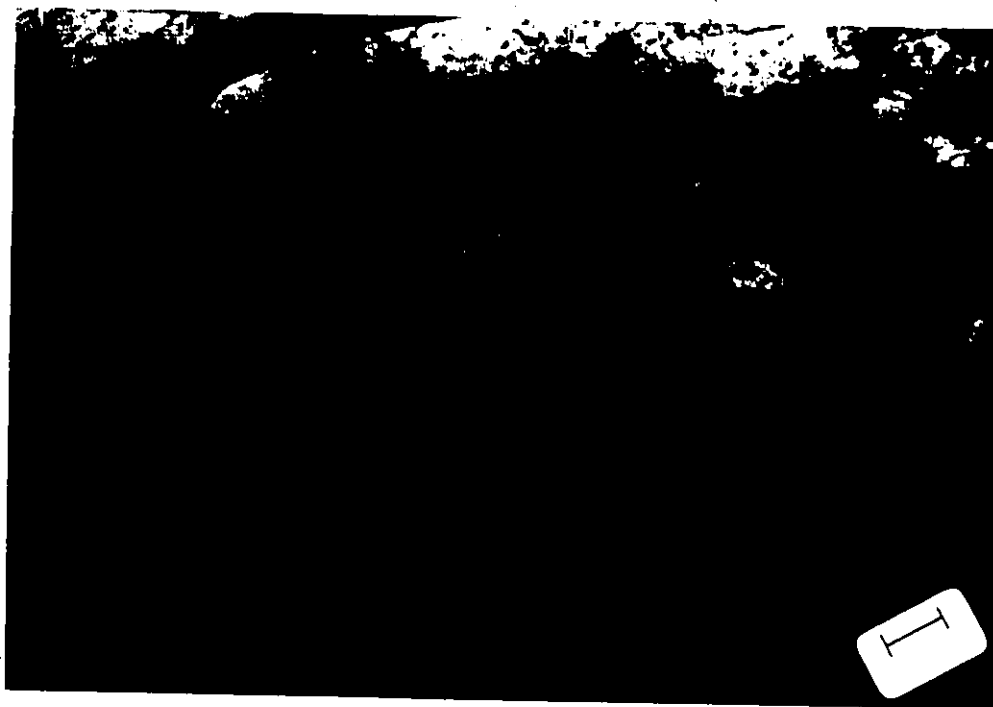
5.17(a)

5.17(b)

Fig. 5.17(a-b)   Dislocation substructure showing elongated subgrains
                 developed in the (a) compression and (b) free faces
                 of the "unstable" crystal at strain $\sim$ 1.0.   Micron
                 marker is along the free direction in (a) and along
                 the compression axis in (b).

Fig. 5.17(c)   Dislocation substructure developed in the die face at
strain of ~ 1.0.   Micron marker is along the free
direction.
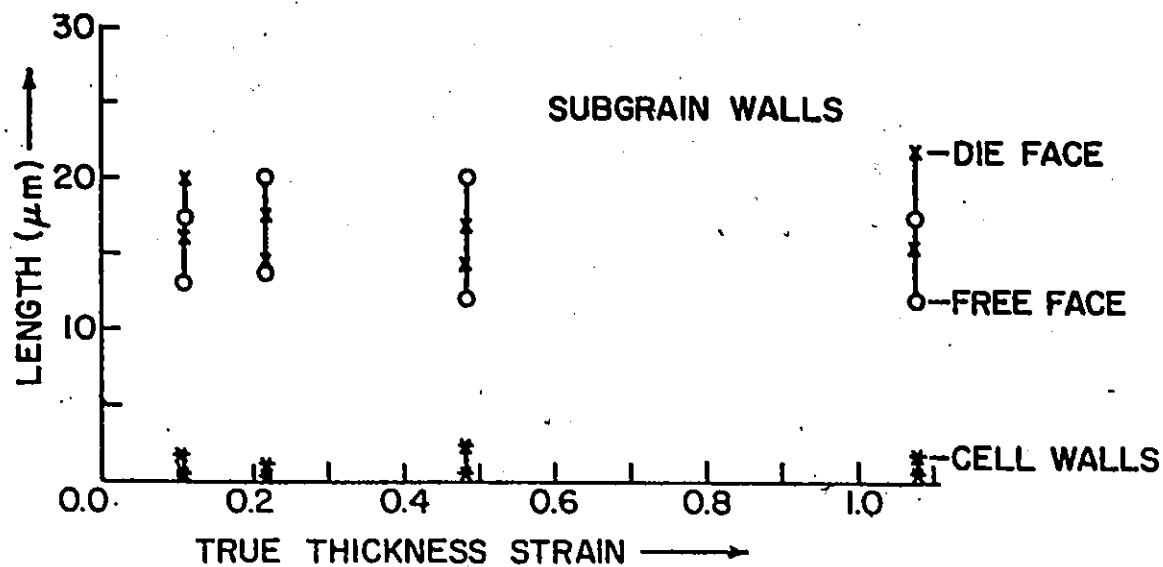
5.18(a)
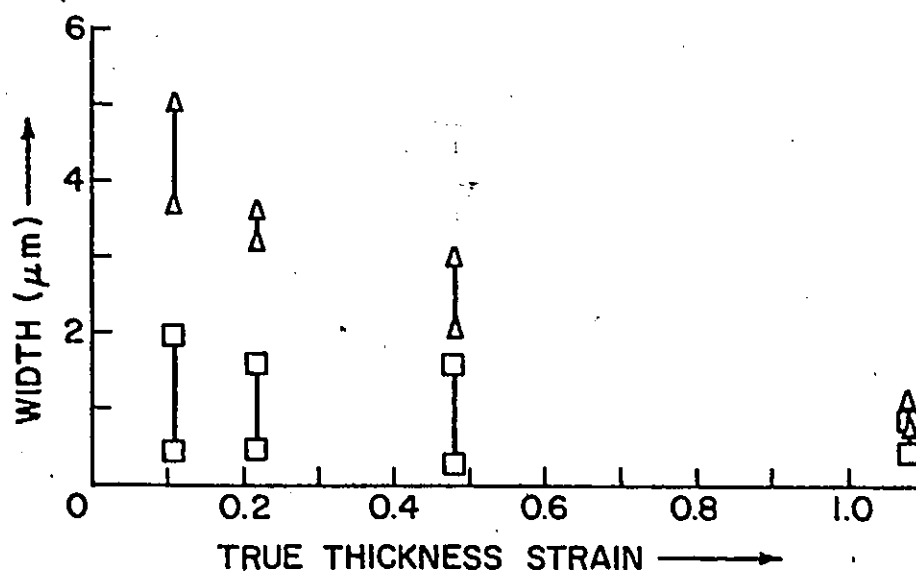
5.18(b)

Fig. 5.18(a)   Variation of the length of the subgrains and
                cells with strain in the "unstable" crystal.

      (b) Variation in the width of the subgrains   (— Δ —)
            and   cells   (— □ —) with strain in the "unstable"
            crystal.

The width of the subgrains decreases with increasing strain, and at strain of 1.0 it correlates with the spacing between the observed slip plane traces. The quantitative data concerning the scale of the substructure was obtained from the die face and free faces which gave mutually consistent data.

5.2.2 Variation of Misorientation with Strain – Development of High Angle Boundaries at Large Strains in the "Unstable" Crystal

The average misorientation increases with increasing strain across both the subgrain walls and cell walls. Data for the free face is shown in Fig. 5.19 (a-b). Misorientation in general oscillates as one traverses across the cell walls up to strain of 0.5 indicating no large accumulation of misorientations. Such oscillations in misorientation with distance traversed are shown in Fig. 5.20 at strain of 0.5.

But striking differences were observed during detailed investigations of the dislocation substructure developed at strain 1.0 in the compression face. High angle boundaries accommodating misorientations of approximately 30° are observed. These were apparent only after detailed investigations of the orientations of individual subgrains, as there is no major difference in the scale of the substructure between those regions bounded by high angle boundaries and those bounded by subgrain boundaries of misorientation 0.5 to 2.0.

The high angle boundaries are numerous when viewed in the compression face. A detailed composite of the corresponding dislocation substructure with the associated diffraction patterns are shown in Fig. 5.21. Only two orientations are recognized, these being (1$\bar{1}$1) and [0$\bar{1}$1]. The (1$\bar{1}$1) orientation which was the initial orientation of the crystal was observed to be retained by the compression face throughout
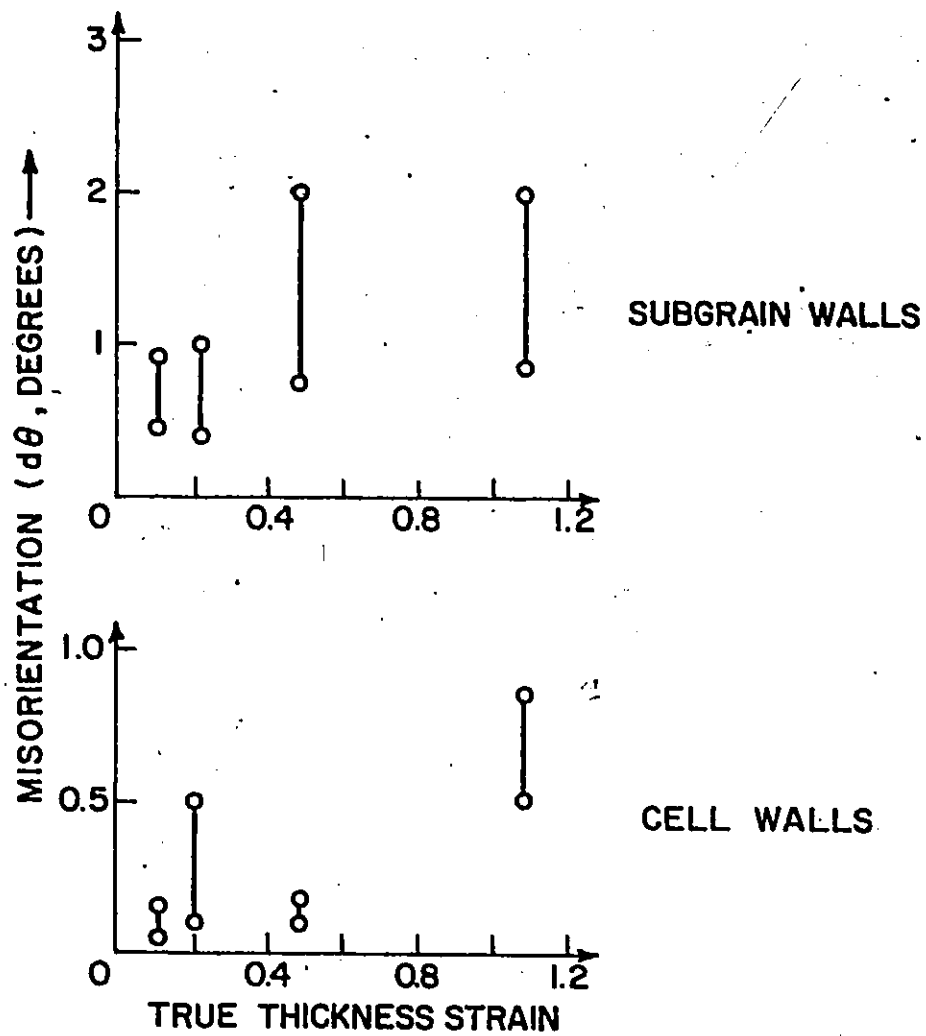
Fig. 5.19 Variations of misorientation with strain in the "unstable" crystal. Data at each level of strain indicates the range of misorientations present.

(a)

(b)
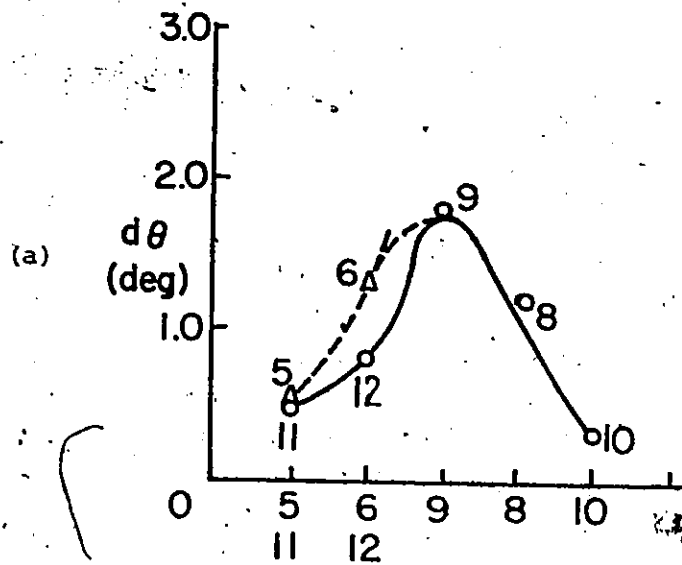
$d\theta$: Deviation from [$\bar{1}$12] orientation; numbers on x axis refer to number of the cell traversed.
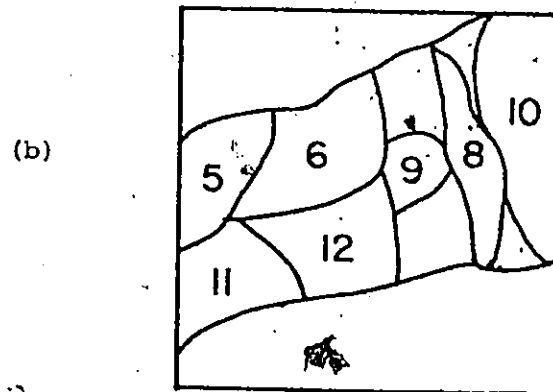
Fig. 5.20 Schematic illustration to indicate that the level of misorientation oscillates. In (a) the degree of misorientation and in (b), the position of the corresponding subgrains are shown.

6
5
3
8
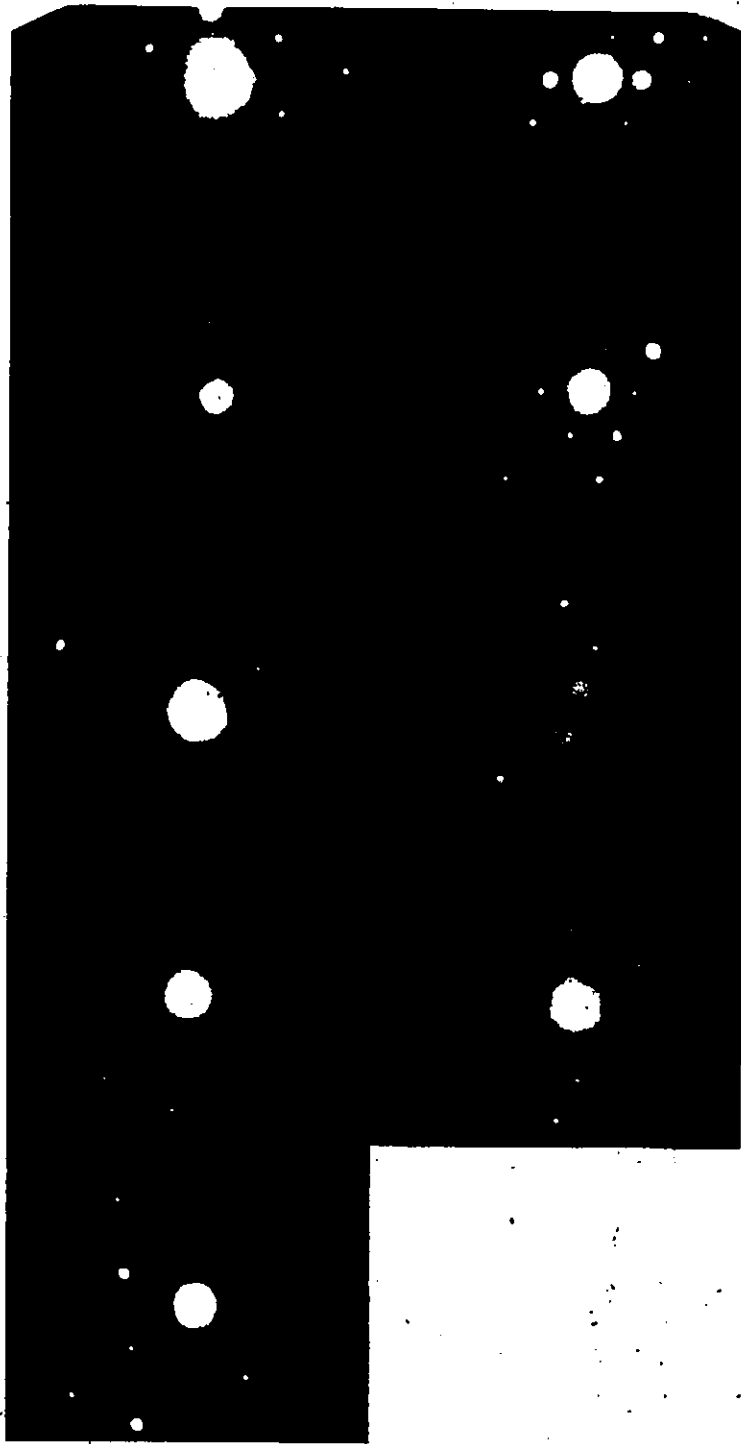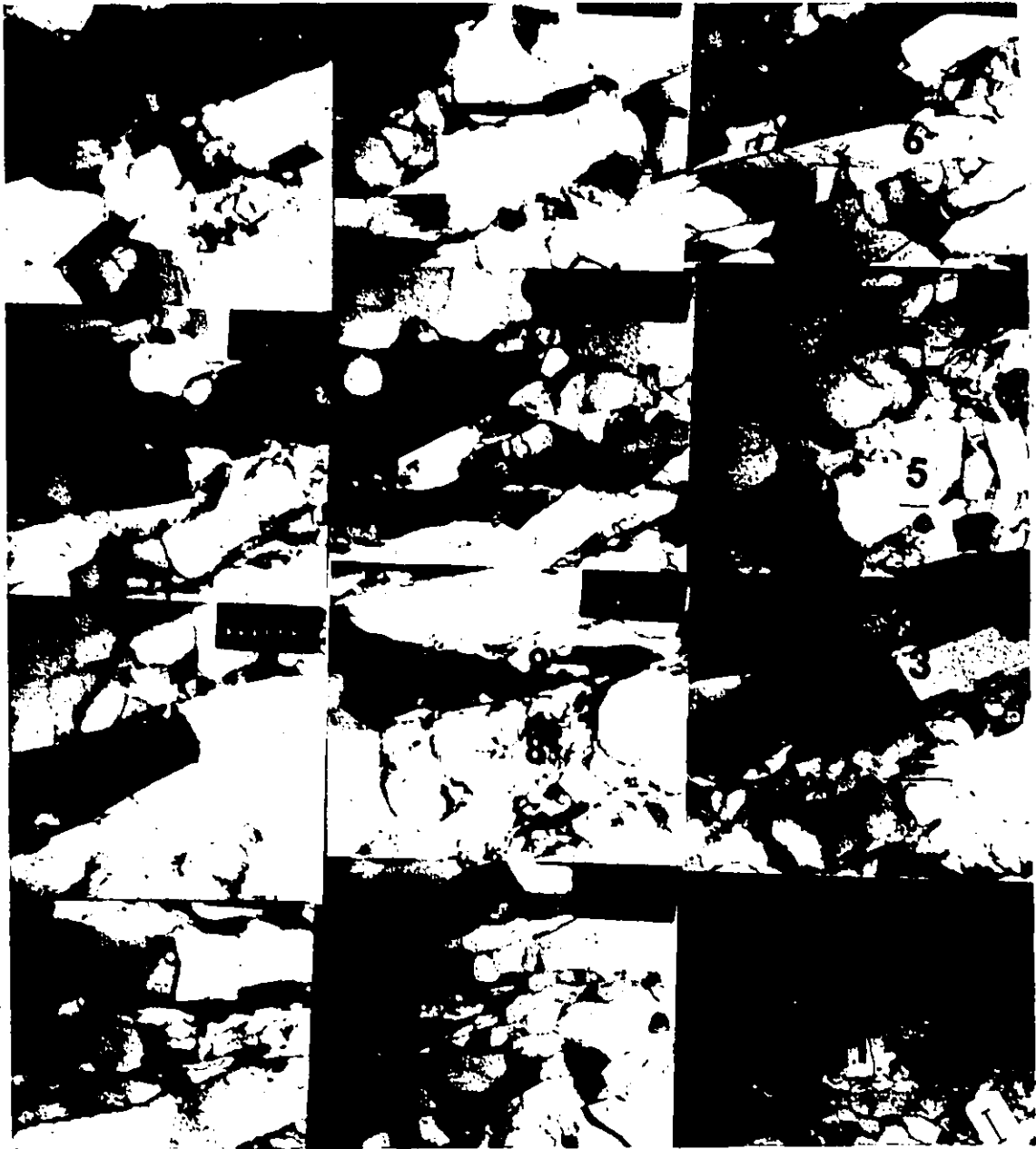
Fig. 5.21(a-b) Detailed view of the substructure as viewed in the compression face of the "unstable" crystal at strain $\sim$ 1.0, indiciating presence of regions of $(0\bar{1}1)$ orientations amidst regions of $(1\bar{1}1)$ orientation. Regions of $0\bar{1}1$ orientation are observed only at the current level of strain. Diffraction patterns taken from within the regions indicated, are shown in Fig. 5.21(b) on the facing page.

the deformation of the "unstable" crystal. The regions with 011 orientations were observed only at this strain level. These are separated from the regions of (1$\bar{1}$1) orientation by high angle boundaries. These highly misoriented regions denoted by A are about 1 - 2 µm wide, approximately 10 µm long and are spaced nearly 5 - 10 µm apart. Two special features connected with these large misorientations are:

(1)   The nature of misorientation is similar across all the observed high angle boundaries.

(2)   The change in orientation occurs abruptly across a single boundary instead of being accommodated over a number of subgrains as within transition bands.

The first aspect is apparent from the diffraction patterns shown in Figs. 5.21 and 5.22. Fig. 5.22 illustrates diffraction patterns taken at the high angle boundary and from within a subgrain close to the boundary. The diffraction pattern taken across the boundary contains both the 1$\bar{1}$1 and 0$\bar{1}$1 orientations and the reflections 022 are common to both. This shows that the rotation axis has a [011] component in the compression face. Diffraction patterns taken from within subgrains on either side of the boundary correspond to either 1$\bar{1}$1 or 0$\bar{1}$1 type.

Detailed analysis of the misorientations developed in the substructure observed in the channel face (perpendicular to the channel direction) is shown in Fig. 5.23 along with a map indicating the distribution of orientations. Mainly two orientations, {112} and {110} types, are observed. The change in orientation occurs across single subgrain boundaries, e.g., subgrains L and M are of [$\bar{1}$12] type orientation whereas the subgrain B located in between L and M is 110 type; similarly subgrains K and O are
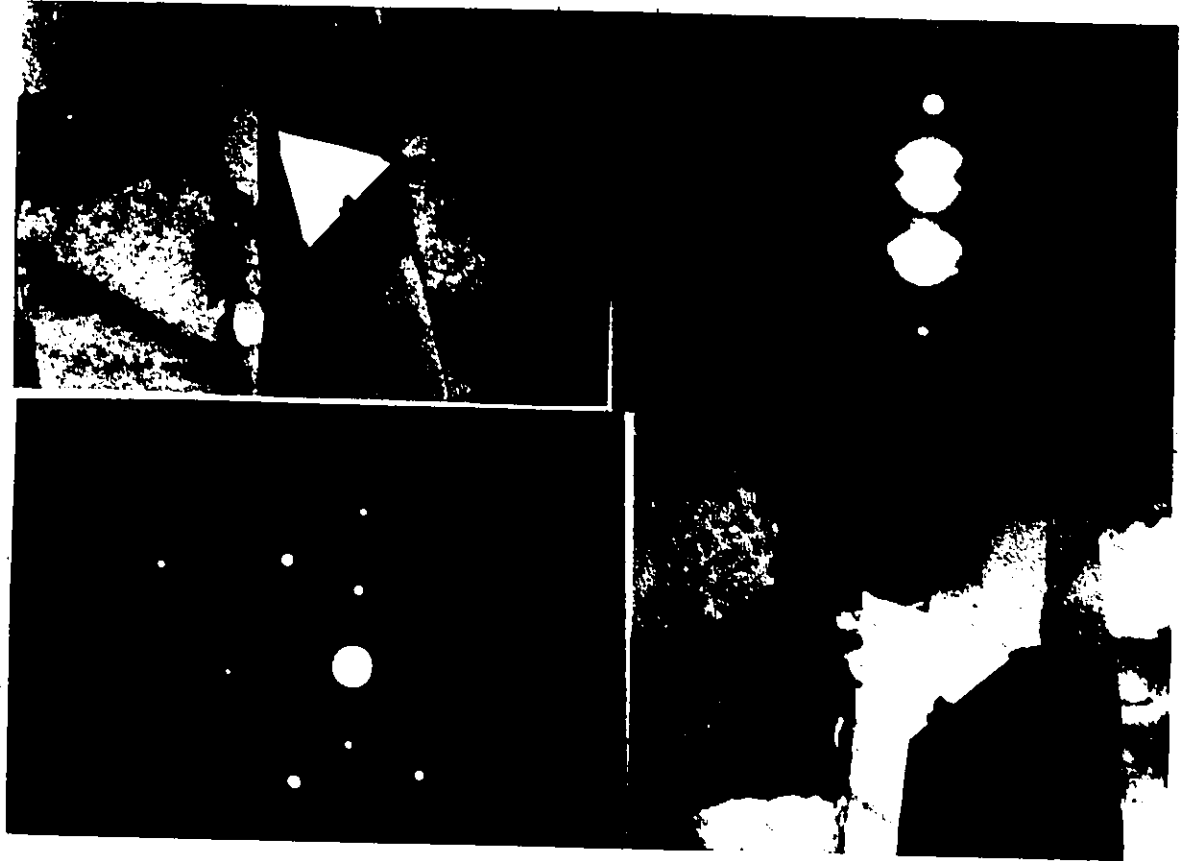
Fig. 5.22 Micrographs illustrating abrupt change in orientation
across a subgrain boundary indicating presence of high
angle boundaries in the substructure developed at
strain 1.0 in the "unstable" crystal. Aperature size
used for taking the diffraction patterns is shown.
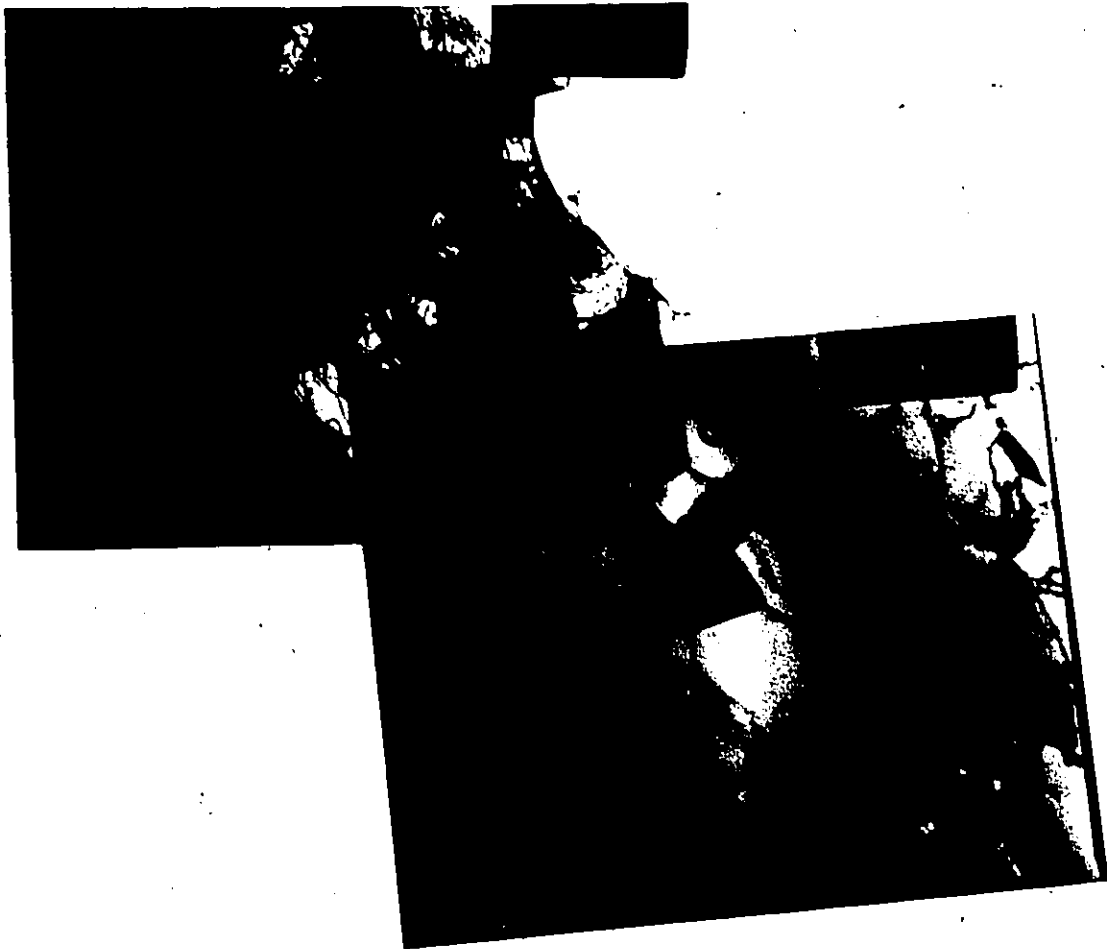
Fig. 5.23 Micrographs illustrating the presence of high angle
boundaries in the dislocation substructure viewed in the
channel face of the "unstable" crystal at strain 1.0.
Boundaries between subgrain L-B, B-M, K-E and E-O are
high angle boundaries. Orientations of these subgrains
are discussed in the text.

of the 112 type whereas E has 110 type orientation. Thus, the scale

and distribution of the regions bounded by high angle boundaries are

different when observed in different sections of the crystal.

While the transmission electron microscope enables a detailed

investigation of the nature of the misorientations associated with areas

in the submicron range, the total amount of area available for observation

is extremely small. Thus, it is difficult to investigate the spatial dis-

tribution of the highly misoriented regions in the deformed crystal.

Observations in the optical microscope of surfaces suitably prepared

to indicate the differences in orientation are more appropriate to study

such distributions. Results of these investigations along with a brief

summary of the thermal stability of the dislocation substructure during

subsequent recovery and recrystallization of the deformed crystals will

be discussed in the next chapter.

CHAPTER 6

THERMAL STABILITY OF THE DISLOCATION SUBSTRUCTURE - RESULTS

OF ELECTRON AND OPTICAL MICROSCOPY OBSERVATIONS

In this chapter, the influence of subsequent recovery and recry-

stallization treatments on the form of the dislocation substructure of

the deformed crystal will be considered. No kinetic studies were made;

but a comparison was made of the substructural changes caused by both

thermal and dynamic recovery.

The spatial distribution of the high angle boundaries (discussed

in Chapter 5) was investigated by examining the anodized surface of the

crystal using polarized light in an optical microscope. Results of

these investigations and observations of the role played by these high

angle boundaries during subsequent recrystallization will be presented.

Recrystallization was followed by both optical microscope investigations

of bulk annealed samples and attempts at in-situ observations in the

transmission electron microscope. The nomenclature adopted in Chapter 5

to distinguish the crystals will be used in this section.

6.1   Results of Recovery and Recrystallization Experiments
       as Observed in T.E.M.

The effect of thermal annealing on the nature of the dislocation

substructure was studied in the transmission electron microscope after

bulk annealing slices about 1 mm thick, spark cut from the deformed

samples. The recovery annealing treatment was usually carried out at

100°C for one hour and the observations were limited to the compression plane unless otherwise specified.

The nature of the dislocation substructure in the "stable" crystals - FC1, FC2 and FC4 in both the deformed state and after thermal recovery are shown in Fig. 6.1 (a-f). It can be seen that in crystals deformed up to strain of 0.2, the tangled nature of dislocations in the cell walls which is characteristic of the deformed condition become rearranged into simpler configurations. The high density of dislocation loops appears to have decreased and the interior of the cells becomes clear. At large strains the configurations of dislocations in the substructure is not greatly influenced by thermal recovery as seen from a comparison of Figs. 6.1 (c) and 6.1 (f).

Annealing at 100°C for one hour appears to exert little influence on the nature of the dislocation substructure developed during deformations up to strain 0.5 of the "unstable" crystal. Representative micrographs of the thermally recovered substructure along with that in as-deformed condition for the HC2 crystal are shown in Figs. 6.2 (a) and (b). The nature of the substructures according to Figs. 6.1 (a-f) and 6.2 (a-b) indicate that similar changes in the dislocation arrangements are caused by both thermal and dynamic recovery. The influence of thermal recovery is most marked at low strains, where the dislocation arrangement in the as-deformed condition resembles tangles. At larger strains, where the extent of dynamic recovery appears to have been greater, as indicated by cleaner substructures with dislocations arranged in cell walls and subgrain walls, the influence of subsequent thermal recovery is much less. Though such short-term recovery treatments did not produce any major changes in the average cell size or
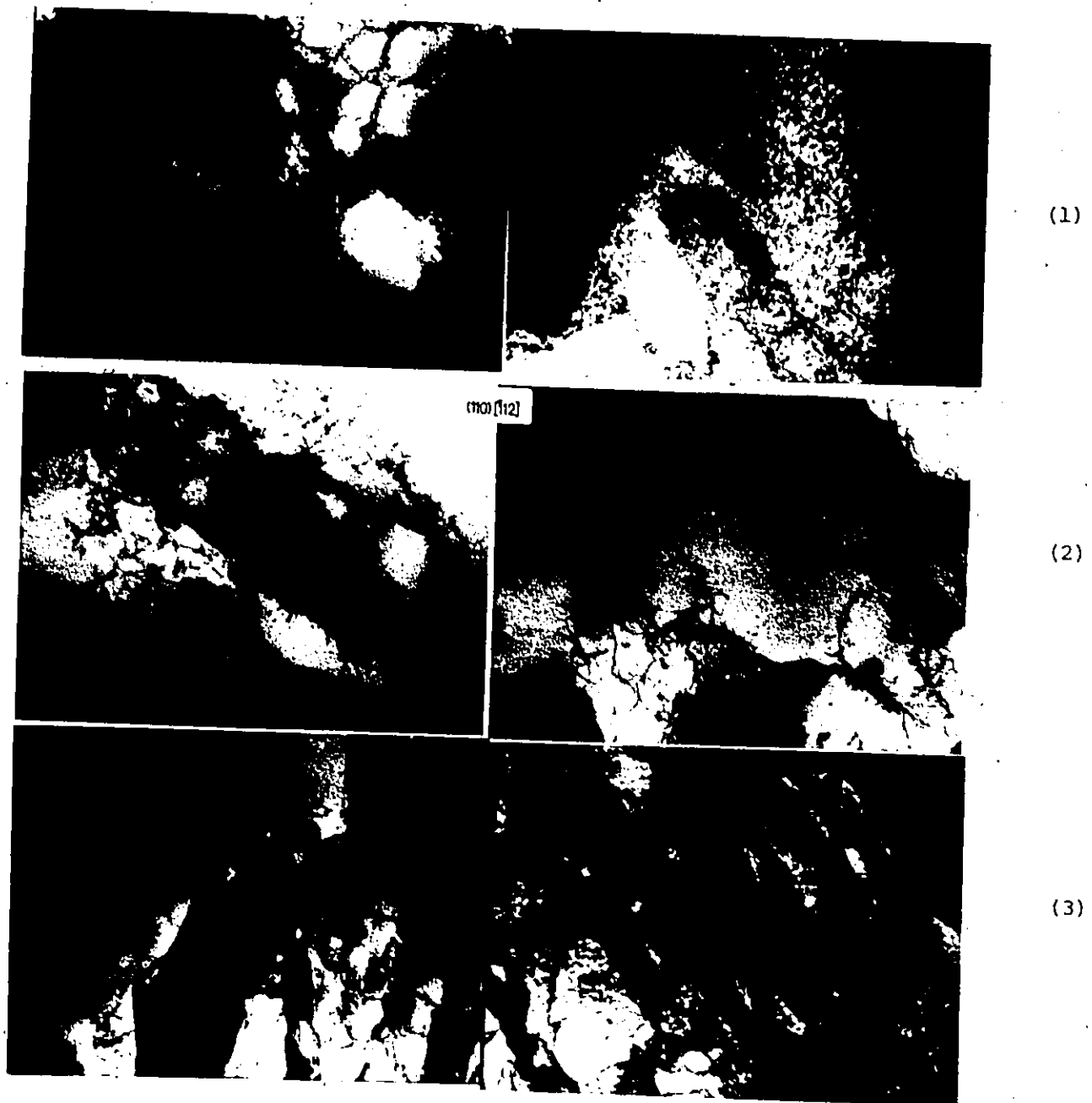
Fig. 6.1 Effect of thermal recovery on the nature of the substructure
as viewed in the compression face of the "stable" crystal.
Micrographs at left refer to the substructure in the as-deformed
condition; those at right to the recovered structure.
Strain: (1) 0.1 (2) 0.2 (3) 0.5
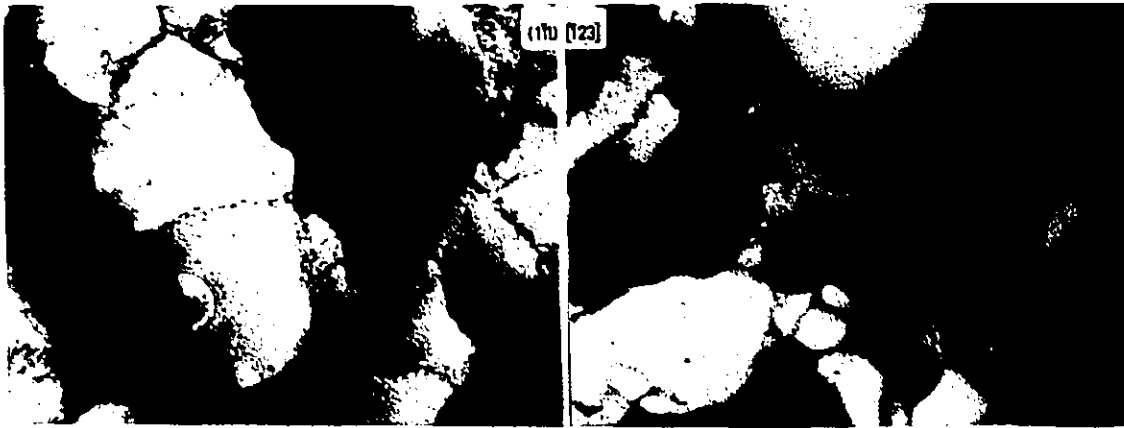
Fig. 6.2 Substructure developed in the "unstable" crystal at strain 0.2
in the as-deformed condition (at left) and after thermal
recovery (at right), illustrating that no major changes occur
due to thermal recovery.

misorientation, striking changes were observed in the dislocation sub-
structure when the "unstable" crystal deformed to strain 0.5, was
stored for long periods (of nearly one year)   at room temperature.
The corresponding substructure shown in Fig. 6.3 reveals development of
regions of new orientation. Regions characteristic of the ($1\bar{1}1$) orienta-
tion (the only component observed immediately after deformation) are
observed along with regions having ($0\bar{1}1$) orientation. The orientations
that are present are identical in nature to the large misorientations
observed in the HC6 crystal, which was described in Chapter 6. The main
difference between the substructures seen in Fig. 5.22 of the HC6 crystal
and Fig. 6.3 of the HC4 crystal is the difference in the average size
of the misoriented regions. The scale of the regions with [$0\bar{1}1$] orienta-
tion in the HC4 crystal is larger by a factor of ten than the region of
($1\bar{1}1$) orientation, while the two regions had the same average scale in
the HC6 crystal. This indicates that the [$0\bar{1}1$] regions in the HC4
crystal have grown in scale accomplished by localized migration of the
high angle boundaries.   /

6.1.1 Results of Recrystallization Experiments

    In order to study the influence of these high angle boundaries
on the recrystallization behaviour, HC4 and HC6 samples of the "unstable"
crystal were subjected to bulk annealing at higher temperatures. It was
observed that complete recrystallization had occurred after annealing
the HC6 crystal for 5 minutes at 250°C and the HC4 crystal for 5 minutes
at 350°C. Many new grains with [$0\bar{1}1$] orientations were recognized in
the thin foils of these annealed samples when observed in T.E.M. No
dislocation substructure characteristic of the deformed condition could
be observed.
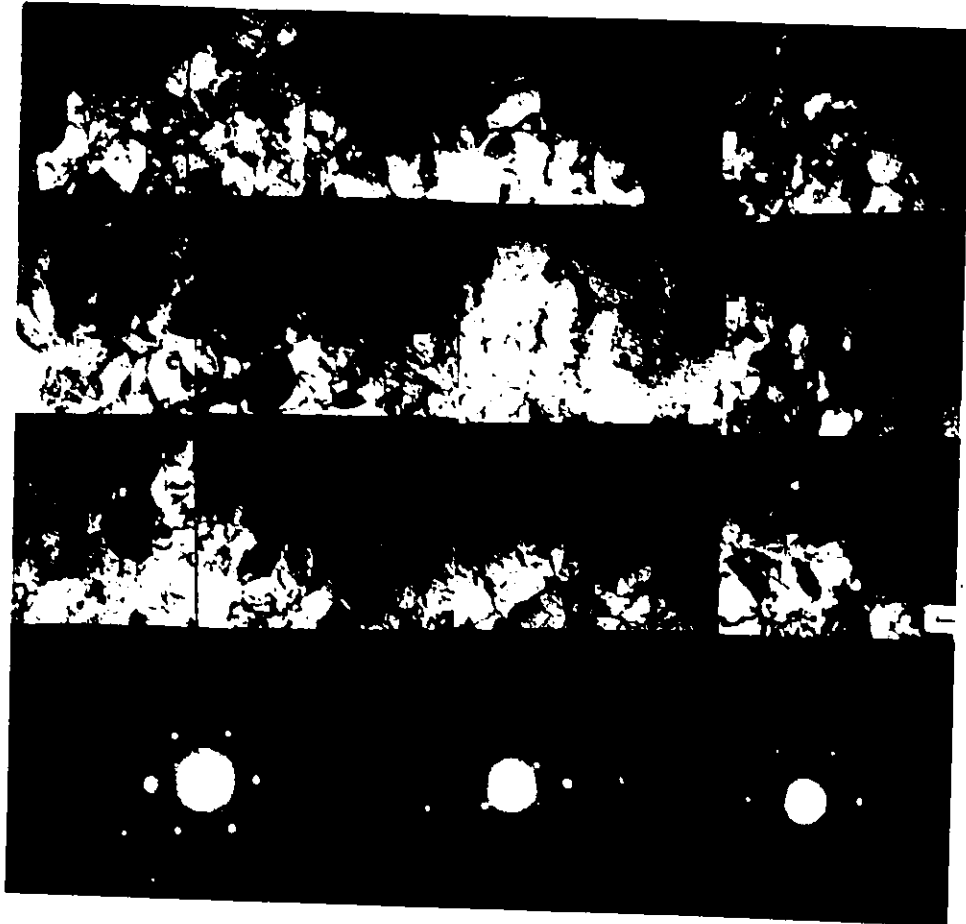
Fig. 6.3 Changes observed in the substructure of the "unstable" crystal
due to storage for long period at room temperature. Diffraction
pattern taken with wide S.A.D. aperatures in indicated areas.
Face: compression; Strain: 0.5

6.1.2 Results of In-Situ Annealing Experiments

The bulk annealing experiments described in the previous section shows that the orientation of the recrystallized grain was observed in the as-deformed crystal. In order to examine whether recrystallization started within the [0$\bar{1}$1] oriented regions observed in the as-deformed condition, in-situ experiments were carried out on thin foils of the HC4 crystal on the hot stage of T.E.M. The temperature of the foil was slowly raised to 100°C and was maintained constant for periods of 1/2 - 1 hour at 100°C and subsequently higher temperatures up to 500°C. Some subgrain coarsening was observed, but no recrystallization was observed even when the foil was heated to nearly 500°C. Because the rate of heating is one of the factors influencing the recrystallization behaviour of thin foils (Sehgal et al., 1975), the temperature of the thin foil was raised to 500°C within 10 minutes. Recrystallization was observed to set in, in the [0$\bar{1}$1] oriented regions. The process was complete within a span of ten seconds and could not be photographed.

6.2 Anodizing Experiments

Anodizing experiments were conducted in order to obtain the following information:

(1) to observe the distribution of the high angle boundaries in the HC4 and HC6 crystals over the entire surface of the crystal,

(2) to be able to relate the distribution to the scale and pattern of the slip plane traces observed on the surface, and,

(3) to investigate the role of these boundaries during subsequent annealing processes.

The regions with large misorientations can be recognized by the colour contrast in the anodized film when observed under polarized light. The

technique of anodizing and the possible origins of the colour contrast
are described in Appendix 2. Observations were done in the Zeiss ultra-
phot optical microscope and were limited to the compression plane of the
deformed sample unless otherwise specified.

6.2.2 Results of Observations

The microstructure observed in the HC6 crystal in the as-deformed
condition is shown in Fig. 6.4. Numerous small regions about 10 μm long
and a spacing of 10 μm apart, aligned close to the free direction are
observed. The larger regions may have developed due to the coalesence
of the smaller regions as can be seen from the composite micrograph of
Fig. 6.5. Only two colours are observed over the entire area indicating
that the structure in the crystal consists of mainly two orientations,
in accordance with the observations made by T.E.M. As a check, similar
observations were conducted on an identical section of the virgin
"unstable" crystal and "stable" crystal deformed to strain 1.0 and no
such highly misoriented regions were detected. -

The influence of thermal annealing was studied by successively
annealing the HC4 crystal at 180°C, 200°C and 250°C. The microstructures
of the sample before and after annealing are shown in Fig. 6.6. The
corresponding periods of annealing are indicated.

·Marked differences can be observed due to annealing at higher
temperatures. These may be summarized as follows. Small grains appear
amidst the deformed structure after annealing for 2 minutes at 180°C.
The highly misoriented regions observed in Fig. 6.6 (a) appear to grow
in size by coalescence of the smaller regions during the annealing
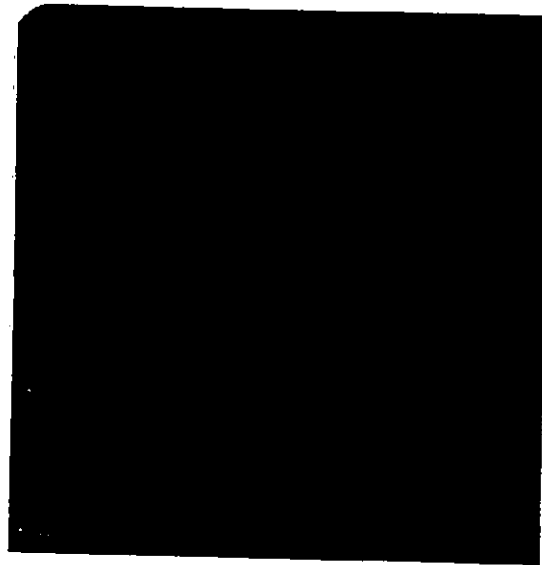
6.4(a)
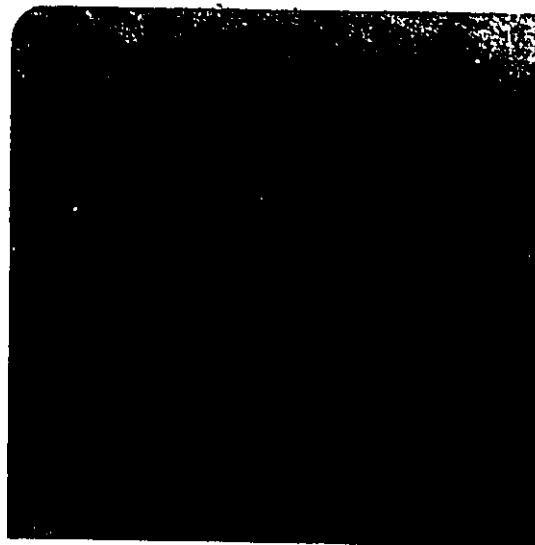
6.4(b)

Fig. 6.4(a-b)   6.4(a) - optical micrographs of the anodized surfaces
of the "unstable" crystal indicating presence of
regions of different orientations in the compression
face at strain 1.0. No such regions are observed in
the compression face of the "stable" crystal at strain
1.0 in 6.4(b). Magnification 30x..
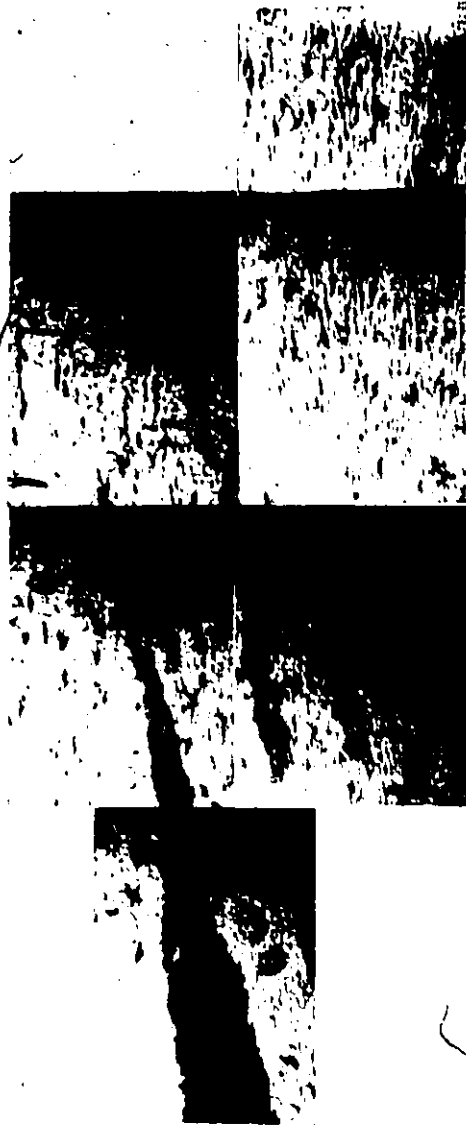
Fig. 6.5 Composite optical micrograph of the anodized surface of
the "unstable"ccrystal indicating regions of different
orientations. Arrow is along the channel direction.
Face: compression; Strain: 1.0
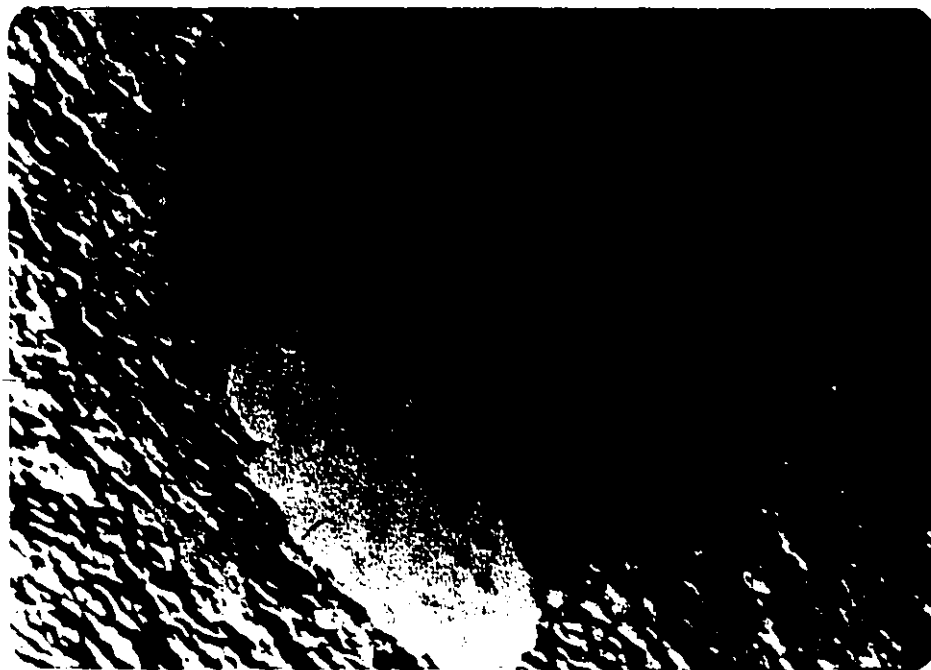
6.6(a)

Fig. 6.6 (a-d) Micrographs of the anodized surface of the
"unstable" crystal illustrating effects of
annealing. Face: compression; Strain: 0.5
(a) after annealing for 2 mins. at 180°C
(b) and (c) show coalescence after 2 mins.
at 200°C (d) new grains appear due to recry-
stallization (1 min. at 250°C). Mag. 30x.

6.6 (b)
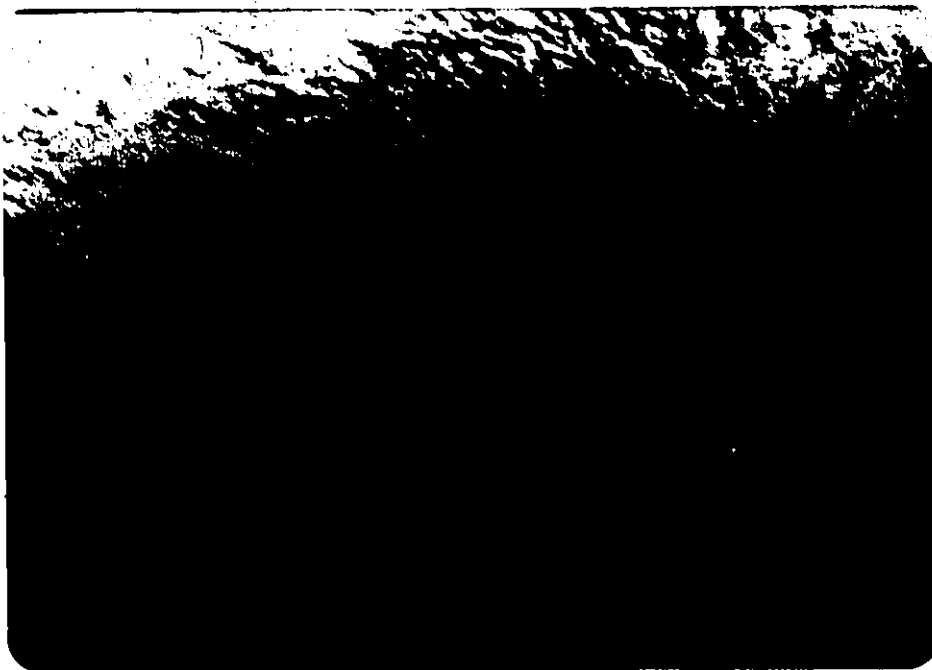
6.6 (c)

6.6(d)

process, as seen in micrographs 6.6 (c) and 6.6 (d). Finally, the entire sample appears to have recrystallized after annealing for 1 minute at 250°C. No regions characteristic of the deformed structure could be detected at this stage. One artifact which may obscure recrystallization studies is the nucleation of new grains at the surface. Beck and Hu (1966) observed this phenomenon when the surface of an aluminum sample rolled to 80% reduction was abraded with emergy paper before annealing. In the present experiments care was taken to try and avoid such surface nucleation by minimizing the mechanical damage of the crystal prior to annealing. The damaged area caused by spark cutting was removed by electro-polishing.

The results discussed so far indicate that the high angle boundaries are produced at large strains, only in the "unstable" crystal. The scale of the regions bounded by the high angle boundaries and the characteristics of the dislocation substructure within these regions indicate that the high angle boundaries must have been produced during deformation. These regions bound by the high angle boundaries act as nuclei for subsequent recrystallization. The origin of these high angle boundaries will be discussed in Chapter 7.

CHAPTER 7

DISCUSSION OF THE RESULTS OF THE
OBSERVATIONS OF DISLOCATION SUBSTRUCTURE

In this chapter; the observations presented in Chapters 5 and 6 regarding the nature of the dislocation substructure developed during large strain deformations, will be discussed. The salient features of the results are summarized at the beginning of the chapter. Various aspects of these observations will be examined in order to clarify the following points:

(1) the evolution of the nature and geometry of the substructure,

(2) the influence of initial crystal orientations on the similarities and differences in the resultant substructure,

(3) the comparison of the scale of the substructure with the scale of slip,

(4) the substructural changes occurring due to thermal and dynamic recovery, and,

(5) the origin of the high angle boundaries in the crystal of "unstable" orientation.

Any comparison between the results of investigations which use transmission electron microscopy with the observations of the surface assumes that both types of observations reflect the behaviour of the bulk of the material. Detailed investigations of the nature of the substructure in the submicron range is possible only in the transmission

Summary of the salient features of the dislocation
substructure observed in "stable" and "unstable" crystals.

	"Stable" Crystal	"Unstable" Crystal
1. Nature of dislocation substructure at strain = 0.1	Equiaxed arrangement of dislocations into cells bounded by walls resembling tangles; beginning of three-dimensional walls can be recognized at major cell walls; high density of dislocation loops and dipoles.	Thin subgrain walls + diffuse tangles; high density of dislocation loops and dipoles.
strain = 0.2	Cells with cell walls in which dislocations are arranged in simple configurations	Subgrain walls + cell walls; clean subgrain interiors.
strain = 0.5	diffuse cell walls + subgrains; clean subgrain interiors	Subgrains with clean interiors.
strain = 1.0	Subgrains with clean interiors.	Subgrains with clean interiors.
2. Alignment with primary slip traces	At low strains, cell walls are arranged along primary slip plane traces. Tangles are not. With increasing strain ($\geq$ 0.5) direction of substructure deviates from the traces of active slip planes.	Nature of alignment is dependent on section observed. Good correlation observed up to strain 0.5. At larger strains substructure follows direction of externally imposed pattern of flow.
3. Variation of the scale of the substructure with strain.	In both the crystals, the scale of the substructure is refined during deformation; the scale decreases more rapidly at the initial stages than at later stages of deformation.	
4. Variation of misorientation with strain.	The average misorientation increases during deformation.	
5. Effect of thermal recovery for 1 hour at 100°C.	Marked influence up to strain 0.2; not much influence at strains > 0.2.	No marked influence of thermal recovery.
6. Special characteristics at large strains.	Dislocation substructure follows externally imposed pattern of flow. No large misorientations.	Dislocation substructure aligned along externally imposed pattern of flow; high angle boundaries with misorientation of 33° are observed at strain 1.0 in as-deformed condition.

electron microscope and where possible these observations have been

supplemented by investigations using the optical microscope. The

results obtained in the present work are explained based on some simple

models and where possible, are correlated with the evidence available

in the literature.

The deformation behaviour at large strains is complex and complete

understanding of the nature of the substructure developed is still not

possible. The results of the current investigations indicate specific

problems associated with large strain deformations. Suggestions for

further studies are made at the end of the chapter.

7.1 The Evolution of the Substructure

As the observations of the dislocation substructure were carried

out in the T.E.M., on thin foils prepared from deformed crystals, it

is important to consider whether the nature of the substructure observed

reflects a relaxation of the dislocation arrangement present in the

deformed crystal and whether it is influenced by rearrangement during

the thinning process.

Malin and Heatherly (1979) recently concluded that the cell

structure in rolled copper must have developed due to relaxation. This

was based on the observation that the scale and shape of the cell struc-

ture observed in edge sections did not vary between strains of 0.05 and

3.5. However, in their study it was observed that flow was restricted

to regions within microbands, the nature of which changed during deform-

ation. In the present work it was observed that the scale of the dis-

location substructure decreases with increasing strain as shown in

Figures 5.7 and 5.20. Also, tangles and cells are observed to coexist

at low levels of strain and these become converted to subgrains at large

strains. These features indicate that gross rearrangement does not occur during the thinning process. Support for this view is also available from the work of Swann (1963), McQueen and Hockett (1970) who observed that in aluminum deformed to a given level of strain, the scale of the dislocation substructure was a function of the deformation temperature. Loss of dislocations is possible during thinning and can be inferred by considering the nature of the substructure near the edge of the foil. The differences that are usually observed are that the substructures near the edge of the foil have cleaner cell interiors and thinner cell walls. In the present investigations, this was particularly apparent in the "stable" crystal deformed to strain of 0.1. Therefore, where possible, investigations of the substructure were carried out in areas away from the edge of the thin foil. Free dislocations were seldom observed. They must either be lost to the surface during thin foil preparation or incorporated into the cell walls. Evidence from literature (Young and Sherill, 1967; Mughrabi, 1968, 1971; Ambrosi et al., 1978) indicates that no major differences are observed in thin foils prepared from deformed crystals which were neutron irradiated before unloading the sample, so as to pin the existing arrangements of dislocations. This leads to the conclusion that cellular arrangement of dislocations occur in the as-deformed condition. The evolution of the cellular arrangement due to the elastic interaction between dislocations stored during deformation has been discussed in Chapter 2.

·7.1.1 The Geometric Arrangement of the Dislocation Substructure

The tangels observed in the compression face of the "stable" crystal at strain 0.1, deviate from the common trace of the primary slip planes (Figure 5.1). They appear to be threading between the primary

slip planes, corresponding to the geometric model of building up cell structure proposed by Steeds (1966).

There is some similarity in the "stable" and "unstable" crystals with respect to the correlation between the substructure and the slip plane traces. Up to strain of 0.5, the cell walls and/or subgrain walls constituting the substructure are aligned along the traces of active slip planes. At larger strains they deviate from these traces and tend towards alignment with the direction of externally imposed pattern of flow. In the "stable" crystal clear deviation from the slip plane trace is observed when the substructure is viewed in the compression face. The alignment of the general direction of the subgrain walls with the imposed direction of external flow is more marked in the "unstable" crystal. These observations suggest that cell walls are developed on the slip planes during the early stages of deformation; at later stages they rotate conforming to the imposed shape change. At large strains cell walls and subgrain walls alignment with the external direction of flow has also been observed during wire drawing, rolling etc., (Langford and Cohen, 1969; Slakhorst and Tien Bonwhuijs, 1977).

Micrographs in Figures 5.6 and 5.17 show that at large strains, the cells and subgrains get elongated along the free direction and that the number of cell walls running perpendicular to the major subgrain walls is reduced. This could occur as a consequence of extensive dynamic recovery. Following Langford and Cohen (1969), f, the fraction of the initial number of cells observed at strain 0.1, remaining at later stages was calculated. The fraction, f, increases at strain 0.2 indicating creation of more cell walls and decreases slightly at larger strains indicating some loss of cell walls. These calculations were

restricted to the number of cells observed in the free face of the "unstable" crystal, as well-defined cell walls could be observed even at strain of 0.1 (Figure 5.10).

7.1.2 Uniformity of the Substructure

The distributions in the sizes of the cells and subgrains present in the substructure developed at various strains in the "stable" and "unstable" crystals are shown in Figures 5.7 and 5.18. At low strains, there is a wide variation in the cell size, varying between 2 to 8 μm at a strain of 0.1 in the "stable" crystal. Nonuniformity in the scale raises two important questions:

(1) the validity in using the average parameter of cell size to correlate with the flow stress, and,

(2) the associated distribution in misorientations.

The latter factor has important implications in the recrystallization behaviour of materials deformed to large strains and will be considered later.

The various empirical relationships that are in use to describe the current level of flow stress in terms of the average cell size were discussed in Chapter 2. The effectiveness of the cell walls as barriers to mobile dislocations will be considered by correlating the scale of the substructure relative to the length of the slip plane traces.

7.1.3 Correlation Between the Scales of the Substructure and Slip Plane traces

Comparison of the data in Figure 4.9(a-b)   with data in Figures 5.7 and 5.18 indicates that the length of the slip plane traces observed is much larger than the scale of the substructure   in the "stable" crystal at low strains. When the slip plane traces are nearly 200 μm

long, the diameter of the cells is of the order of 5 μm. At large

strains, when the spacing between the cell walls is about 1/2 to 1 μm,

the slip line length varies between 10 - 50 μm. Similarily, in the

"unstable" crystal, the length of slip plane traces is much larger than

the spacing of the cell walls, the difference being larger at low strains.

Long slip plane traces were observed on the surface of "stable" crystals

rolled to 90% thickness reduction (Hu et al., 1966). Slip plane traces

longer than average cell size has also been observed by Thompson et al.

(1974). These results indicate that cell walls are not effective barriers

to mobile dislocations in the same way as high angle grain boundaries.

The spacing of the cell and subgrain walls correlates better with

the minimum spacing of the slip plane traces. This is true especially

at large strains, for both orientations. At lower strains, the spacing

between cell walls is smaller compared to the average spacing of slip

plane traces. It is possible that not all the slip plane traces are

observed in the present investigations, which are based on optical micro-

scopy. Using the replica technique, Malin and Hatherly (1979) were able

to measure slip plane traces of spacing 0.03 μm which correlated with the

scale of the dislocation free regions within the cells.

In correlating the scales of the slip plane traces and of the dis-

location substructure, the changing nature of the alignment of the cell

walls during deformation must be considered. At low strains, the cell

walls being parallel to the slip plane traces must have developed as

debris left behind by mobile dislocations on the slip planes. Long slip

plane traces could develop easily at this stage. Only at large strains

when the subgrain walls are rotated away from the active slip planes

the mobile dislocations will move essentially between the subgrain walls.

At this stage the spacing between the slip plane traces correlates
with the separation between the subgrain walls. The cell walls present
in between the subgrain walls are characterized by low misorientation
and may not be effective barriers to dislocation motion.

At large strains extremely coarse and wavy slip plane traces were
observed on the surfaces of the "stable" crystal, the width of individual
traces corresponding to the average cell size.

7.1.4 Variation of Misorientation During Deformation

Investigation of the accumulation of misorientation with strain
across the cell walls and subgrains is important both with respect to
the effectiveness of the subgrain walls as barriers to dislocation
motion and with respect to their role during any subsequent recrystalli-
zation process. Data presented in Chapter 5 indicates that in general
the average misorientation across the dislocation walls increases with
increasing strain, indicating accumulations of excess dislocations at
pre-existing cell walls. It must be noted that at all strain levels
the substructure consists of walls across which the degree of misorien-
tation is small ($\simeq 0.5°$). This could be caused by the production of
new walls continuously during deformation. It is also possible that
some areas of the substructure become inactive during further deforma-
tion, in the sense that no new slip is generated near these walls and
hence there is no accumulation of dislocations. At large strains, mis-
orientations of the order of 30° develop in the as-deformed "unstable"
crystal. The nature and origin of such large misorientations will be
discussed in Section 7.3.

7.2 Similarities in Dynamic and Thermal Recovery

The detailed investigation of the substructures presented in Chapters 5 and 6 indicate that with increasing strain, the extent of dynamic recovery increases in both the crystals. The observations that should be emphasized are the following:

(1) subgrains develop at a lower strain in the "unstable" crystal compared to "stable" crystal, and,

(2) both thermal and dynamic recovery treatments lead to similar structural changes, i.e., cleaner subgrain interiors and simpler walls.

In relation to the first point, micrographs in Figure 6.1 reveal striking differences in the nature of the substructures up to a strain of 0.2 in the "stable" and "unstable" crystals; the substructure in the "stable" crystal being composed of tangles and cells and that in the "unstable" crystal being composed of subgrains and cells.

The stress-strain behaviour of the two orientations also indicate similar tendencies.

The stress-strain behaviour was determined by measuring the flow stress at 0.2% offset in uniaxial compressive deformation, from crystals which were predeformed in the channel die (the details of the uniaxial deformation mode are given in Chapter 3). In Figure 7.1(a) the flow stress at 0.2% offset for both "stable" and "unstable" crystals is plotted as a function of the strain at the end of predeformation in the channel die. In Figure 7.1(b), the data is represented in terms of shear stress and shear strain, calculated according to the relations $\sigma = M\tau$ and $Md\varepsilon = \Sigma d\gamma$. M was calculated based on the initial orientation of the crystal. The variation in M due to variation in lattice orientation has been neglected here. The stress-strain curve for the "stable"
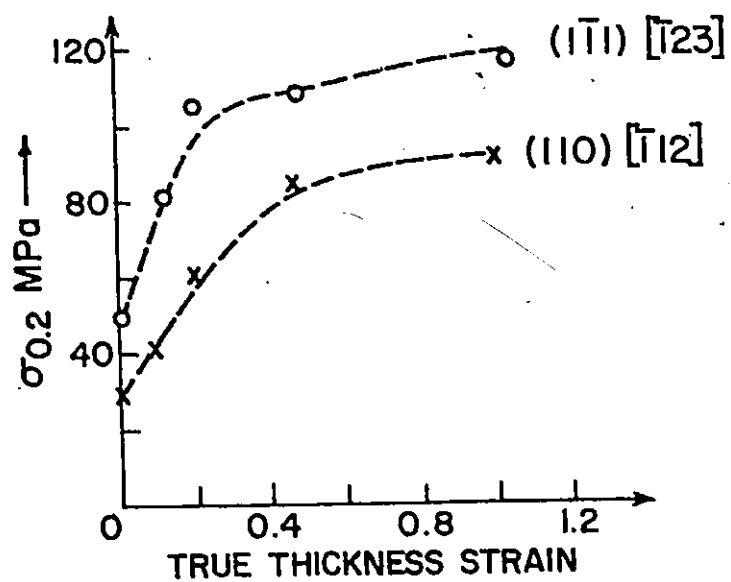
Fig. 7.1(a)   Flow stress ($\sigma_{0.2}$) – thickness strain curves for
the "stable" and "unstable" crystals.
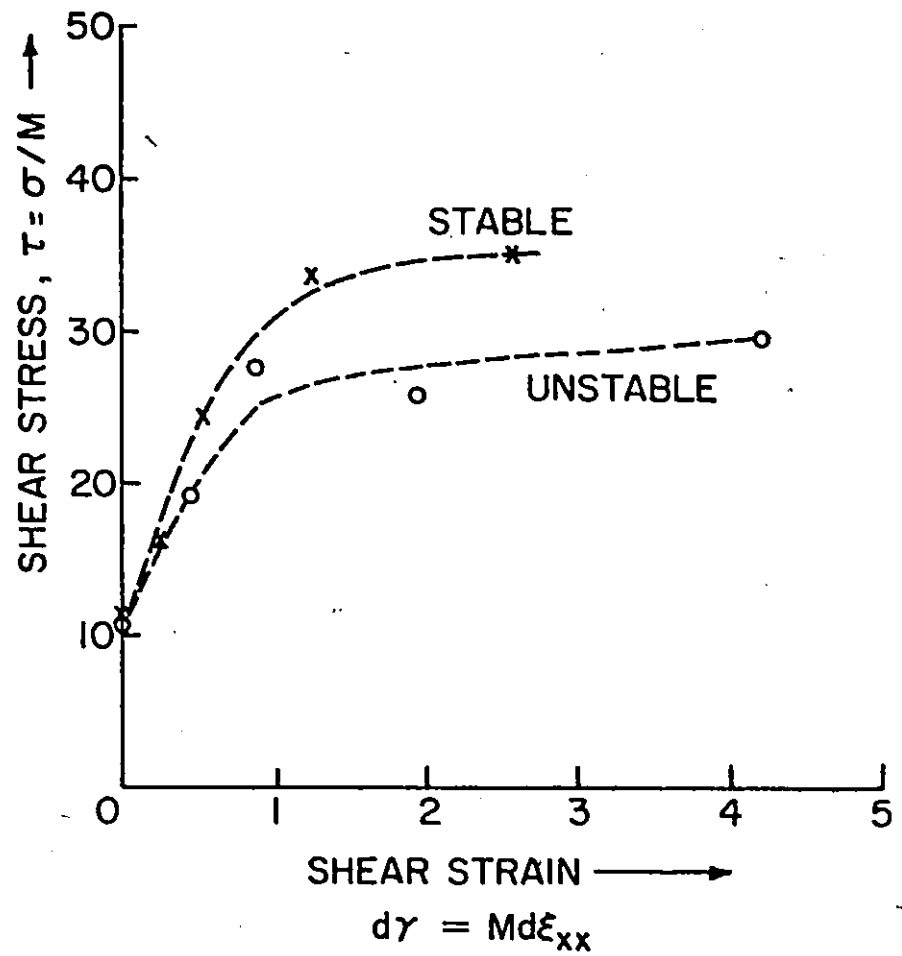
Fig. 7.1(b)   Shear stress vs. total shear strain curves for the "stable" and "unstable" crystals. M is defined in the text.

crystal indicates that high work hardening rate (though much less than θ_{II} - the rate of work hardening in Stage II), is maintained till about a strain of 0.5, whereas a decrease in work hardening rate compared to the initial rate indicating extensive dynamic recovery can be observed at low levels of strain in the "unstable" crystal.

Hosford (1966) reported that the stress-strain behaviour of single crystals of aluminum deformed under plane strain conditions did not show large variations in the stress level, all the curves falling within a band. But the variation in the rate of work hardening is of more significance than the variations in the level of stress at a given strain. The data available for copper single crystals (Wonsiewicz and Chin, 1970) and aluminum single crystals (Serpoul and Driver, 1979) both deformed in channel die show significant variations in the rates of work hardening in crystals of different orientations (the data of copper is complicated because of its ability to develop deformation twins). The data indicates that crystals whose orientations are stable during deformation and/or which deform on fewer number of slip systems, continue to work harden. For crystals of "unstable" orientations and with large number of possible set of active slip systems, the rate of work hardening decreases more rapidly during deformation.

As discussed in Chapter 2, orientation dependence of stress-strain behaviour in single crystals of aluminum deforming under polyslip conditions have been reported (Kocks, 1960; Hosford et al., 1960; Sakei and Miura, 1977). Striking differences were observed in <111> and <100> oriented crystals during room temperature deformation. Extensive cross slip was observed at low strains in the <100> crystals. This raises important questions:

(1)   What is more sensitive to crystal orientation - is it the rate

      of work hardening or is it the rate of dynamic recovery?

(2)   What is the mechanism of dynamic recovery?

It is well established that the orientation dependence of work hardening

rate in Stage II, where no dynamic recovery occurs is small (Hirsch,

1975), whereas the stress-strain characteristics in Stage III are orien-

tation dependent (Kocks and Brown, 1966).

     For extensive dynamic recovery to occur during deformation, the

dislocations which are being held up at tangles and cell walls must be

able to overcome these obstacles. Cross slip is one of the possible

mechanisms of escape for dislocations.

     Branching out of slip plane traces at the end of slip plane traces

are observed in Stage III indicating again that cross slip processes are

an important mechanism of dynamic recovery. As the activation energy

for cross slip decreases with increasing flow stress, dynamic recovery

events are easier at higher stresses and thus occur easily in Stage III

and not in Stage II. A model of dynamic recovery based on cross slip

events being dependent on τ, the external flow stress, has been derived

by Lücke and Mecking (1973).   For cross slip to occur the magnitude

of the resolved shear stress on the cross slip system is of importance.

The low work hardening rate in <100> crystals compared to <111> crystals

have been explained on the basis of the nature of the available cross

slip systems among the primary slip systems (Kocks and Brown, 1966).

      The slip systems primarily operative in the "stable" and "unstable"

crystals, as derived based on the yield subsurface analysis in Chapter 4,

are summarized along with their cross slip systems in Table 7.1. As

shown in this table, the cross slip planes available in the "stable"

Table 7.1

Primary slip systems with corresponding cross slip
systems for the "stable" and "unstable" crystals.

	"Stable"	"Unstable"
Primary slip systems	$\bar{a}$ $\bar{b}$ $\bar{j}$ $\bar{k}$	b c d $\bar{e}$ j $\bar{l}$
Corresponding cross slip systems	g $\bar{e}$ d $\bar{h}$	e l j $\bar{b}$ d $\bar{c}$
Resolved shear stres on the cross slip system in terms of unit stress on primary slip system	0 0 0 0	-1 -1 1 -1 1 -1

crystal are ($1\bar{1}1$) and ($\bar{1}11$) type, on which the resolved shear stress

is zero. In contrast, the primary slip systems themselves can act as

mutual cross slip systems in the "unstable" crystal. Consequently, the

extent of dynamic recovery at low strains may be larger in the "unstable"

crystals. The magnitudes of the resolved shear stresses given in Table

7.2 are in terms of the primary compressive stress. In the channel die,

due to the development of reaction stresses, the actual magnitudes of

these resolved shear stresses may be different. As the magnitudes of

the reaction stress components were not measured in the present study,

the actual magnitude of resolved shear stresses on the cross slip

systems is not known.

Apart from the fact that the primary slip systems of the "unstable"

crystal can act as cross slip systems, another equally important factor

which may contribute to dynamic recovery even at strain of 0.1 in the

"unstable" crystal, is the fact that the nature of operative slip system

changes during the deformation of the "unstable" crystal. This is indi-

cated by the changing nature of the slip plane traces shown in Figures

4.4 to 4.6. On the contrary, the same slip plane traces are observed

during the entire deformation of the "stable" crystal (Figure 4.3).

Based on latent hardening experiments, Kocks and Brown (1966) concluded

that changing the operative slip system may lead to rearrangement of

dislocations. This factor has important consequences on the nature of

the substructure developed at large strains. Thus, models of dynamic

recovery have to be extended to incorporate the influence of orientation

in order to relate the kinetics of the detailed mechanisms of dynamic

recovery. The available models of dynamic recovery (Lücke and Mecking,

1973; Kocks and Mecking, 1979) are based on establishing the distribution

of recovery events as a function of τ, the external stress.

Experimental observations discussed so far show that the extent of dynamic recovery is not only a function of stress τ, but is also dependent on orientation; or more specifically, on the number and type of slip systems that are active. Experiments in crystals of polyslip (Kocks, 1960; Wonsiewicz and Chin, 1970) and present investigations show that even though equivalent shear stress levels are reached in crystals of different orientations, the overall rates of work hardening are dependent on orientation. Other important observations made in the present investigations concerning the effects of recovery are:

(1) short-term thermal recovery is similar to dynamic recovery, both resulting in cleaner cell interiors and simpler configurations of cell walls.

(2) long-term thermal recovery, unlike dynamic recovery, leads to coarsening of substructure.

Thermal recovery is observed to exert marked influence only in the regime where the extent of dynamic recovery is small. This is clearly seen in the changes occurring in the nature of the substructure of the "stable" crystal, as shown in Figure 6.1.

Detailed investigations of the nature of the dislocations constituting the walls in crystals subjected to thermal recovery were not undertaken. But it is observed that the configuration of the walls becomes simpler and that density of local debris - dipoles and dislocation loops - is reduced. There is no major difference in the degree of misorientation in keeping with this observation. Similar observations have been reported in niobium by Boyd et al. (1976), as discussed in Chapter 2. Investigations of the fraction of stored energy which is

released during thermal recovery (Gordon, 1955) and influence of the

thermal recovery on subsequent recrystallization behaviour (Kaspar and

Pluhar, 1975) in samples prestrained to various extents indicate simi-

larities in thermal and dynamic recovery processes.

·Similarities between thermal and dynamic recovery emphasized here,

concern only the changes occurring in the nature of the substructure in

the as-deformed condition. Differences in the two processes particularly

with respect to subsequent mechanical behaviour has been discussed in

Chapter 2. Differences are also manifest in coarsening of the substruc-

ture seen in micrographs in Figure 6.3 shown in Chapter 6. which show

the development of regions of large misorientation due to storage at

room temperature in the "unstable" crystal deformed to strain of 0.5.

The nature of these misorientations was discussed in detail in Chapter

6. It was emphasized that the regions of [0$\bar{1}$1] orientation which are

observed are much larger in size compared to the regions of (1$\bar{1}$1) orien-

tation. That such regions of [0$\bar{1}$1] orientations were not observed in

the T.E.M. in the as-deformed conditions must only indicate that these

regions were much smaller and so were not detected in T.E.M. investiga-

tions. Thermal recovery treatments carried out for 1 hour at 100°C did

not reveal any change in the nature of the substructure as observed in

samples prepared from the free face. In contrast, storing the crystal

at room temperature for long periods changed the nature of the substruc-

ture, enabling growth of the regions of the new orientation. (Consistent

orientation changes were observed in the compression and free faces but

only the data for the compression face is reported in Chapter 6.)

Hasegawa and Kocks (1979) have also reported subgrain coarsening observed

during thermal recovery. In order to examine whether the subgrain boundary

migration is the operative mechanisms leading to such coarsening, the time, t_m, required for the subgrain size to increase by a factor of two by boundary migration was estimated following Kreisler and Doherty (1978) according to the relationship:

$$t_m = \frac{2\beta L^2}{K'} \quad . \tag{7.1}$$

β is a geometrical parameter which depends on subgrain shapes and sizes. and is assumed to be 2 (Kreisler and Doherty, 1978). K', a parameter which depends on the boundary energy and mobility was deduced by the values known at various temperatures for copper. It is assumed here that at equivalent homologous temperature (same fractions of the melting point), boundaries in copper and aluminum have similar mobilities. Then at room temperature $K' \simeq 2 \times 10^{-17}/295$ m^2/sec (Viswanathan and Bauer, 1973), and t_m the time for migration of the boundary of misorientation $\sim 30°$ (orientation difference between 011 and 11 regions) of subgrain of size 1 µm is approximately 340 days. Whereas this time is calculated for an increase in size by a factor of two, nearly tenfold increase in size occurs in the present investigations, in equivalent length of time. This could be due to the influence of the nature of the boundary on mobility. Models of subgrain boundary migration and boundary rotation (Li, 1962) have been used to examine whether the regions of the new orientation were created during the thermal recovery event, the 0$\bar{1}$1 oriented then developing due to accumulated misorienta – tion during the process. The time required for subgrain coarsening of boundaries of average misorientation 1 – 2°, calculated according to Eq. (7.1) is several orders of magnitude larger than the observed time. Even the time required for development of increased misorientations by boundary rotation according to Li (1962) is orders of magnitude larger.

This implies that the regions of large misorientation must have developed during deformation.

7.3 Investigation of High Angle Boundaries

The most striking difference in the "stable" and "unstable" crystals deformed to large strains is the development of high angle boundaries in the "unstable" crystal. The nature of these high angle boundaries was discussed in Chapter 5. Micrographs in Figure 5.21 reveal that there is essentially no difference in either average scale or misorientation in the subgrains present in regions bounded by these high angle boundaries compared to the rest of the substructure. Therefore, these high angle boundaries must have been created during deformation. Detailed investigation of the spatial distribution of the regions bounded by high angle boundaries examined by optical microscopy technique has been described · in Chapter 6. These investigations confirmed the T.E.M. observations that only two orientations are present. The regions bounded by the high angle boundaries are about 10 - 15 μm long, 2 - 3 μm wide and are distributed periodically, aligned close to the channel direction. During the early stages of recovery, these regions coalesce. Coalescence is observed to occur in a particular direction as shown in Figure 6.5. The direction of coalescence is close to [011], the direction along which the high angle boundaries are aligned in Figure 5.21.

7.3.1 Origin of the High Angle Boundaries

The development of such large misorientations as observed in the present investigations, will be discussed by comparing the observed features with the characteristics of some established mechanisms associated with the production of large misorientations. As summarized in Table 2.6 (Chapter 2), large misorientations observed in as-deformed

materials have been usually associated with kink bands, deformation bands, microbands or shear bands and with occurrence of dynamic recry-stallization.

Kink bands and bands of secondary slip are special types of deformation bands. In general, deformation bands represent regions in which the combination of operative slip systems is different compared to the rest of the material. Structural observations reveal that kink bands and deformation bands are usually associated with transition bands which accommodate the observed orientation difference. Kink bands in particular are characterized by a [112] type roller axis and are not observed in crystals oriented for multiple slip. Other structural details are summarized in Table 2.6 of Chapter 2.

The regions of large misorientation observed in the present investigations do not conform to the usual characteristics of deformation bands. The orientation difference in the present case occurs abruptly across a single boundary, and are observed only at large strains, unlike the deformation bands which develop gradually throughout the deformation. The scale of the $0\bar{1}1$ regions being $2-4$ μm wide and $10-15$ μm long, thus it would be necessary for different sets of slip systems to be operative over distances which are equivalent to the spacing between two-three slip plane traces and further the combination of slip systems must vary so as to always produce the same kind of misorientation, which seems an improbable situation.

Presence of deformation bands may not be the reason for the formation of high angle boundaries. Continued observations of the surface slip plane traces discussed in Chapter 4 show that deformation bands were observed only on the die face of the "unstable" crystal and only

at strain of 1.0. No such deformation bands were observed at lower

strains, though it was discussed earlier that similarly misoriented

regions develop in the crystal deformed to strain of 0.5.

Microbands are another type of feature characteristics of rolled

and drawn crystals. As summarized in Table 2.6, investigations of micro-

bands indicate they develop early in deformation, are elongated even at

low strain, and occur between equiaxed cells. It is not known whether

unique misorientation exists across the microbands at a given strain.

The regions of large misorientations observed in the present investiga-

tions do not conform to any of these characteristics. They do not

appear within equiaxed structure; instead there is no difference between

these regions and the rest of the substructure with respect to either

the misorientation   or the scale of the substructure present within

the regions bounded by high angle boundaries.

Shear bands are other regions across which large misorientations

could develop, but the characteristic surface features associated with

the shear bands were not observed here.

Yet another possibility of development of new orientations is due

to occurrence of dynamic recrystallization during deformation. Experi-

mental evidence of dynamically recrystallized material available in the

literature (Cairns et al., 1971) indicate presence of regions clear of

substructure. As discussed earlier, no such differences were observed

in the present work. It is, of course possible that the regions were

dynamically recrystallized and the substructure observed within developed

due to further deformation. But the observations that:

(1)   the scale and nature of the substructure is not different from that

      of the rest of the material, and, that

(2)   unique misorientation develops

indicate that the origin of these regions may not lie in dynamic recry-

stallization.   Also, the general shape of the recrystallized region

(Figure 6.6), is much different from what was observed here.

In further understanding the origin of the high angle boundaries,

the following factor must be recalled: that large misorientations are

developed only in the "unstable" crystal and not in the "stable" crystal.

The essential difference exhibited by the "stable" crystal during deform-

ation is with respect to the operation of same slip systems throughout

the deformation.

As discussed earlier in Section 7.2, the changing nature of opera-

tive slip systems in the "unstable" crystal leads to dynamic recovery

early on in the deformation process and to the development of well-

defined subgrains.

According to Figure 5.19, the general direction of the substructure

at large strains is along the direction of free flow.   The coarse slip

plane traces observed at large strains have developed at an angle to

this direction.   The length of the region bounded by high angle bound-

aries is approximately the same as the spacing between these coarse slip

bands.   This indicates that the high angle boundaries may have developed

due to the intersection of the slip bands with previously developed sub-

structure, similar to the development of local kinking proposed by

Argon and Orowan (1961).

7.4   Homogeneity of Slip

That highly misoriented regions were created only in the "unstable"

crystal and not in the "stable" crystal gives rise to the question whether

it is possible to create high angle boundaries during the deformation of

"stable" crystals. The variation in the nature of operative slip systems during the deformation of the "unstable" crystal is equivalent to subjecting the crystal to changes in the path of deformation. As discussed in Chapter 2, the stress-strain behaviour of crystals deformed in a different direction after prestraining in a given direction, is associated with changes in the level of flow stress and rate of work hardening. Slip is observed to occur in coarse bands (Kocks and Brown, 1966; Jackson and Baskinski, 1967). Substructural investigations carried out by Sharp and Makin (1966) indicated that coarse slip bands penetrate through the cell walls of the substructure developed during predeformation. Predeformation in the investigations of Sharp and Makin (1967) was carried out into Stage III and the strain in the second deformation varied between 4 - 18%. No experimental evidence is available where the crystal was subjected to frequent changes in the path of deformation at low intervals of strain and where the crystal was predeformed to large strains before being deformed in a different direction. Predeformation to large strains will result in well-developed dislocation substructure and subsequent deformation in a different direction leads to information about the mechanical stability of these subgrain walls - whether the walls will be locally destroyed or whether large misorientations are created at the intersections of the new slip and existing subgrains.

It is known that the rate of work hardening is reduced drastically in a cube-shaped polycrystalline material compressed alternately in different directions compared to the sample compressed in a given direction (Hecker, 1979). No substructural observations are available under such deformation conditions.

In order to investigate the possibility of creating large mis-

orientations in the "stable" crystal, a sample of the crystal deformed to strain 0.5 by compression along 110 direction in the channel die was subsequently compressed along 1$\bar{1}$1 direction in the uniaxial mode.

During the subsequent compression, the deformation became localized. The band of localized deformation observed only on the side faces, does not follow the expected direction of slip plane traces, but instead makes an angle of ~ 55° to the new compression axis (or 35° to the trace of the compression plane) similar to the shear bands reported in the literature (Malin and Heatherly, 1979; Dillamore and Bush, 1978). After 10% strain in the second deformation, the width of the band is about 85 μm and detailed investigations of the surface indicate that these must be clusters of shear bands. The surface characteristics of the shear bands as observed on the (110) plane (compression plane in predeformation) shown in Figure 7.2, indicates severe bending of slip plane traces on either side of the band. The traces correspond to the (111) and (11$\bar{1}$) slip planes. The density of the slip plane traces decreases away from the shear bands.

Electron microscope investigations of the changes resulting in the nature of the substructure due to the subsequent deformation, were difficult due to the problem of producing a thin foil from the region of the shear bands. The substructure developed in a region away from the shear bands, is shown in Figure 7.3. The micrograph in Figure 7.3(a) indicates coarse bands penetrating through cell walls developed during predeformation. A magnified view of these bands in Figure 7.3(b) shows, that these bands are composed of tangels of dislocations. No major changes in misorientation were observed across these bands of dislocations.
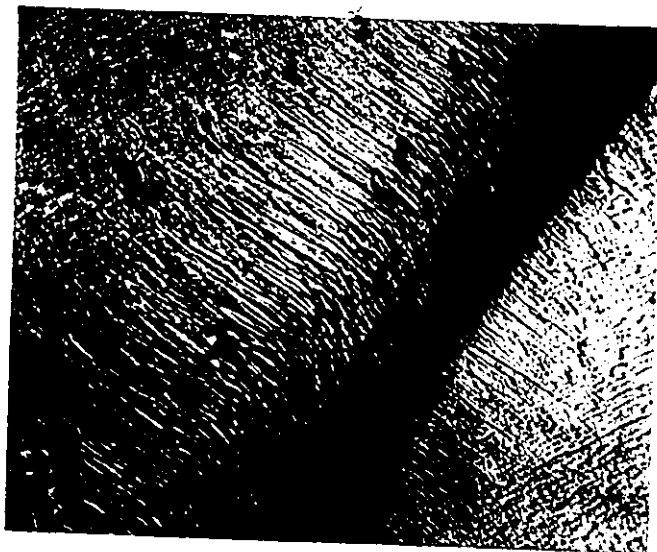
7.2(a)
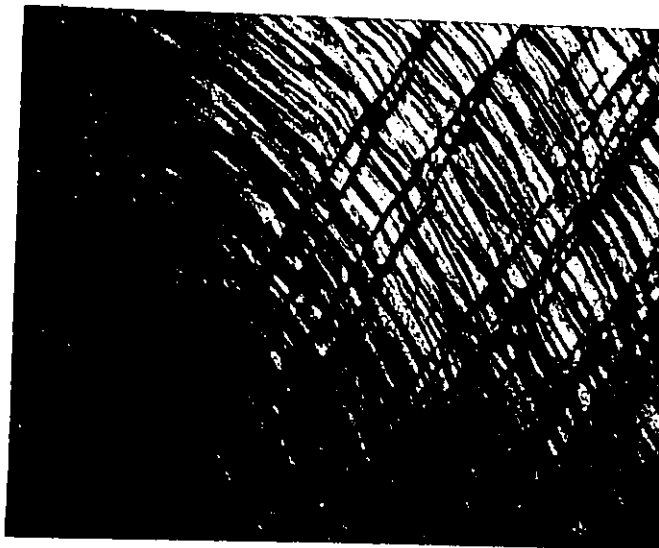
7.2(b)

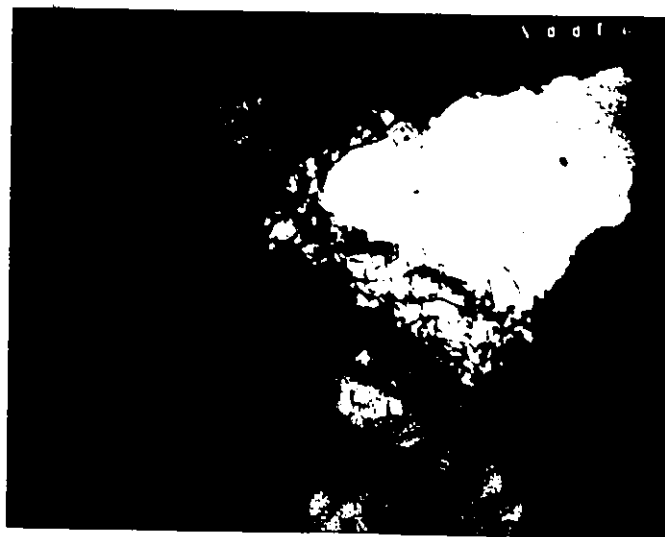Fig. 7.2(a-b)   Surface features indicating formation of shear
                bands. A magnified view is given in (b);
                magnification 600x.

7.3(a)

7.3(b)

Fig. 7.3(a-b)   (a) Micrographs illustrating bands developed
during second deformation running across the
cell walls and subgrains developed during the
pre-deformation. (b) shows the bands to be
tangles of dislocations.

Possible development of large misorientation across the shear bands compared to the rest of the crystal is seen in Figure 7.4 which shows the anodized surface of the crystal taken in polarized light.

These results indicate that large misorientations may develop in the "stable" crystal due to changing the operative slip systems as a consequence of changing the path of deformation. The exact nature of and degree of misorientation and the resulting changes in the nature of the dislocation substructure are not known.

7.5 Conclusions

The observations made in the present study lead to the following conclusions:

(1) Both the spatial homogeneity of slip and the sequence of active slip systems are dependent on the orientation of the crystal. These factors have important implications on the nature of the substructure developed during deformation, and the extent of dynamic recovery, particularly at low strains and the creation of high angle boundaries at large strains.

(2) The dislocation substructure develops according to the following stages during deformation. In the early stages, tangles are created as debris in the active slip planes; these get converted into cells and subgrains at later stages. At large strains the cell walls and subgrain walls are not confined to the active slip planes, but instead, move toward the overall flow direction.

(3) Thermal and dynamic recovery processes are similar to the extent that they lead to similar structural changes.

(4) Extent of dynamic recovery is dependent on orientation. It is well established that the case of cross slip influences
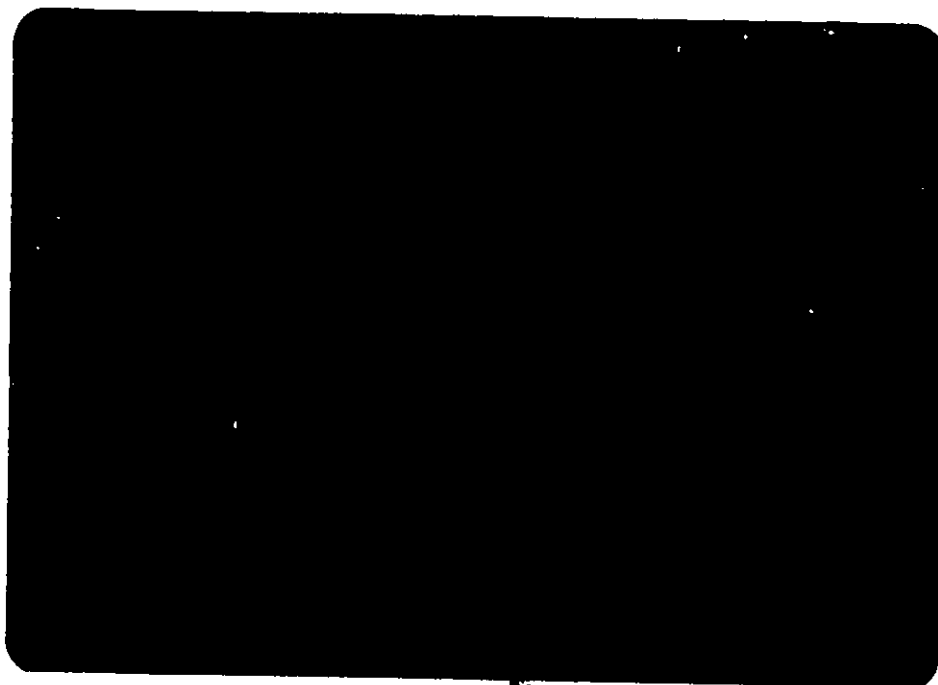
Fig. 7.4   Optical metallograph of the anodized surface illustrating
            change in contrast and thus possible change in orientation
            at the band.   Magnification 30x.

the extent of dynamic recovery. A significant contribution to
dynamic recovery must arise from changes in the operative slip
systems. This can be concluded by comparing the nature of the
dislocation substructure and of slip in the "stable" and "unstable"
crystals.

(5) The origin of the high angle boundaries is not clear, though it
is undoubtedly related to the inhomogeneity of slip.

(6) The nuclei for recrystallization are created during deformation.

7.6 Suggestions for Future Work

Future work in the area of large strain deformation must be
directed towards the following investigations. These can be broadly
classified into four sections:

(1) orientation dependence of dynamic recovery.

(2) importance of similarity between thermal and dynamic recovery.

(3) importance of homogeneity of slip, and,

(4) creation of nuclei for recrystallization, during deformation.

It has long been established by investigations of the stress-strain
behaviour of Stage III hardening in fcc single crystals that the extent
of dynamic recovery is dependent on orientation. The present investiga-
tions confirm the importance of changes in the nature of operative slip
systems in causing extensive dynamic recovery. But the actual changes
in the dislocation configurations which result due to such changes in
operative slip systems are not yet known. Extensive macroscopic obser-
vations of the nature of slip are available for [100] and [111] oriented
aluminum single crystals (Sakei and Miura, 1977). It is known that
marked dynamic recovery is observed in [100] crystals (Kocks, 1960).
Electron microscopic investigations of the [100] crystals concerning

nature of the dislocation configurations and the changes that occur due to dynamic recovery, may provide more insight as to why the extent of dynamic recovery is dependent on orientation.

The similarities observed in the structural changes caused by thermal and dynamic recovery processes have important implications in the processing of materials. It is known that the influence of dynamic and thermal recovery processes on the mechanical properties differ and that a drop in flow stress and increased rate of work hardening are observed immediately after thermal recovery. The similarities and differences in the dynamic and thermal recovery processes can be used to increase the regime of useful strain in materials by subjecting them to short recovery annealing treatments, intermittently. It is also possible that such treatments enable the metal to be worked at lower stresses.

The homogeneity of slip has important implications on the extent of dynamic recovery as discussed earlier and on the creation of large misorientations during deformation. That the extent of homogeneity of slip is orientation dependent has important implications in the recrystallization behaviour and processing behaviour of polycrystalline materials. It is possible to create a material of mixed strength-ductility characteristics by recrystallizing a heavily deformed poly-crystalline material, because the recrystallization behaviour will vary from grain to grain.

That large misorientations are observed only in crystals which exhibit inhomogeneity of slip highlights the necessity of detailed investigations in which the path of deformation is changed. Operative slip systems can be changed by varying the path of deformation. The

nature of influence of such changes, whether it leads to extensive

dynamic recovery, or creates major changes in the previously developed

substructure which are dependent on the detailed nature of the strain

path.

Detailed investigations of the nature of substructure produced by

subjecting crystals of "stable" orientation to changes in the path of

deformation may lead to elucidation of the origin of the large misorien-

tations observed in the present investigations.

APPENDIX 1

THE CONCEPT OF A YIELD SURFACE

A yield surface is a schematic representation of yield criterion, which is a function of the applied stresses responsible for yielding. To represent the influence of a general applied stress, σ_{ij}, the yield surface must be considered in a six-dimensional space. In the present study, we are concerned with yield surface of single crystals. The shape of the yield surface of a virgin single crystal depends on the symmetry of the crystal structure and the nature of expected slip systems, which defines the number of slip systems intersecting at a given point.

A two-dimensional, schematic representation of a section of a yield surface for a single crystal is shown in Figure A.1, to illustrate the concepts of an "edge" and "corner". The diagram also serves to illustrate the equivalence between the Taylor and Bishop-Hill analyses following Kocks (1970).

In Figure A.1, DA, AB and BC represent edges of the yield surface DABC. A and B are the corners. The strain vector normality rule is assumed to be obeyed at the yield surfaces. A stress acting along the vector σ_1 will activate only the slip system s_1 and in so doing cause a positive strain along $\underline{d\varepsilon_1}$. Similarly, the stress vector $\underline{\sigma_2}$ will activate only the slip system s_2 and cause a strain along $\underline{d\varepsilon_2}$. Stress $\underline{\sigma}$ to the corner B will activate both the slip systems s_1 and s_2.
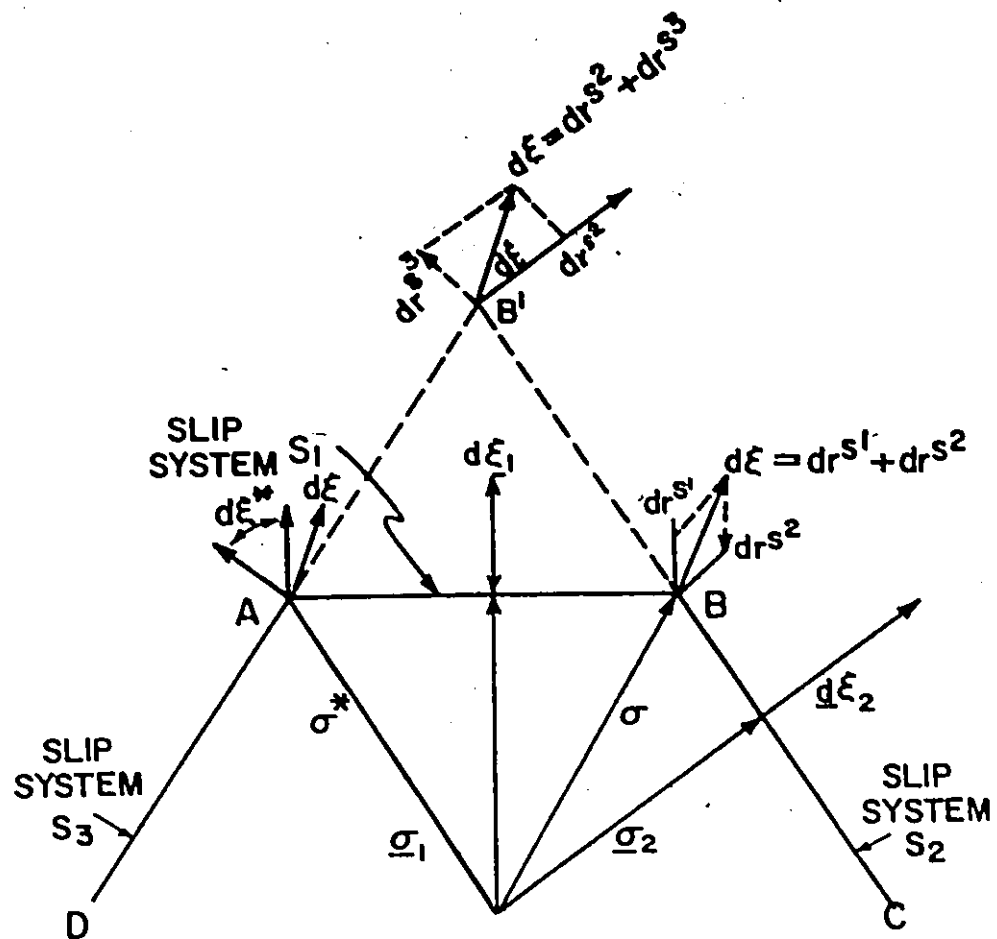
Fig. A.1   Schematic illustration of a section of a general
two-dimensional yield surface.

At a corner the strain vectors are contained within a cone of normals. This gives rise to uncertainty in the relative activity on the slip systems, meeting at the corner.

To predict which combination of slip systems will be active under given deformation conditions, Taylor (1938) proposed that the sum of shears of the set of active slip systems is less than the sum of shears on all other possible sets. That such a set of slip systems also satisfies a yield criterion can be shown in Figure A.1 following Kocks (1970).

In Figure A.1 a prescribed strain $\underline{d\varepsilon}$ (as at corner B) can be achieved by a stress vector $\underline{\sigma}$ which satisfies the yield condition and activates the slip systems s_1 and s_2. The sum of the shears is $\underline{dr}^{S1} + \underline{dr}^{S2}$. Here the length of the vectors $\underline{dr}$ is considered to represent the amount of shear on the particular slip system. From Figure A.1 it is also seen that if the same prescribed strain $\underline{d\varepsilon}$ can be achieved as at corner B' by a suitable stress vector, it will result in the following:

(1) The total amount of shear caused on slip systems s_1 and s_3 is $\underline{dr}^{S1} + \underline{dr}^{S2}$ which is larger than $\underline{dr}^{S1} + \underline{dr}^{S2}$.

(2) Such a stress vector which causes larger shear will violate the yield criterion because the stress to corner B' must in fact activate the slip system s_2, to satisfy the yield criterion.

The Bishop-Hill criterion of selecting the set of active slip systems is based on the principle of maximum external work. A stress vector $\underline{\sigma}$ which produces the strain $\underline{d\varepsilon}$ at corner B does the maximum amount of work and satisfies the strain normality rule. The strain vector $\underline{d\varepsilon}$ is contained within the cone of normals only at corner B.

Any other stress $\underline{\sigma}^*$ to corner A cannot produce $\underline{d\epsilon}$.

The above treatment also illustrates the equivalence between the Taylor and Bishop-Hill analysis.

APPENDIX 2

ANODIZING TECHNIQUE

In order to examine the spatial distribution of the regions
bounded by high angle boundaries, an anodizing technique was adopted.
The technique has been widely adopted and regions differing in orien-
tations can be identified due to the colour contrast developed in the
anodized film when examined in polarized light with crossed nicols.
The details of anodizing technique are summarized in Table A.1.

The structure of the film depends on the type of the solution
used.

Discussion of the Observed Contrast

With crossed nicols colour contrast is observed where phase
differences are created in the incident plane polarized light such
that it can be converted into elliptically polarized light during
reflection from the surface of the sample. The reasons for develop-
ment of colour contrast in the oxide film have been discussed in
detail in books dealing with metallography and optics (Phillips, 1971;
Conn and Bradshaw, 1952). Clearly it is possible that the nature and
structure of the oxide film depends on the orientation of the area on
which it develops. In order to understand whether such a structure
is present in the oxide film developed in the present work, the film
was examined in a scanning electron microscope. The structure of the
film observed at a magnification of 9900x shown in Figure A.2 indicates

Table A.1

Anodizing procedure.

| Specimen preparation:	Mechanically polish the surface on 600 grade emery paper. Electropolish in ethanol - 20% perchloric acid solution. Wash thoroughly in distilled water.
Anodizing procedure:	
Solution	2% fluoboric acid in distilled water.
Cathode	Stainless steel strip.
Voltage	Approximately 20 volts.
Time	1 minute Wash thoroughly in distilled water and ethanol. Dry in air.
Examination	In polarized light with crossed nicols.
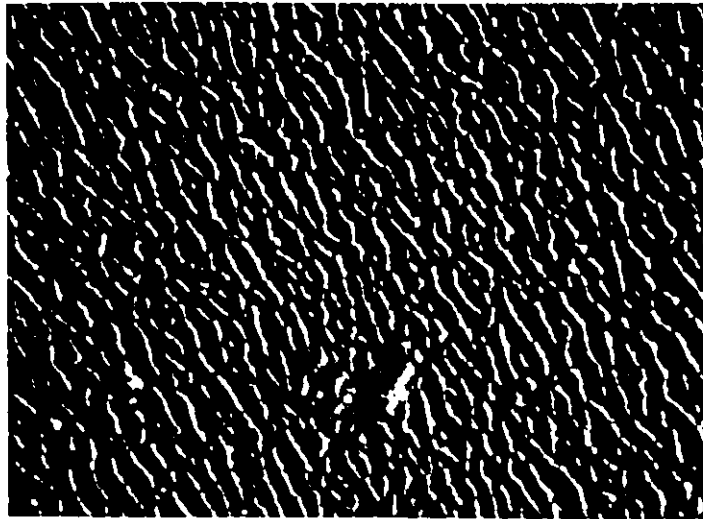
Fig. A.2   Scanning electron micrograph indicating
ridges and valleys in the oxide film
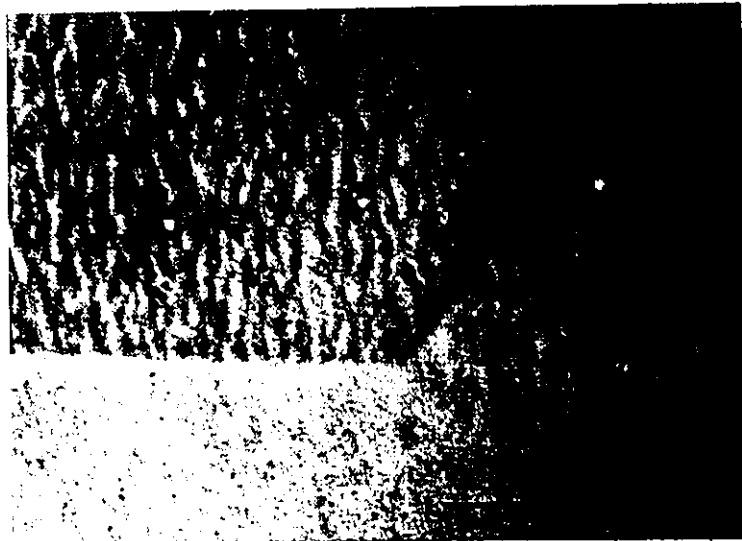developed during anodization.   Mag. 9900x.

Fig. A.3   Micrograph illustrating that the structure
of the oxide film varies from grain to
grain.   Ref. Conn and Bradshaw (1952)

regular presence of ridges and valleys in the oxide film. The separa-
tion between the ridges varies between 0.1 - 0.2 μm. The region indica-
ting colour contrast is about 2 - 6 μm wide. It is believed that
the topography of the oxide film converts the plane polarized light
into elliptically polarized light. That the nature of the topography
varies depending on the orientation of the region was shown by the
examination of the oxide film in phase contrast microscope (Conn and
Bradshaw, 1952) reproduced in Figure A.3. Colour contrast was observed
even when a layer of optically isotropic silver was deposited on the
oxide film which eliminates the possibility that the colour contrast
was due to the optical anisotropy of oxide film (Perryman and Lack, 1951).

Because the topography of the oxide film gives rise to the colour
contrast necessary to identify regions of different orientations, extreme
care must be taken to ensure that the surface before anodizing is flat
and free of scratches. Although it is known that regions bounded by high
angle boundaries can be identified, it is not yet clear as to what the
lower limit of misorientation is, that can be identified.

APPENDIX 3

STORED ENERGY AND WORK HARDENING BEHAVIOUR

Both the current values of flow stress and stored energy of a metal are influenced by the density and distribution of the accumulated dislocations. No experimental study of stored energy was undertaken in the present investigation. Instead, what is presented is a survey of some of the data available in the literature. Bever et al (1973) have presented a comprehensive review of stored energy studies related to plastic deformation. No attempt is made here to review the data in detail. Instead, the data is analysed in two ways: 1) the fraction of energy stored per increment of strain to examine the nature of deformation at large strains, and 2) variation of E_s, the energy stored vs σ^2 (where σ is the flow stress) to examine the constancy at large strains of the parameters α and β which relate the flow stress and stored energy respectively to the density of stored dislocations.

Energy Stored During Deformation

According to the first law of thermodynamics:

$$\Delta u = \Delta Q + \Delta w \tag{1}$$

where Δu = change in internal energy,

ΔQ = amount of heat absorbed or given out,

Δw = amount of work done.

The change in internal energy during deformation is the energy stored and is considered to contribute to the major portion of the free energy change of a cold worked material. The change in internal energy is due to the elastic strain energy of the increased number of dislocations that are stored during deformation (Cottrell, 1953).

Experimental investigations indicate that a major/portion of the stored energy is released when the deformed metal undergoes recrystallization (Bever et al, 1973).

E_w, the energy supplied to the material during plastic deformation, is the amount of mechanical work done per unit volume of the material and is computed as the area under the stress-strain curve. In Fig.A.4, data representing E_w, the amount of energy supplied, and E_s, the amount of energy stored during deformation of aluminum, is given.

Relation Between Work Hardening Rate, Stored Energy and the Density of Stored Dislocations

Neglecting the contribution of friction stress σ_o, the flow stress σ is related to ρ, the average dislocation density as

$$\sigma = \alpha \mu b \sqrt{\rho} \tag{2}$$

when the density of stored dislocations increases by $d\rho$, the amount of energy stored increases by dE_s, where

$$dE_s = \beta \mu b^2 d\rho \tag{3}$$

The value of the coefficient α in Equation (2), defined as the strength parameter, is estimated to vary between 0.05 - 1.0, based on a variety of work hardening models (Nabarro et al, 1964).

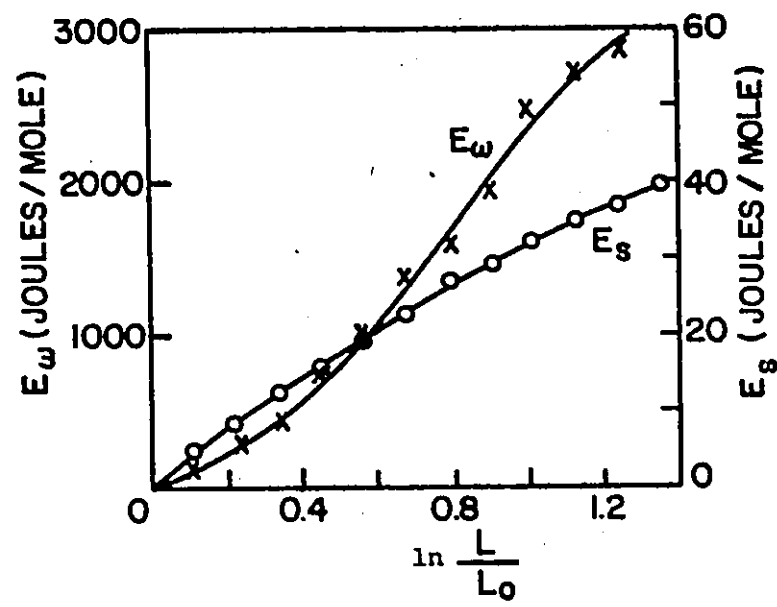The parameter β in Equation (3) is the arrangement factor and is

Fig. A.4 Variation of E_w, energy supplied and E_s, energy stored with strain ($\ln\frac{L}{L_o}$) during deformation of polycrystalline aluminum.

(Note difference in scales for E_w and E_s).

From Williams, R.O., 1962, Trans. A.I.M.E., 224, 719.

related to the energy of the dislocation configuration.

Following Nabarro, the energy stored during Stage II hardening of fcc single crystals can be estimated as follows: the work hardening rate $\frac{d\sigma}{d\epsilon}$ in Stage II is given by

$$\theta_{II} = \frac{\mu}{K} \tag{4}$$

where μ is the shear modulus of the material and $K \simeq 100\text{-}300$, depending on the orientation of the crystal. The work done/unit volume of the material is given by

$$dE_w = \sigma d\epsilon \tag{5}$$

Considering that $dE_s = \frac{1}{2}\mu b^2 d\rho$, Nabarro estimated that in Stage II,

$$\frac{dE_s}{dE_w} = \frac{1}{K\alpha^2} \tag{6}$$

With $\alpha = 0.25$, a maximum of about 5% of the energy supplied is stored in the crystal in Stage II.

Parameter α

In Stage II, hardening where no dynamic recovery occurs, the value of α is known to be quite insensitive to the actual distribution of dislocations and mechanisms of work hardening (Nabarro et al, 1964); Hirsch, 1975). Thus, α is usually considered to be insensitive to strain. At large strains such an assumption may not be valid.

Parameter β

In Stage II, β is also considered to be independent of strain. Nabarro's treatment of Stage II hardening assigns a constant value of $\frac{1}{2}$ to β. The changes occurring in the configuration of dislocations at large strains have been discussed in detail in Chapters 2, 5 and 7. It

it possible that the magnitude of β, the arrangement factor, changes at large strains and is dependent on strain.

Bever et al (1975) treat β (referred to as α_s in their article) as the interaction parameter. The self energy per unit length of dislocations is defined as

$$\frac{\mu b^2}{4 \pi K} \ln \frac{R}{r_o} + \text{Core energy}$$

where K = 1 for screw dislocations,

and K = 1-ν for edge dislocations

R = radius of the area in which the stress field of the dislocation is felt,

r_o = core radius of the dislocation.

Bever et al (1973) treat β as follows, to give an idea about the arrangement of dislocations:

When

$$\beta > \frac{\ln R/r_o}{4 \pi K}$$

the interaction is positive. The stress fields of dislocations reinforce one another. This is typical of tangled structure and dislocation pileups.

$$\beta = \frac{\ln R/r_o}{4 \pi K}$$

represents zero interaction. This is true only for a truly random distribution of equal number of positive and negative dislocations.

$$\beta < \frac{\ln R/r_o}{4 \pi K}$$

represents negative interaction. This is when the dislocations are arranged so that stress fields cancel one another. This is true of dislocations arranged in low energy configurations as in subcell walls.

Based on Equations (8.2) and (8.3), β is given by

$$\beta = \mu\alpha^2 (\frac{E_s}{\sigma^2})$$

(7)

Bever et al, op cit, estimated β to have a value between 2 and 14 in different metals. When compared with the value of $\frac{\ln R/r_0}{4\pi K}$ which is 0.8 when $R = 1$ μm and $r_0 = 2$ Å, the large value of β means that a positive interaction occurs between dislocations stored in cold worked, nominally pure, polycrystalline materials. This is possible in metals deformed such that the extent of dynamic recovery is small. The excess stress field represented by the large positive value of β is relieved when the metal is subjected to thermal recovery subsequent to deformation.

Method of Analysis to Examine the Constancy of α and β

Based on Equation (7), it is possible to examine the variation of α and β during deformation (Gottstein, 1974). If both α and β are constants, the plot of E_s vs σ^2 will be linear with a constant slope = $\frac{\beta}{\mu\alpha^2}$ throughout deformation.

In Fig. A.5, the effect of varying α and β on the slope of E_s vs σ^2 is shown schematically. Plot 1 represents the case where both α and β are independent of strain. Plot 2 represents the case where only β is a decreasing function of strain. If both α and β decrease with strain, but α decreases more rapidly than β, the variation of E_s with σ^2 follows Plot 3. The magnitude of deviation from the linear plot indicates the level of variation of α and β.

Equations Relating Stored Energy Data and Work Hardening Behaviour

Based on Equation (2), the work hardening rate $\frac{d\sigma}{d\varepsilon}$ is given by

$$\frac{d\sigma}{d\varepsilon} = \frac{(\alpha\mu b)^2}{2} \frac{d\rho}{d\varepsilon}$$

(8a)

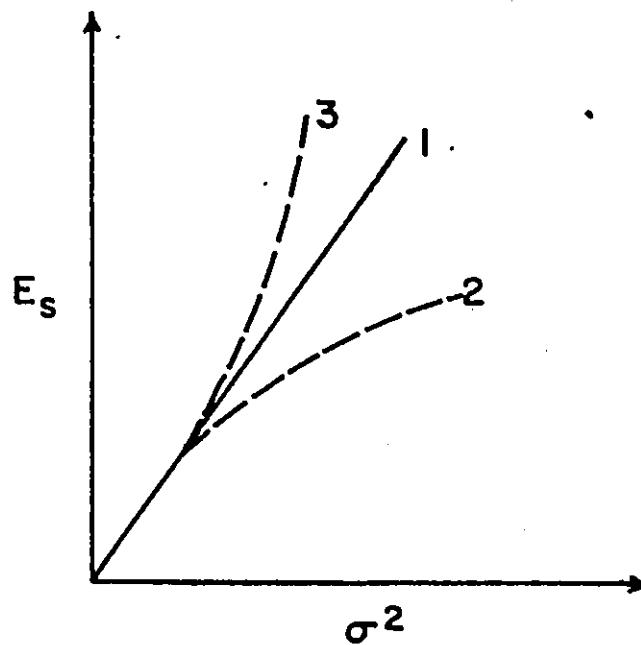Fig. A.5 Schematic illustration of the effect of the variation of parameters α and β during deformation on the slope of E_s vs σ^2.

$$\sigma\frac{d\sigma}{d\epsilon} = \frac{(\alpha\mu b)^2}{2}\frac{d\rho}{d\epsilon} \tag{9a}$$

$\sigma\frac{d\sigma}{d\epsilon}$ can be evaluated from stress-strain plots and is considered to represent the rate of dislocation storage during deformation.

Equation (6) can be rewritten for a general work hardening rate $\frac{d\sigma}{d\epsilon}$ as

$$\frac{dE_s}{dE_w} = (\frac{2\beta}{\mu\alpha^2})\frac{d\sigma}{d\epsilon} \tag{10a}$$

and

$$\frac{dE_s}{dE_w} = \frac{\mu b^2 \beta}{\sigma}\frac{d\rho}{d\epsilon} \tag{11a}$$

Equations (9a) and (11a) relate the rate of work hardening to the fraction of energy stored during deformation. Variations of $\frac{d\sigma}{d\epsilon}$ and $\frac{dE_s}{dE_w}$ with σ and of $\sigma\frac{d\sigma}{d\epsilon}$ and $\sigma\frac{dE_s}{dE_w}$ with should follow similar trends.

Incorporating that α and β are also functions of strain, Equations (8) to (11) should be modified respectively as:

$$\frac{d\sigma}{d\epsilon} = \frac{\alpha\mu^2 b^2}{\sigma}(\frac{\alpha}{2}\frac{d\rho}{d\epsilon} + \rho\frac{d\alpha}{d\epsilon}) \tag{8b}$$

$$\sigma\frac{d\sigma}{d\epsilon} = \alpha\mu^2 b^2(\frac{\alpha}{2}\frac{d\rho}{d\epsilon} + \rho\frac{d\alpha}{d\epsilon}) \tag{9b}$$

$$\frac{dE_s}{dE_w} = \frac{\mu b^2}{\sigma}(\beta\frac{d\beta}{d\epsilon} + \rho\frac{d\beta}{d\epsilon}) \tag{10b}$$

$$\sigma\frac{dE_s}{dE_w} = \mu b^2(\beta\frac{d\beta}{d\epsilon} + \rho\frac{d\beta}{d\epsilon}) \tag{11b}$$

Unless the functional dependence of α and β with strain is known, the correlation of the rate of work hardening with the fraction of energy stored is difficult.

Parameters Used to Define Stored Energy Data

The two parameters most often used to describe the stored energy data are:

1) the level of energy stored, E_s,

2) the fraction of energy stored to energy supplied, $\dfrac{dE_s}{dE_w}$.

Measurement of the energy stored during deformation is extremely difficult. The available techniques and the level of accuracy that is possible have been discussed in detail (Bever et al, 1973). The precise measurement of E_w, the energy supplied, is also difficult, because it includes contributions due to work done against friction and that due to elastic energy stored in the specimen and the testing machine. The problem is more acute at large strains.

Some of the data in the review of the article of Bever et al(1973) show that $\dfrac{dE_s}{dE_w}$ reaches a steady value as dE_w, the energy supplied increases. It would be interesting to examine whether this is because there is an optimum level of energy that can be stored in the material or is due to the difficulty in measuring the parameters involved.

Alternatively, the strain undergone by the material can be determined more accurately by measuring its shape change. The parameter $\dfrac{dE_s}{d\varepsilon}$, the change in energy stored per increment of strain, may give a better understanding of the question of whether there is an optimum level of energy that can be stored during deformation.

In Fig A.6 is shown the variation of $dE_R/d\gamma$ with γ, the shear strain, from the data of Hessner and Hemminger (1979). dE_R is the fraction of the energy released during recrystallization (and
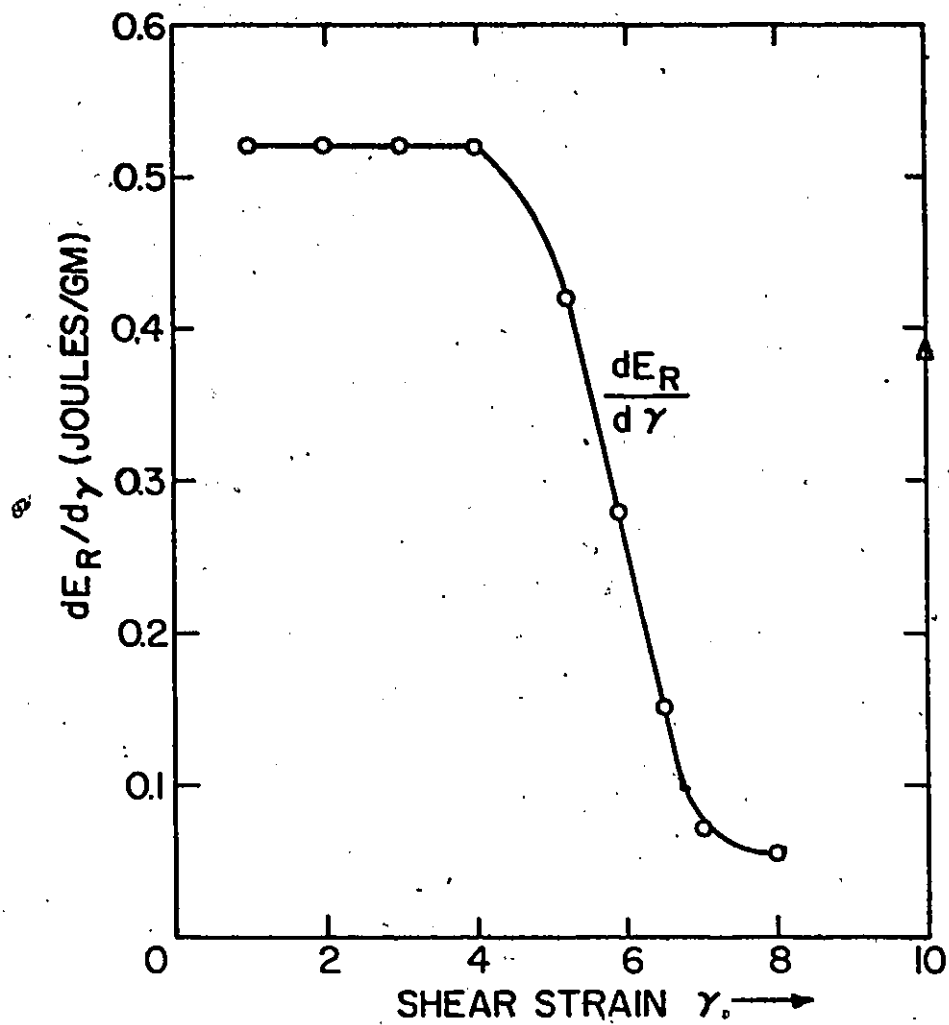
Fig. A.6 Illustration of the sensitivity of variation of the fraction of the energy stored ($\frac{dE_R}{dr}$) with strain

thus is related to dE_s) and $d\gamma$ is the shear strain in torsion. The data

shows that a   sensitive variation is followed by $\dfrac{dE_R}{d\gamma}$. In the

initial stages of deformation, the energy stored per increment of strain

is constant. The rapid decrease of $\dfrac{dE_R}{d\gamma}$ at later stages may reflect

major changes in dislocation configuration.

Salient Aspects of Stored Energy at Large Strains - Analysis of the Data Available in Literature

The work hardening behaviour and the accompanying changes in dis-

location substructure are well documented for single crystals, as dis-

cussed in Chapter 2. In most of the experimental studies of single

crystals where stored energy and work hardening behaviour were measured,

the deformation was carried out only up to moderate strains possible in

uniaxial tension mode. Therefore, the data available for polycrystals

must be considered to understand the behaviour at large strain. Impor-

tance of dynamic recovery in single crystals deformed beyond the linear

hardening stage has been discussed earlier in detail. Dynamic recovery

occurs at early stages of deformation in polycrystals (Lucke and Mecking,

1973). Therefore, some relevant data of stored energy measured at large

strains in polycrystals will be analysed with a view to investigate

whether the stored energy data reflects the changes occurring during

deformation at large strains.

Data of stored energy and work hardening behaviour are taken from

the works of Williams (1962, 1965); and Hessner and Hemminger (1979).

These are analysed and plotted in terms of $\dfrac{d\sigma}{d\epsilon}$, $\sigma\dfrac{d\sigma}{d\epsilon}$, $\dfrac{dE_s}{dE_w}$ and $\dfrac{dE_s}{d\epsilon}$ as

functions of stress. In Figs. A.7 to A.9, σ is considered here because it is a

structure sensitive parameter. Plots of E_s vs σ^2 obtained from the

above data are plotted in Fig. A.10(a-b).

Although, as discussed earlier, exact analysis of the parameters $\frac{d\sigma}{d\epsilon}$, $\sigma\frac{d\sigma}{d\epsilon}$, and $\frac{dE_s}{dE_w}$ are difficult because the functional dependence of α and β on strain is not known, the data can be analysed qualitatively.

In Fig. A.7, the data for polycrystalline aluminum deformed at 42°C by impact compression is given (Williams, 1962). The work hardening rate $\frac{d\sigma}{d\epsilon}$ is seen to decrease more rapidly than $\frac{dE_s}{dE_w}$. Variations of ρ, the dislocation density and α with strain are built up in $\frac{d\sigma}{d\epsilon}$ whereas $\frac{dE_s}{dE_w}$ reflect the variation of ρ and β with strain. That $\frac{d\sigma}{d\epsilon}$ decreases more rapidly in the initial stages may mean that α is changing more rapidly than β. The decrease in β which must occur due to rearrangements of dislocation substructure at large strains, is shown by the more rapid decrease in $\frac{dE_s}{dE_w}$ at large strains. This interpretation is consistent with the data shown in Fig. A.7(b). The rate of increment of energy stored per increment of strain decreases more rapidly at large deformations, reflecting the variation of β at these strains.

The results indicate that changes in α are more important in the early stages of deformation, while the changes in β are important at later stages.

The data presented here must be approached with caution, because of the strain rates and the temperatures involved. At the specified deformation temperature 42°C, simultaneously thermal recovery during deformation will occur in aluminum and the data may not indicate the real effects of dynamic recovery. The extremely high strain rates involved, the changes occurring in the dislocation configuration may be completely different from that characteristic of low strain rates.
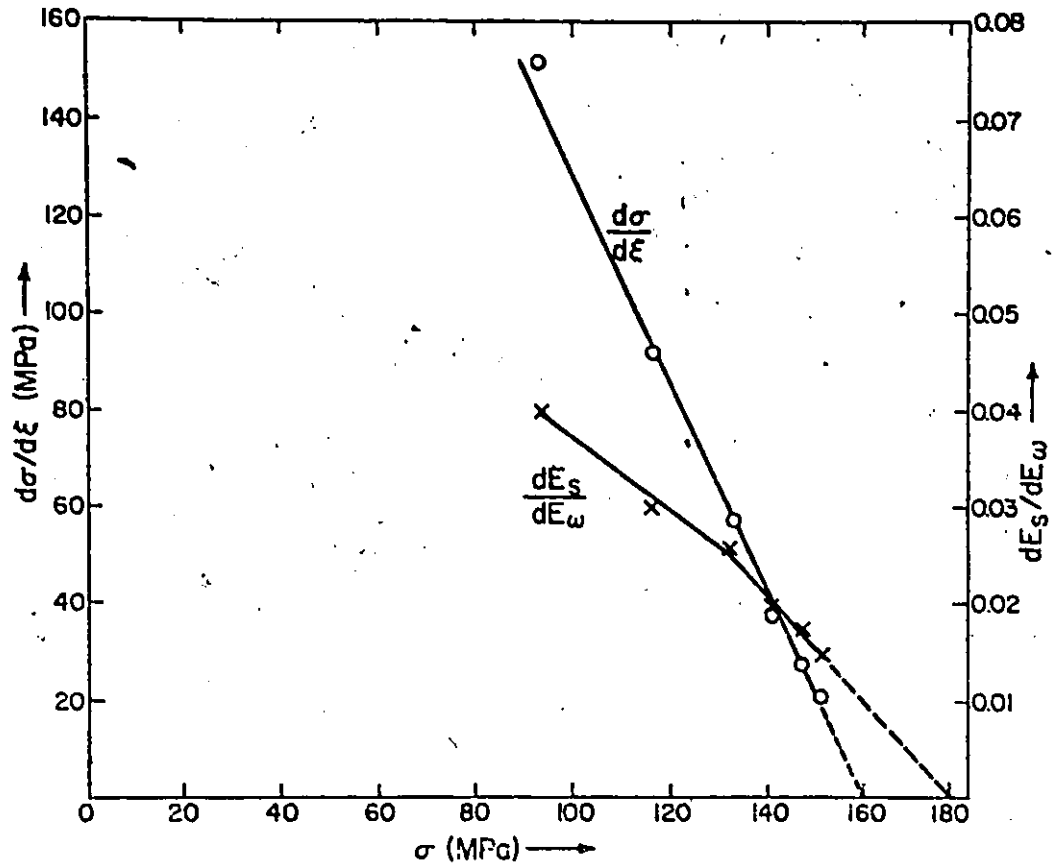
Fig. A.7(a) Comparison of stored energy data with work hardening behaviour for polycrystalline aluminum, from Williams, R.O., 1962, Trans. A.I.M.E., 224, 719.

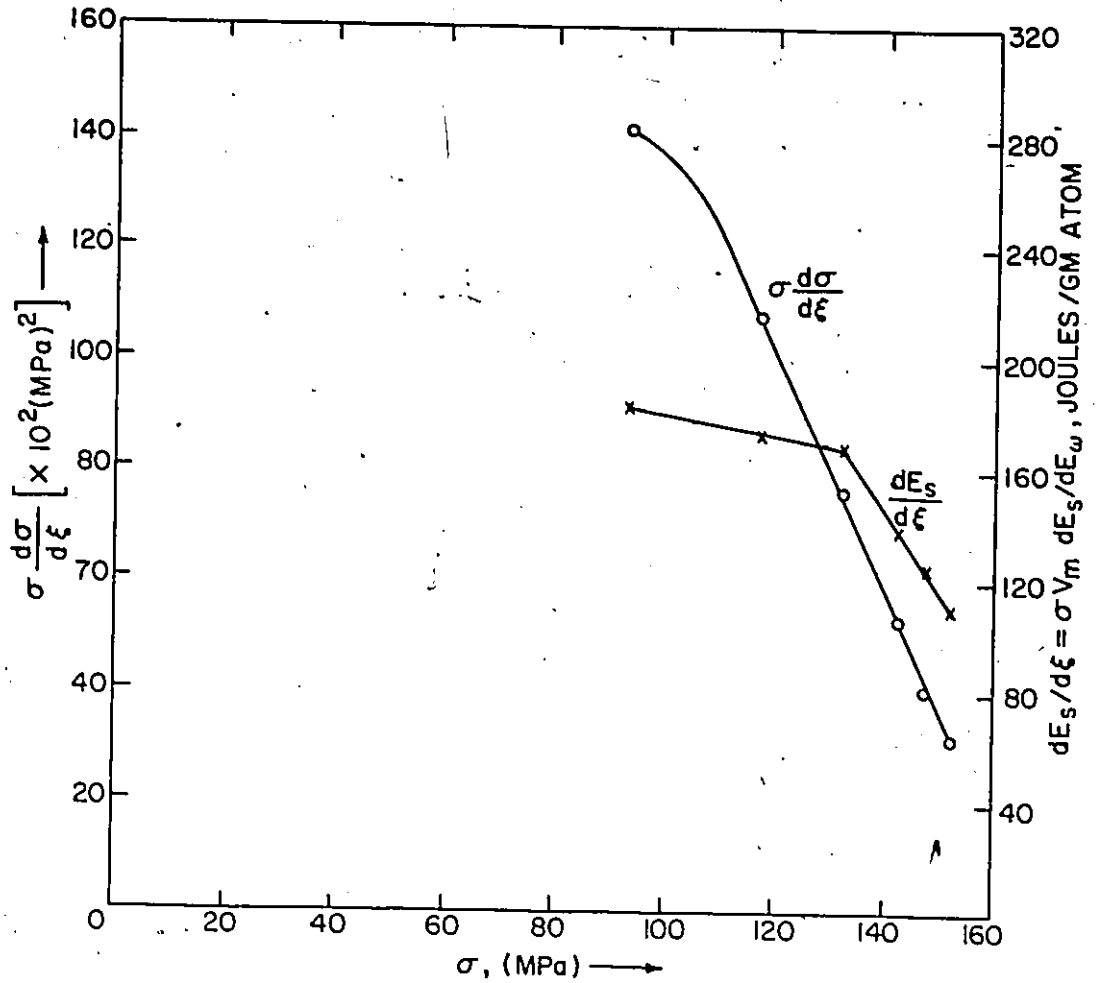Plots of $\dfrac{dE_s}{dE_w}$ and $\dfrac{d\sigma}{d\varepsilon}$ vs σ

Fig. A.7(b) Comparison of stored energy data with
work hardening behaviour for polycrystalline
aluminum, from Williams, R.O., 1962, Trans.
A.I.M.E., 224, 719.

Plots of $\dfrac{dE_s}{dE_w}$ and $\sigma\dfrac{d\sigma}{d\epsilon}$ vs σ

In order to examine the effect of strain rate ($\sim 10^4$/min. in the impact test), data for two different strain rates are compared in Figure 5 for polycrystalline copper (Williams, 1965). Surprisingly, no major changes due to the effects of strain rate can be detected. Comparing the level of $\frac{dE_s}{dE_w}$ at the two strain rates shows a lower fraction of the energy supplied is stored at the higher strain rate. The experimental findings of Titchener and of other workers reported by Bever et al (1973) which indicate that the level of energy stored increases with increasing deformation rate may not be true when the rate of deformation is of the order of 10^4/min. This is faster by an order of magnitude than the maximum rate reported by Bever et al (1973).

The results in Fig. A.8 are contradictory when the variation of the work hardening rate with stress is considered for the two different strain rates. At a given stress, the work hardening rate is higher for the impact compression test than for tensile test, but lower fraction of energy is stored during the impact compression test. This could be due to the inaccuracy of measurements of E_s and E_w and the effects of friction in the compression tests.

Figs. A.9(a-b) show some of the data generated by Hessner and Henninger (1979) from torsion tests on polycrystalline copper. The work hardening rate attains a constant level but the fraction of energy stored decreases continuously. Even in the range where the rate of dislocation storage does not change appreciably, $\frac{dE_r}{d\gamma}$ decreases drastically as shown in Fig. A.9(b). Both these plots reflect the relative variations of α and β with strain and the regime of deformation
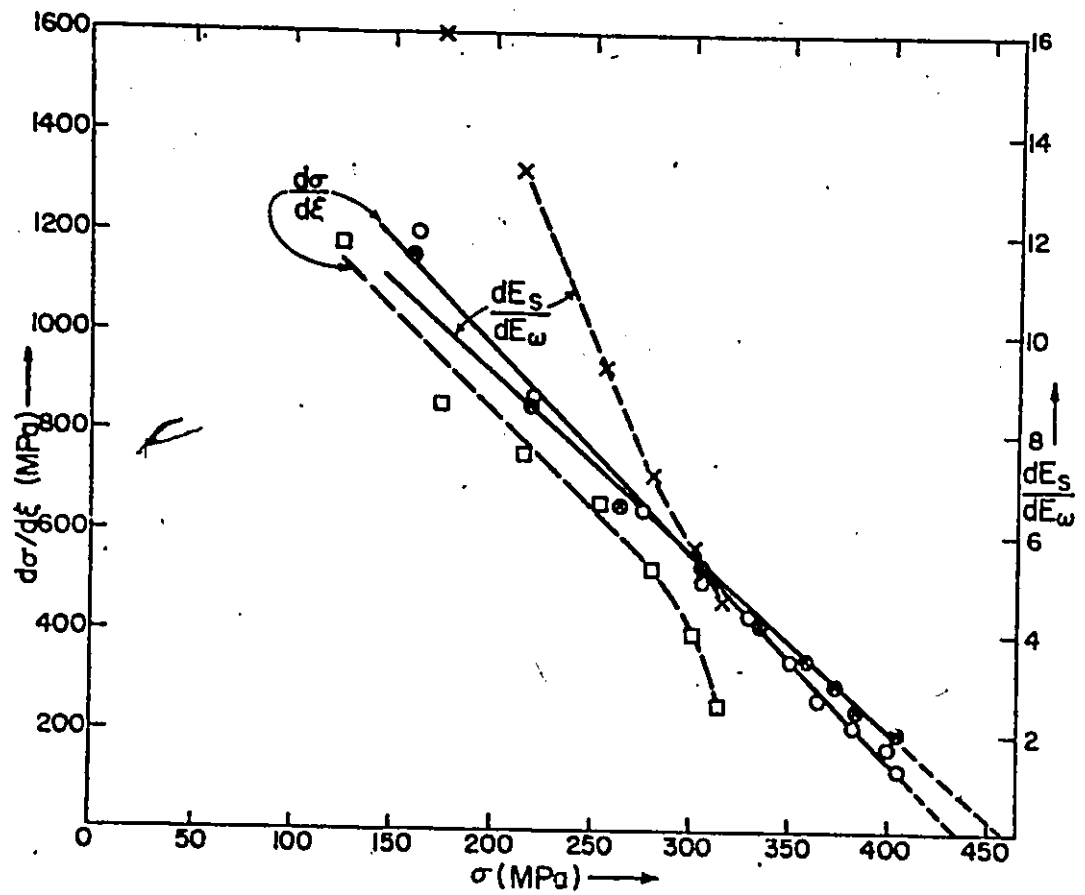
Fig. A.8 Comparison of stored energy data with
          work hardening behaviour in polycrystal-
          line copper at two different strain rates.
          From Williams, R.O., 1965, Acta. Meta.,
          13, 163.
          Solid lines represent large strain rate(40,000/min)
          Dotted lines represent low strain rate(0.022/min).

Fig. A.9(a)   Comparison of stored energy data with work hardening
              behaviour of polycrystalline copper.
              From Hessner, F. and Hemminger, H., Z. Met. 69
              (1979), 553.

              Plots of $\frac{d\tau}{d\gamma}$ and $\frac{dE_R}{dE_w}$ vs σ
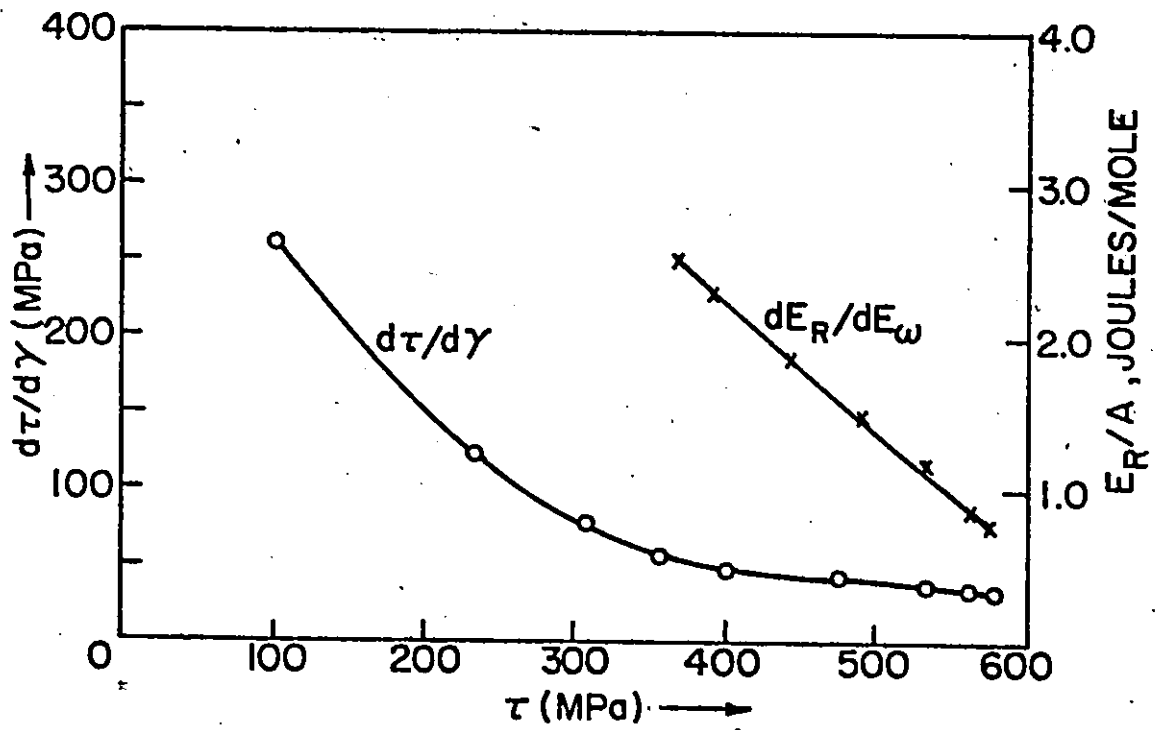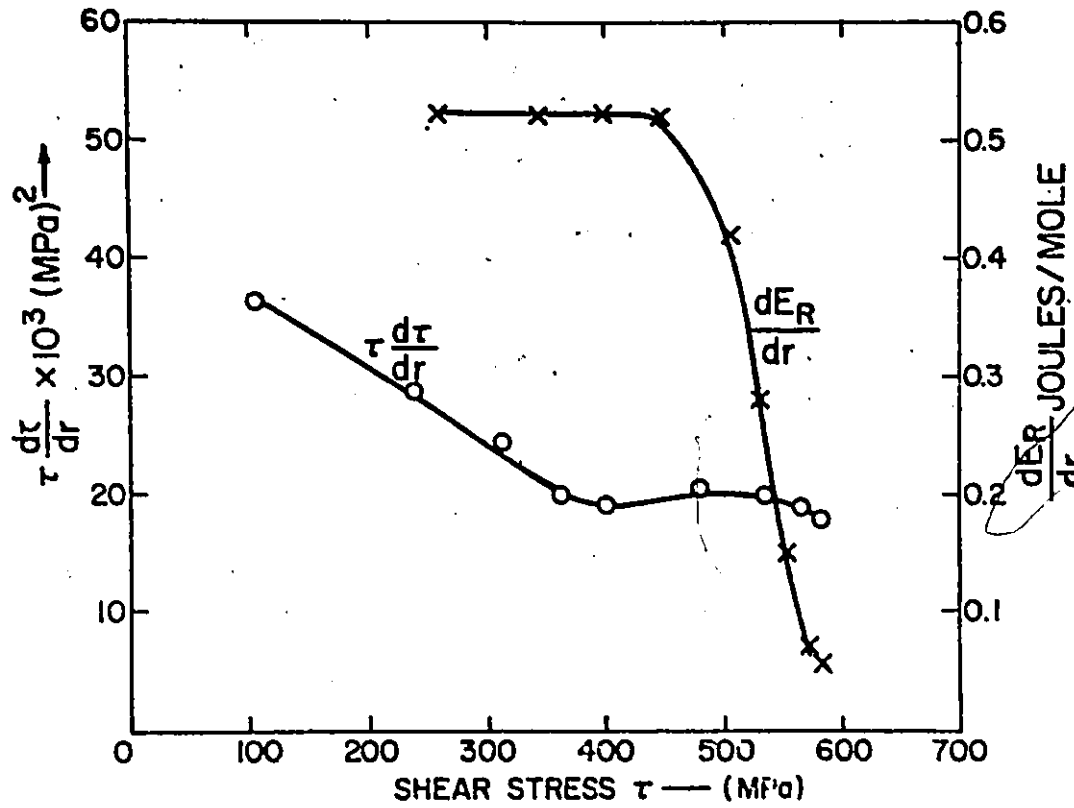
Fig. A.9(b)   Comparison of stored energy data with
work hardening behaviour of poly-
crystalline copper.   From Hessner, F.
and Hemminger, H., Z. Met. 69 (1979), 553.

Plots of $\tau\dfrac{d\tau}{d\gamma}$ and $\dfrac{dE_R}{d}$ vs τ

where these changes are important.

In Figures A.10(a-b), the data for polycrystal aluminum and copper (Williams, 1962, 1965) are replotted in terms of E_s vs σ^2. Upon comparing with Fig. A 5, it is seen that the deviation of the experimental data indicates that the parameter α is decreasing with increasing strain. That β also decreases with strain is not apparent from these plots, because the change in α has more effect on the slope of E_s vs σ^2, according to the section dealing with the method of analysis to examine the constancy of α and β. To separate the effect of variation in α and β, plots shown in Figs. A.7-A.9 seem to be more appropriate.

Possible Reasons for Variation of α and β With Strain

Equation (2) relates the flow stress to the average dislocation density and is valid for a random arrangement of dislocations. Neglecting the dependence of α on strain, an increment of $d\rho$ in the stored dislocation density should increase the level of flow stress $d\sigma$ according to the relation

$$d\sigma = \frac{\alpha\mu b}{2\sqrt{\rho}}\, d\rho$$

$$= \frac{(\alpha\mu b)^2}{2\sigma}\, d\rho \tag{12}$$

What Equations (2) and (12) do not consider is how the flow stress is influenced by recovery events which are influenced at large strains by an increment $d\rho$ in the stored dislocation density. At large strains, the nature of influence of the substructure on the flow stress is complicated and Equation (2) may not be an adequate description of the flow stress.

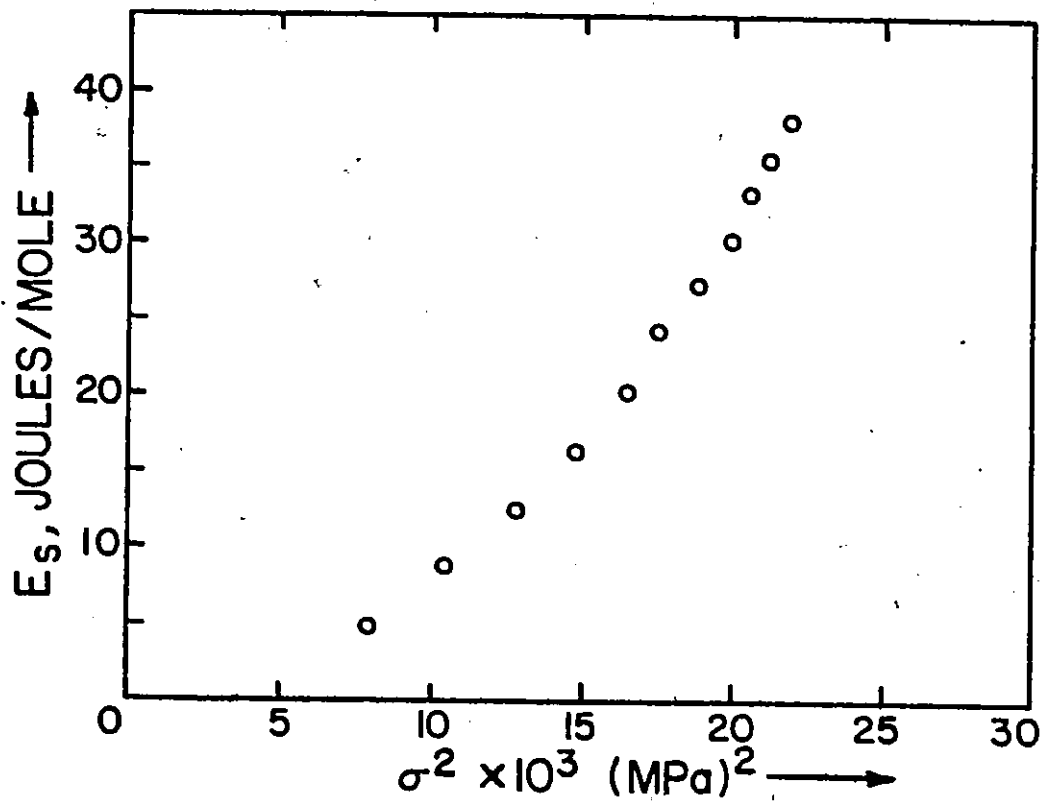Similarly, Equation (3) for the energy stored, implies that every

Fig. A.10(a) Plot of E_s vs σ^2 for polycrystalline aluminum.
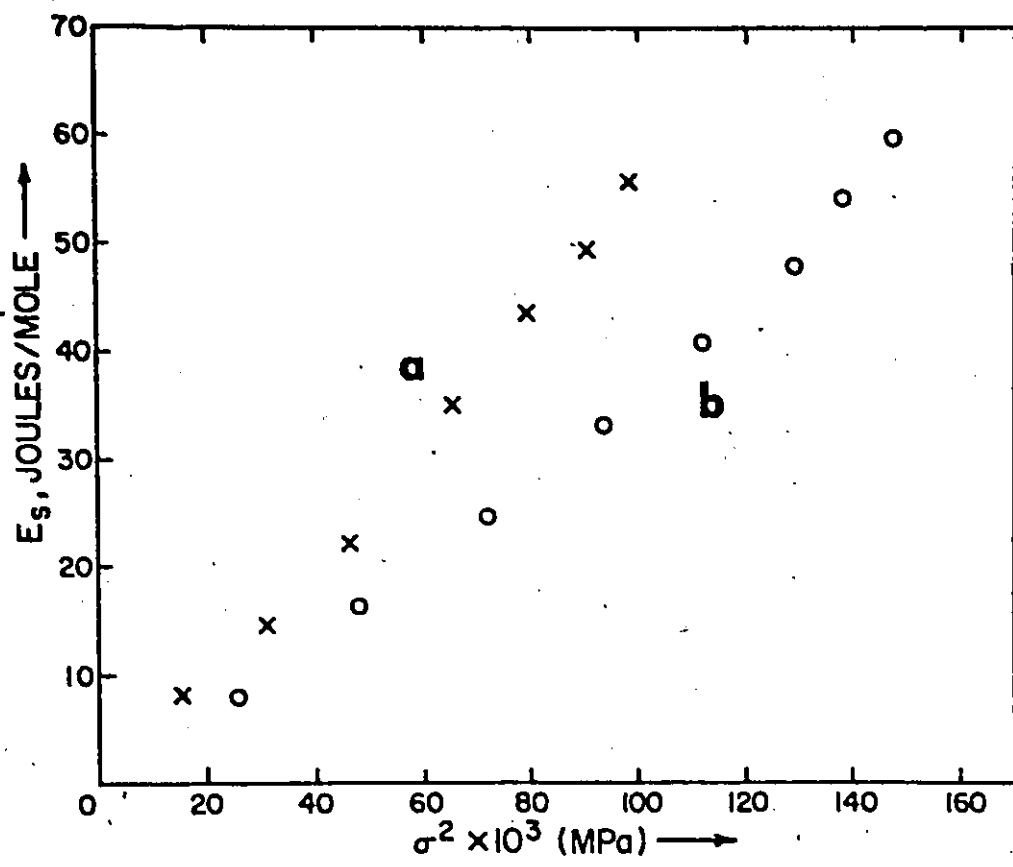From Williams, (1962).

Fig. A.10(b)   Plots of E_s vs σ^2 for polycrystalline copper.

From Williams, (1965).

Strain rates: (a) 0.022/min.
(b) 40,000/min.

dislocation added to the structure increases the stored energy according to the relation $E_s = \beta\mu b^2 \rho$. Actually, due to an increase in $d\rho$ in the dislocation density, on the increase in energy stored depends on how the additional dislocations get incorporated in the existing dislocation substructure. Considering a simplified picture, where the existing dislocation substructure is made up of simple tilt walls, the energy increase due to an increase due to an increase in dislocation density depends on how the dislocations increase the angle of misorientation across the tilt walls. The energy of a simple tilt wall of misorientation θ is given by Read (1953):

$$E = E_o \, \theta(A - \ln \theta) \qquad (13)$$

where $E_o = \dfrac{\mu b}{4\pi(1-\nu)}$ and A is a constant. θ is related to ρ, the density of dislocations in the tilt wall, according to the relation

$$\theta = b\rho \qquad (14)$$

Incorporating Equation (2) in Equation (13) results in

$$E = \beta^1 \mu b^2 \rho - \frac{\beta^1}{A} \mu b^2 \, \rho \ln(b\rho) \qquad (16)$$

where
$$\beta^1 = \frac{A}{4\pi(1-\nu)} \; .$$

The first term in the expression (16) is similar to Equation (3), but there is an additional logarithmic term in Equation (16), the details of which depend on the nature of the substructure. This term influences the level of energy stored.

Thus, at large strains, the details of the substructure in terms of the characteristics of the dislocation components making up the subgrains, the scale and the misorientation of the substructure, are important in considering the flow stress and the level of stored energy.

In fact, Equations (2) and (3) may not contain all the appropriate parameters necessary to describe the stored energy E_s and the flow stress σ.

Conclusions

Based on the limited data of stored energy considered here, the following conclusions can be drawn:

(1)   the parameter $\dfrac{dE_s}{d\varepsilon}$ gives a clearer view compared to the parameter $\dfrac{dE_s}{dE_w}$ of the fraction of energy stored at large strains;

(2)   the rate of energy storage per increment of strain decreases rapidly at large strains, indicating possible, major changes in the dislocation configurations;

(3)   the parameters α and β vary during deformation at large strains.

REFERENCES

Ahlborn, H., 1966 in Recrystallization, Grain Growth and Texture, ASM, p.374.

Ambrosi, P., Göttler, E. and Schwink, Ch., 1974, Scr. Met., 8, p.1093.

Ambrosi, P. and Schwink, Ch., 1978, Scr. Met., 12, p.303.

Amelinskx, S. and Dekeyser, W., 1958, J. Appl. Phys., 29, p.1000.

Argon, S.A. and Orowan, E., 1961, Nature, 4, p.447.

Bailey, J.E. and Hirsch, P.B., 1960, Phil. Mag., 5, p.485.

Ball, C.J. and Hirsch, P.B., 1955, Phil. Mag., 46, p.1343.

Basinski, Z.S., 1959, Phil. Mag., 4, p.393.

Basinski, Z.S. and Dove, D.B., 1963, unpublished (see Basinski, Z.S. and Basinski, S.J., 1966)

Basinski, Z.S. and Basinski, S.J., 1966 in Recrystallization, Grain Growth and Texture, ASM, p.1.

Basinski, Z.S. and Basinski, S.J., 1970, Vol. 2, Proc. ICSMA 2, ASILOMAR, p.189.

Barrett, C.S., 1952, Structure of Metals, McGraw-Hill.

Barrett, C.S. and Masalski, T.B., 1966, Structure of Metals, McGraw-Hill.

Beck, P.A., 1949, J. Appl. Phys., 20, p.633.

Beck, P.A. and Sperry, P.R., 1950, J. Appl. Phys., 21, p.150.

Beck, P.A. and Hu, H., 1966 in Recrystallization, Grain Growth and Texture, ASM, p.393.

Bellier, S.P., 1971, D. Phil. Thesis, University of Sussex.

Bellier, S.P. and Doherty, R.D., 1977, Acta Met., 25, p.521.

Bever, M.B., Holt, D.L. and Titchener, A.L., Vol. 17, Progress in Material Science, Pergamon.

Bishop, J.F.W. and Hill, R., 1951, Phil. Mag., 42, p.414, 1298.

Blewitt, T.H., Coltman, R.R. and Redman, J.K., 1967, J. Appl. Phys., 28, p.65.

Bridgmann, P.W., 1925, Proc. Am. Acad. Arts Sci., 60, p.305.

Brown, A.F., 1952, Adv. in Phys., 1, p427.

Buckley, S.N. and Entwistle, K.W., 1956, Acta Met., 4, p.352.

Byrne, J.G., 1965, Recovery and Recrystallization and Grain Growth, MacMillan.

Cahn, R.W., 1966 in Recrystallization, Grain Growth and Texture, ASM, p.99.

Cash, R.W., 1970, Physical Metallurgy, North Holland Publishing Co., 2nd Ed.

Cairns, J.H., Clough, J., Dewey, M.A.P. and Nutting, J., 1971, J. Inst. Metals, 99, p.93.

Carpay, F.M.A., Chin, G.Y., Mahajan, S. and Rubin, J.J., 1975, Acta Met. 23, p.1473.

Cherian, T.V., Pietrokowsky, P. and Dorn, J.E., 1949, Met. Trans., 185, p.948.

Chin G.Y., Nesbitt, E.A. and Williams, A.J., 1966, Acta Met., 14, p.467.

Chin, G.Y. and Mammel, W.L., 1969, Trans. AIME, 245, p.1211.

Crussard, C., 1945, Rev. Met. 42, p.286, 321.

Conn, G.K.T. and Bradshaw, F.J., 1952, Polarized Light in Metallography, Butterworth.

Cotterill, P. and Mould, P.R., 1976, Recrystallization and Grain Growth in Metals, Surrey University Press.

Dillamore, I.L., Butler, E. and Green, D., 1968, Metal Sci. J., 20, p.161.

Dillamore, I.L., Morris, P.L., Smith, C.J.E., and Hutchinson, W.B., 1972, Proc. Roy. Soc. (L), A329, p.405.

Dillamore, I.L. and Bush, A.C., 1978, Proc. ICOTOM 5, Aachen, p.367.

Doherty, R.D., 1974, Metal Sci. J., 8, p.132.

Doherty, R.D. and Cahn, R.W., 1972, J. Less Common Metals, 28, p.279.

Embury, J.D., 1971 in Strengthening Mechanisms in Crystals, Ed. A. Kelly and R.B. Nicholson, Appl. Sci. Pub. (London).

Embury, J.D., Keh, A.S. and Fisher, R.M., 1966, Trans. AIME, 236, p.1252.

Frank, F.C., 1950, Symp. on the Plastic Deformation of Crystalline Solids, p.150.

Faivre, P. and Doherty, R.D., 1979, J. Mat. Sci., 14, p.897.

Gordon, P., 1955, Trans. AIME, 203, p.1043.

Göttler, E., 1973, Phil. Mag., 28, p.1057.

Gottstein, A., 1974, Diplom Thesis, Aachen.

Grewen, J., Huber, J. and Hatherly, M., 1978, Metals Forum, 1, p.115.

Haessner, F., 1979, Recrystallization in Metallic Materials, 2nd Ed., Riederverlag.

Hansen, N., 1969, Trans. AIME, 245, p.2061.

Hasegawa, T. and Kocks, U.F., 1979, Acta Met., 27, p.1705.

Hasegawa, T., Yakou, T., Shimizu, M. and Karashima, S., 1976, Trans. J.I.M., 197, p.414.

Hecker, S., 1979, Private communication.

Himmel, L., 1963, Recovery and Recrystallization of Metals, Gordon and Breach.

Hirsch, P.B., Howie, A., Nicholson, R.B., Pashley, D.W. and Whelan, M.J., Electron Microscopy of Thin Crystals, Butterworth, 1965.

Hirsch, P.B., 1959, Internal Stresses and Fatigue in Metals, Ed. G.M. Rassweiler and W.L. Grube, Elsevier, p.89.

Hirsch, P.B. and Kellar, 1952, Acta Cryst., 5, p.162.

Holt, D.L., 1970, J. Appl. Phys., 41, p.3197.

Honeycombe, R.W.K., 51-52, J.I.M., 80, p.49.

Inokuti, Y. and Doherty, R.D., 1978, Acta Met., 26, p.61.

Jackson, P.J. and Basinski, Z.S., Canad. J. Phys., 1967, 45, p.707.

Johnson, L., 1969, Trans. AIME, 245, p.275.

Karduck, P., Gottstein, G. and Mecking, H., ICSTOM 5, Aachen, p.377.

Kaspar, R., and Pluhar, J., 1975, Metal Sci., 9, p.104.

Kawasaki, Y., 1979, Japan. J. Appl. Phys., 18, p.1429.

Kear, B.H., 1962, Met. Trans., 224, p.674.

Keh, A. and Weissmann, S., 1963 in Electron Microscopy and Strength of Crystals, Ed., G. Thomas and J. Washburn, Interscience.

Kishi, T., 1969, Plasticity and Working 10, p.868.

Kocks, U.F., Chen, H.S., Rigney, D.A. and Schaefer, R.J., 1966 in Work Hardening, Gordon and Breach, p.151.

Kocks, U.F., 1959, Ph.D. Thesis, Harvard University.

Kocks, U.F., 1960, Acta Met., 8, p.345.

Kocks, U.F. and Brown, T.J., 1966, Acta Met., 14, p.87.

Kocks, U.F., 1970, Met. Trans 1, p.1121.

Kocks, U.F., and Mecking, H., ICSMA 5, Aachen, 1979.

Korbel, A. and Swiatkowski, K., 1972, Metal Sci. J., 6, p.60.

Kuhlmann-Wilsdorf,D., 1962, Trans. AIME, 224, p.1047.

Kuhlmann-Wilsdorf, D., 1975, Work Hardening in Tension and Fatigue, Ed. Thompson, A.W., AIME, p.1.

Langford, G. and Cohen, M., 1969, Trans. ASM, 62, p.623.

Langford, G. and Cohen, M., 1975, Met. Trans. 6A, p.901.

Li, C.H., Washburn, J. and Parker, E.R., 1953, Trans. AIME, 197, p.1223.

Li, J.C.M., 1962, J. Appl. Phys., 33, p.2958.

Li, J.C.M., 1966 in Recrystallization, Grain Growth and Texture, ASM.

Lücke, K. and Lange, H., 1952, Z. Met., 43, p.55.

Lücke, K. and Mecking, H., 1973, Inhomogeneity in Plastic Deformation, ASM, p.223.

Mader, S., 1963, in Electron Microscopy and Strength of Crystals, Ed. G. Thomas, J. Washburn, Intersci.

Malin, A.S., and Hatherly, M., 1979, Metal Sci., 13, p.463.

Martin, J.B., 1975, Plasticity M.I.T. Press.

Masima, M. and Sachs, G., 1929, Z. Phys., 56, p.394.

McQueen, H.J. and Hockett, J.E., 1970, Met. Trans., 1, p.2997.

McElroy, R.J. and Szkopiak, Z.C., 1972, Int. Met. Rev., 17, p.175.

Mecking, H., 1978, ICSTOM 5, Aachen, p.25.

Mitchell, T.E., 1964, Prog. Appl. Mat. Res., 6, p.119.

Mitchell, J.W., Chevrier, J.C., Hockey, B.J., Monaghan, J.P., Canad. J. Phys., 45, p.453.

Mott, N.F., 1952, Phil. Mag. 43, p.115.

Mughrabi, H., 1968, Phil. Mag., 18, p.1211.

Mughrabi, H., 1971, Phil. Mag., 23, p.897.

Nabarro, F.R.N., Basinski, Z.S., and Holt, D.B., Adv. in Phys., 13, p.193.

Noggle, T.S., 1953, Rev. Sci. Instr., 24, p.184.

Perryman, E.C.W., and Lack, J.M., 1951, Nature (London), 167, p.479.

Phillips, V.A., 1971, Modern Metallographis Techniques and Their Applications, Wiley-Interscience.

Price, W.L. and Washburn, J., 1963, J. Aust. Inst. Metals, 8, p.1.

Ratsuzek, E. and Karp, S., 1976, Metal Sci., 10, p.214.

Roberts, W., 1976, Proc. ICSMA 4, Nancy, p.146.

Rosi, F.D., 1954, J. Metals, p.1010.

Saeki and Miura, 1977, Trans. J.I.M., 18, p.843.

Sandström, R., 1977, Acta Met., 25, 897, p.905.

Sandström, R., 1978, J. Mater. Sci., 13, p.1229.

Schuh, F. and von Heimendahl, M., 1974, Z. Met., 65, p.346.

Schnell, C. and Grewe, H.G., 1978, ICSTOM 5, Aachen, p.389.

Schmid, E., Proc. Int. Cong. Appl. Mech., Delft, 1924, p.342.

Seeger, A., 1956 in Dislocations and Mechanical Properties of Crystals.

Sehgal, H.K., Butler, E.P. and Swann, P.R., 1975, Sci. Met., 9, p.165.

Serpoul, J.J. and Driver, S.H., 1979 in Proc. ICSMA 5, Aachen, Vol. 2, p.875.

Sevillano, J.G., van Houtte, P., Aernoudt, E., to be published.

Sharp, J.V. and Makin, M.J., 1967, Canad. J. Phys., 45, p.519.

Slakhorst, J.W.H.G. and Tien Biewjohs, M.J., 1977, Sci. Met., 11, p.1947.

Smith, C.J.E. and Dillamore, I.E., 1970, Metal Sci. J., 4, p.161.

Swann, P.R., 1963, Electron Microscopy and Strength of Crystals, Ed. G. Thomas and J. Washburn, Intersci. p.131.

Taylor, G.I., 1938, J. Inst. Met., 62, p.307.

Thompson, A.W., Baskes, M.I., Flanagan, W.F., 1973, Acta Met., 21, p.1017.

Thompson, A.W., 1977, Met. Trans. 8A, p.83.

Viswanathan, R., and Bauer, C.L., 1973, Acta Met., 210, p.1099.

von Drunen, G. and Saimoto, S., 1971, Acta Met., 18, p.213.

Walter, J.L. and Koch, E.F., 1963, Acta Met., 10, p.1059.

Weertman, J., 1963, Met. Trans. 227, p.1439.

Warrington, D.W., 1960, Proc. European Conf. on Electron Microscopy, Delft, p.354.

Washburn, J., and Murty, G., 1966, J. Appl. Phys., 37, p.2511.

Wilsdorf, H., and Kuhlmann-Wilsdorf, D., 1952, Z. Angew. Phys., 361, p.409.

Wonsiewicz, B.C. and Chin, G.Y., 1970, Met. Trans., 1, p.2715.

Wonsiewicz, B.C., Chin, G.Y., and Hart, R.R., 1971, Met. Trans. 2, p.2093.

Young, F.W. and Sherill, F.A., 1967, Canad. J. Phys. 45, p.707.